Alma Mater Studiorum – Università di Bologna

DOTTORATO DI RICERCA IN

CHIMICA

Ciclo XXIX

Settore Concorsuale di afferenza: 03/C2

Settore Scientifico disciplinare:CHIM04

Synthesis and characterization of mesoporous material for catalytic applications

Presentata da: **Sara Andreoli**

Coordinatore Dottorato
Prof. Aldo Roda

Relatore
Prof.ssa Stefania Albonetti

Correlatore
Prof. Giuseppe Fornasari

Esame finale anno 2017

Table of Contents

General Introduction

This PhD project dealt with different topics mainly linked together by fluorinated compounds. The work started from the preparation and characterization of mesoporous materials as supports for catalysts for the production of fluorinated monomers of industrial interest.

From these monomers, fluorinated polymers are obtained through industrial processes, with all their interesting properties, due to the presence of fluorine, such as thermal and chemical stability, flame resistance. This particular family of polymers find many applications, but their use as catalyst in gas-phase reactions is still poorly investigated. Indeed, the research work was also focused on the use of fluorinated polymers, in particular perfluorosulfonic superacid resins, as acid catalysts in gas-phase reactions. Consequently, this work can be divided in three main sections.

Section 1: preparation and characterization of PdCu/MCM-41 catalysts for hydrodechlorination (HDC) reaction of chlorofluorocarbons compounds with the aim to obtain fluorinated monomers. In previous works, it has been demonstrated that microporous texture of activated carbon used as support, significantly limited possible applications of this catalytic system, because of reduced mass transfer.

Supports with larger pores can overcame these drawbacks; in particular, MCM-41 silicate mesoporous materials can be an alternative support.

The work was focused on the optimization of the synthetic procedure and the catalyst features, such as the active phase particle size, and on the performances in the reaction of interest.

Section 2: The competences achieved during the first part of the work were exploited for the synthesis and characterization of mesoporous carbon materials, always with the aim to solve the problems related to microporous features of active carbon based materials. This part of the work is strongly linked with the previous section due to mesoporous features of materials. The prepared materials were characterized and modified through post-synthesis oxidative treatments or heteroatom insertion, with the aim to increase their catalytic activity. Indeed, benzyl alcohol liquid-phase oxidation was employed as a model reaction to demonstrate the catalytic activity of the pristine carbon material in absence of metals.

Section 3: Study of Aquivion® PFSA, a perfluorosulfonic resin produced by Solvay Specialty Polymers, as aid catalyst in gas-phase dehydration reaction. The application of this polymer, with an acidity close to that of sulphuric acid 100%, as catalyst in gas-phase reaction has never been explored before.

Recently, there has been considerable interest, driven by environmental consideration and safety concerns, to find solid alternatives for very hazardous and corrosive mineral acid catalysts such as hydrofluoric and sulphuric acid used in commercial chemical processes. Acid ion-exchange polymer resins, as Aquivion, represent one class of potential solid acid materials.

Aquivion material was used as catalyst for dehydration of ethanol to ethylene, employed as a model reaction to explore the possible applications of this material in heterogeneous acid catalysis.

Chapter 1: Mesoporous silica based materials

1.1 Introduction

Porous materials, frequently used as support in heterogeneous catalysis, can be classified in different type[1]:

- Microporous, with pore diameter less than 20 Å;
- Mesoporous, with pore diameter between 20 and 500 Å;
- Macroporous, with pore diameter larger than 500 Å.

The application of porous materials in catalysis is mainly due to their high surface area but, at the same time, it is limited by the pore size, leading the use of porous material only in reaction involving small molecules. Indeed, with the aim to overcome this drawback, new materials with larger pores have been searched, as mesoporous material. Thanks to the larger pores, these materials can be employed also in reaction involving larger molecules, increasing the fields of applications in catalysis.

1.1.1 MCM-41 synthesis and applications

In 1992, the researchers of the Mobil Oil Company synthesized MCM-41 material (Mobil Crystalline Material number 41) which has an ordinated porous structure with hexagonal arrangement[2,3]. Changing the synthesis conditions, other pores dispositions could be obtained, such as cubic disposition (MCM-48) or lamellar disposition (MCM-50).

MCM-41 is probably the best known member of the molecular sieve M41S family and, besides similar characteristics to microporous materials, it has also other interesting features. For example [4]:

- Sharp distribution of pore dimension between 15 and 100 Å;
- Very well ordinated porous structure with hexagonal arrangement;

1. Mesoporous silica based materials

- High surface area (over 1000 m^2/g);
- Moderated acidity due to uncoordinated Si atoms;
- High thermal stability (over 400°C);
- High chemical resistance in strong acid environment, but not in basic media.

The MCM-41 synthesis is performed through sol-gel method, staring from a silica source and a templating agent, which usually is a big organic molecule with a hydrophilic head and a hydrophobic tale of variable length. In aqueous media, the molecules of templating agent organized themselves in micelles on which the silica condensation takes place. Indeed the templating agent provides an ordinated structure mimed by the silica and after its removal, the desired porosity can be obtained[5]. Many methods can be found in literature for MCM-41 synthesis and they are similar to the original procedure of the Mobil Oil Company, only the reagents have been changed. The synthesis is performed at room temperature, than it is followed by a hydrothermal treatment, a fundamental step to obtain the ordinated structure of MCM-41 with hexagonal arrangement of the pores. This treatment consists in leaving the synthesis batch between 100 and 150 °C with autogenic pressure for a long period of time (for example 144 hours[6]) which can be largely reduced using new technologies, such as microwave.

The next step is the solid filtration and the calcination at temperature over 500°C; this last treatment is useful for the removal of the templating agent and the formation of the desired porosity.

The parameters, which influence the structure of the final material, are numerous:

- Si/templating agent molar ratio;
- Templating agent concentration in solution;
- Length of the alkyl chain of the templating agent molecules;
- Silica source type;
- Hydrothermal treatment conditions (time and temperature).

Concerning the first parameter, it has been observed that changing the moral ratio between Si and templating agent from 0.5 to 2, the structure obtained in the final material changed from hexagonal to cubic and finally to lamellar type[4]. After various studies[7], it has been stated that for obtaining a hexagonal structure (MCM-41) the Si/templating agent molar ratio has to be less than 1; for a cubic structure (MCM-48) it should be between 1 and 1.5, while for a lamellar structure (MCM-50) a ratio between 1.5 and 2 is needed.

For obtaining a hexagonal disposition of the micelles in solution, the optimal concentration of the templating agent in solution is 25% wt[4].

Indeed, increasing the templating agent concentration, the form of the micelles and consequently the obtained structure change (**Figure *1***).

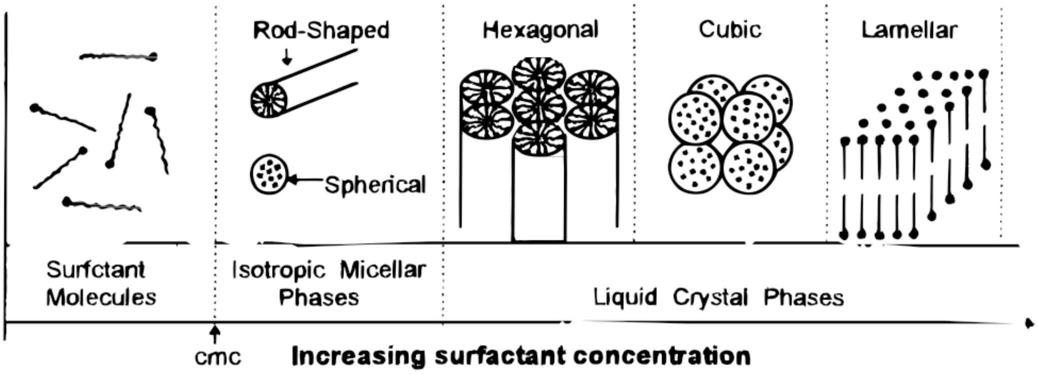

Figure 1 Trend of the micelles disposition with the templating agent concentration[4].

Moreover, at room temperature a basic pH is needed to favour the formation of cylindrical micelles necessary for the hexagonal arrangement.

The main parameters, which can influence the pores dimensions, are:

- Length of the alkyl chain of the templating agent molecules;
- Hydrothermal treatment conditions;
- Possible presence of expanding agents.

It has been demonstrated that increasing the length of the alkyl chain of the templating agent, the pores size increased; but at the same time, if the alkyl chain is too short (less than 8 C atoms), the micelles cannot be obtained[3].

Concerning the hydrothermal treatment, the ideal temperature to obtain the hexagonal phase should be less than 150°C[3], otherwise other types of phase are obtained due to a higher solubility of the templating agent, which does not self-assemble in micelles.

Even the length of the hydrothermal treatment is important for the formation of the desired structure. Indeed, for treatments longer than 144 hours, the crystallinity and the porosity increase; after 10 days, the loss of order and the formation of other type of phase, beside the hexagonal one, is observed[5] (**Figure *2***).

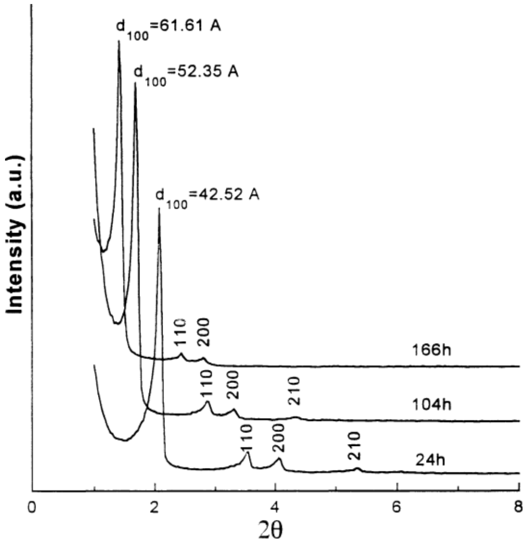

Figure 2 Influence of the length of hydrothermal treatment on hexagonal phase[5].

With the aim of exploit the particular structure and the morphological properties of this material, also for catalytic applications, a large number of investigations were proposed regarding the inclusion of dopants[8], as reported in **Table *1***.

The interest in doping mesoporous silicates with metals lies primarily in the development of catalytically active materials.

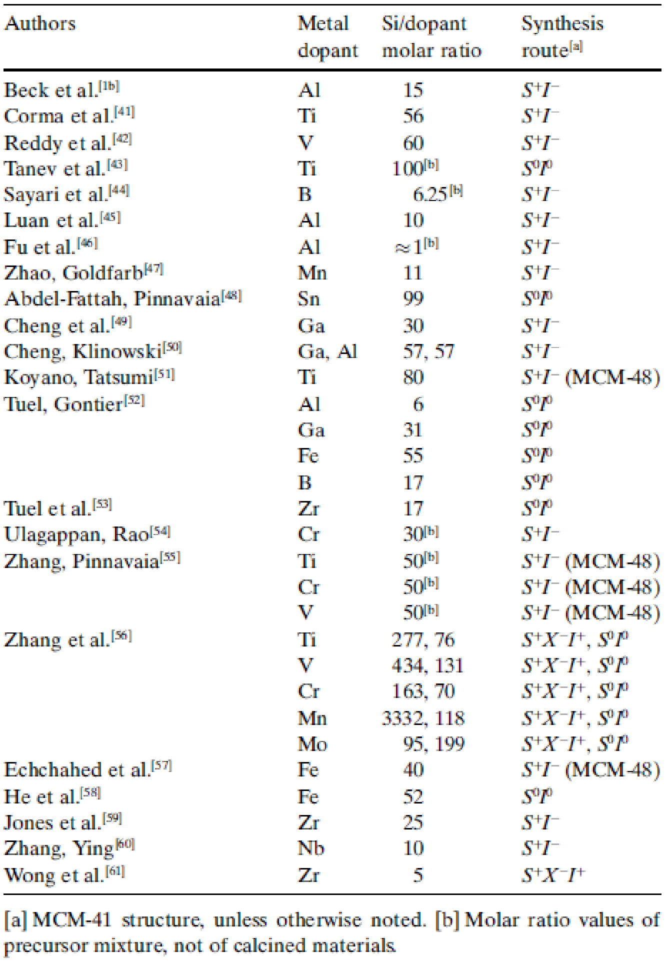

Authors	Metal dopant	Si/dopant molar ratio	Synthesis route[a]
Beck et al.[1b]	Al	15	S^+I^-
Corma et al.[41]	Ti	56	S^+I^-
Reddy et al.[42]	V	60	S^+I^-
Tanev et al.[43]	Ti	100[b]	S^0I^0
Sayari et al.[44]	B	6.25[b]	S^+I^-
Luan et al.[45]	Al	10	S^+I^-
Fu et al.[46]	Al	≈1[b]	S^+I^-
Zhao, Goldfarb[47]	Mn	11	S^+I^-
Abdel-Fattah, Pinnavaia[48]	Sn	99	S^0I^0
Cheng et al.[49]	Ga	30	S^+I^-
Cheng, Klinowski[50]	Ga, Al	57, 57	S^+I^-
Koyano, Tatsumi[51]	Ti	80	S^+I^- (MCM-48)
Tuel, Gontier[52]	Al	6	S^0I^0
	Ga	31	S^0I^0
	Fe	55	S^0I^0
	B	17	S^0I^0
Tuel et al.[53]	Zr	17	S^0I^0
Ulagappan, Rao[54]	Cr	30[b]	S^+I^-
Zhang, Pinnavaia[55]	Ti	50[b]	S^+I^- (MCM-48)
	Cr	50[b]	S^+I^- (MCM-48)
	V	50[b]	S^+I^- (MCM-48)
Zhang et al.[56]	Ti	277, 76	$S^+X^-I^+$, S^0I^0
	V	434, 131	$S^+X^-I^+$, S^0I^0
	Cr	163, 70	$S^+X^-I^+$, S^0I^0
	Mn	3332, 118	$S^+X^-I^+$, S^0I^0
	Mo	95, 199	$S^+X^-I^+$, S^0I^0
Echchahed et al.[57]	Fe	40	S^+I^- (MCM-48)
He et al.[58]	Fe	52	S^0I^0
Jones et al.[59]	Zr	25	S^+I^-
Zhang, Ying[60]	Nb	10	S^+I^-
Wong et al.[61]	Zr	5	$S^+X^-I^+$

[a] MCM-41 structure, unless otherwise noted. [b] Molar ratio values of precursor mixture, not of calcined materials.

Table 1 Reports of dopant incorporation in silicate M41S materials[8].

The great number of the studied systems has evidenced also that other mesoporous ordered oxides were found to be possible for such metals as Sb, Fe, Zn, Ob, W and Mo. However, most mesophases not yield porous materials and collapse when the template is removed.

The interest in doping MCM-41 with other metals meanly comes from the intention of conferring catalytic properties, but the amount of incorporation, the reproducibility and the shape of the mesophase and the stability of the obtained structure cannot be predicted.

The incorporation of dopant in the MCM-41 structure can be performed mainly through two ways: the direct incorporation during the MCM-41 formation or the insertion after the synthesis of the mesoporous material.

1. Mesoporous silica based materials

In general, the structure of MCM-41 can contain only a determined amount of metals; with higher amounts, the stability of the entire material is compromised. Moreover, the amount of incorporated metal depends also on the pH of the synthesis and the employed synthetic procedure[8].

The most common dopant for siliceous material is aluminium, having a tetrahedral coordination, as Si, and a Bronsted-type acidity. For these features, Al is easy to be incorporated in mesoporous silica.

Although a great knowledge has been achieved about microporous alumina-silicates materials (zeolites), is difficult to predict the effect of the Al insertion on the MCM-41 features[9,10].

There are also other examples of metal incorporated in MCM-41 structure, such as Ti, V, Cr, Na, or Cs. In particular, MCM-41 containing Ti, V and Cr is used for oxidation reactions with hydrogen peroxide, while Ti and V are also used in environment catalysis, for the decomposition on nitrogen oxides[4]. Na and Cs in MCM-41 are used in reactions requiring basic catalysts[4]. The catalytic activity of these hybrid systems can be limited by the loading capacity of the siliceous support. Indeed, it has been reported that for metals having a coordination different from the Si one, the metal molar loading should not exceed 2% [9]. The low metal loading that MCM-41 can bear without compromises its structure stability, is due also to the synthetic conditions. Indeed, the mesoporous support is usually obtained in strong basic conditions and in such environment the metal/Si exchange capacity is very limited. The metals which can be incorporated in MCM-41 with higher loading are Zr (17% mol) and Nb (10% mol)[11].

Although the insertion of metal in MCM-41 is not so easy, there is a huge amount of publications in this field, thanks to the great synthetic flexibility of these materials and the appreciable fine-tuning possibilities.

In industrial catalysis field, MCM-41 material find many applications. Concerning the acid catalysis, MCM-41 is used for cracking and hydrocracking reactions. For example, in the gasoline cracking process, the mesoporous features of MCM-41 based catalyst is fundamental. Moreover, the MCM-41 containing Pt and Al systems have shown high catalytic activity for the cracking of TIPB (1,3,5-triisopropylbenzene)[12, 13].

The MCM-41 based systems find applications in basic catalysis, if doped with Cs or V; but they are also used in environmental catalysis, when doped with Ti or V for the abatement of NO_x species[4].

In general, the M41S materials, find applications not only in the heterogeneous catalysis, but also in the field of separation and adsorption. For example, MCM-41 systems can be used for the adsorption of hydrocarbon from water media, or for gas storage and separation of pharmaceutical or biological compounds[4].

In conclusion, the mesoporous materials have brought a great innovation in the heterogeneous catalysis field, because they have interesting features. Indeed, besides the ordinated structure and the pore dimensions, their characteristics can be easily tuned changing synthetic parameters. Moreover, the templating agent seems to cover a fundamental role in determining the pore size. Finally, the fields of applications and the type of catalytic reactions grow thanks to the possibility to insert metals directly in the MCM-41 structure.

1.1.2 Proposed formation mechanism

Many different mechanisms of formation of MCM-41 structure during its synthesis have been proposed in literature; the most important are here reported.

<u>LCT mechanism</u>

The LCT (Liquid Crystal Templating) mechanism, firstly proposed by the Mobil Oil Company researchers, is based on two possible mechanistic pathways of synthesis[4, 8, 14](**Figure *3***).

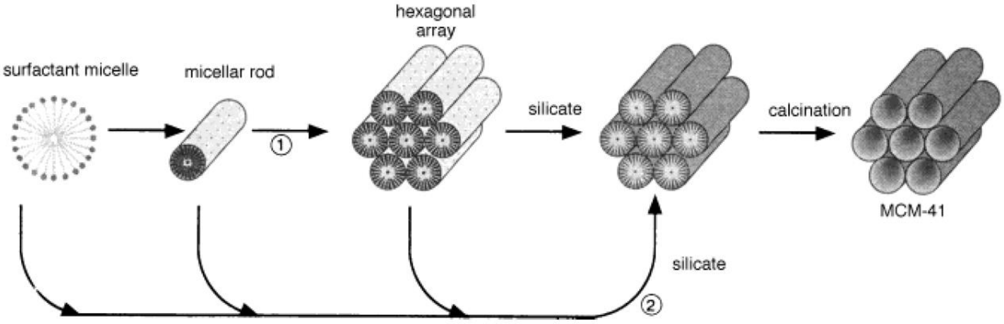

Figure 3 LCT mechanism proposed by the Mobil Oil Company researchers.

In the first one, the templating agent molecules organize themselves independently from the inorganic silicate crystallization; then the siliceous framework polymerizes around these previously formed hexagonal arrays composed by micellar rods. Consequently, in this case, the disposition of cylindrical micelles in a hexagonal arrangement took place spontaneously and then the silica precursor polymerized on the pre-formed structure.

In the second proposed mechanism, the inorganic precursors interact with the templating agent, favouring the formation of the hexagonal disposition. Taking into account the synthesis conditions in terms of pH (basic conditions), the organic template could be considered as a positive centre, interacting with the inorganic precursors, which finally condense into a solid. The obtained mesoporous material could be viewed as a continuous silica framework with encapsulated organic compunds[2]. The subsequent treatment for the template removal produced the typical MCM-41 opened mesopores.

Furthermore, as it is now known, the templating agent concentration, used for preparing the mesophase, following the method proposed by Beck et al., is far below to the critical micellar concentration (CMC) required for the formation of the hexagonal LC (liquid crystal), excluding the first proposed pathway[8].

Consequently, the second proposed mechanism seems to be the really followed one; in this case, the interaction between the silica precursor and the templating agent stabilizes the cylindrical micelles with a hexagonal arrangement below the necessary CMC.

The important aspect for this type of synthesis is that there are two CMCs: the first one is needed for the formation of spherical micelles, while the second one is higher and requested for the formation of cylindrical micelles. The presence of the silica precursor is enough to obtain cylindrical micelles with hexagonal disposition at the first CMC.

Silicate rod assembly

Davis and co-workers, carrying out 14N-NMR in situ study, have proposed that the formation of MCM-41, under the Mobil conditions, began with the deposition of multiple layer of silicate over the micellar rods. The final steps of hydrothermal treatment and aging favoured the complete condensation of the silica source, leading to the ordered MCM-41 phase, previously constituted of disordered silicate-encapsulated rods[15] (**Figure *4***).

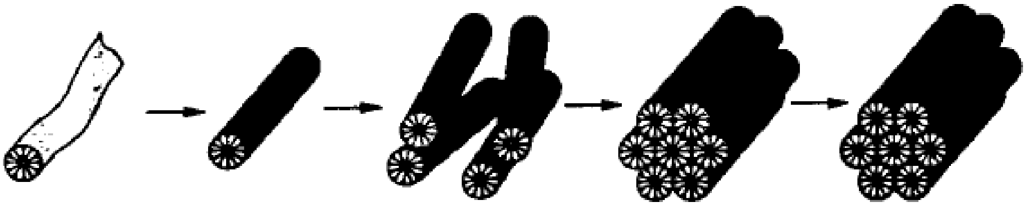

Figure 4 Silicate-encapsulated rods, ordered in the hexagonal array[8].

Silicate layer puckering

Steel et al.[16], realizing the same 14N-NMR study of the LC formation mechanism, postulated that the surfactant molecules assembled directly into the hexagonal LC phase upon the addition of the silicate species. The silicates were organized into layers, with rows of the cylindrical rods intercalated between the layers (**Figure 5**). Ageing the mixture caused the layers to packer and collapse around the rods, which then transformed into the surfactant-containing MCM-41 hexagonal-phase mesostructured.

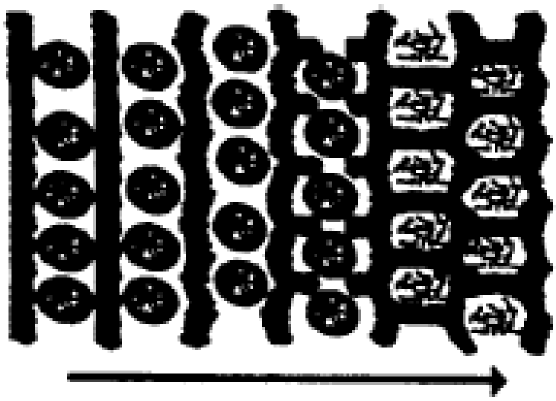

Figure 5 Puckering of silicate layers proposed by Steel at al.[16].

Charged density matching

This mechanistic model was proposed by Monnier et al.[17] and Stucky et al.[18] and suggested that MCM-41 could be derived from a lamellar phase. The initial phase of the synthesis mixture was layered and was formed from the electrostatic attraction between the anionic silicates and the cationic surfactant head groups (**Figure 6**). As the silicate began to condense, the charge density was reduced. Accompanying this process, curvature was introduced into layers to maintain the charged density balance among the surfactant head groups and the lamellar mesostructured became hexagonal.

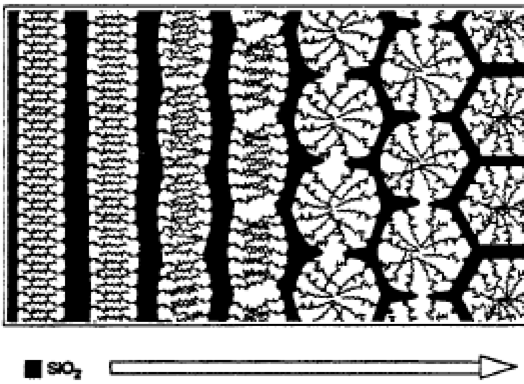

Figure 6 Charge density matching mechanism[8].

In general, the different proposed mechanisms of MCM-41 formation, reported above, consider the interaction between the silica precursors and the templating agent as electrostatic interactions. Taking into account this aspect, the different way of synthesis could be explained, basing them on the electrostatic interactions between the inorganic silica precursor (I) and the templating agent (S). In particular, the charged of I can be changed by varying the pH of the synthesis. At basic pH, the silica is over its isoelectric point and I is negatively charged; at acid pH, the silica is under its isoelectric point and I is positively charged.

So different combination are possible[8] (**Figure** *7*):

- Anionic silica precursor and cationic templating agent (I^-S^+);
- Cationic silica precursor and anionic templating agent (I^+S^-);
- Silica precursor and templating agent with the same charge and addition of a counter ion (X or M)

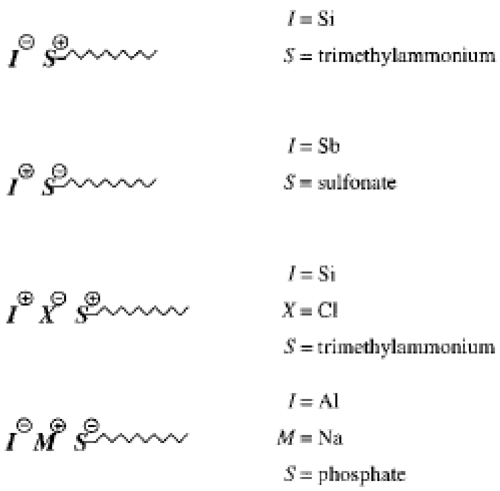

Figure 7 Different combination of silica precursors and templating agent through electrostatic interactions[8].

Hydrogen bonding interactions

Following the synthetic procedure proposed by Tanev and Pinnavia[19,20], which required the use of neutral templating agent, the charged density matching mechanism is no more valid. In this particular case, the templating agent and the silica precursor interact through hydrogen bonding; this type of interaction is weaker than the electrostatic one. Consequently, the templating agent removal can be performed through a simple solvent extraction. This neutral templating synthesis route produced mesoporous silicates with less long-range order of pores, granted by the electrostatic interactions, thicker walls and higher thermal stability compared to the LCT-derived silicates[21].

1.2 Hydrodechlorination (HDC) reaction and fluoropolymers

The hydrodechlorination (HDC) reaction consists in the removal of one or more Cl atoms from halogenated molecules through the use of hydrogen, which in some cases can substitute the removed atoms from the molecules. This process takes place through the interaction between a halogenated substrate and a hydrogen source and it leads to the formation of mixture of products, such as de-halogenated molecules (saturated or unsaturated), halogenated substrate and halogenated acid (HCl in the case of the selective removal of Cl).

In the last years, this process has been the subject of many studies regarding its possible application for CFC (chlorofluorocarbon) conversion in more useful products with lower environmental impact. The products that are usually achieved by these processes are HFC (hydrofluorocarbon) and unsaturated fluorocarbons. The former are not harmful to the ozone layer being completely dechlorinated (lack of radical initiator), while fluorinated olefins are used as monomers for the synthesis of highly technological fluoropolymers.

1.2.1 Fluoropolymers

Fluoropolymers are polymeric materials containing fluorine atoms in their chemical structures. From general organic polymer concepts, there are two types of fluoropolymers: perfluoropolymers and partially fluorinated polymers[22]. In the former case, all the hydrogen atoms, in the analogous hydrocarbon polymer, are replaced by fluorine atoms. In the latter case, there are both hydrogen and fluorine atoms in the polymer structures.

The development of the fluoropolymer industry began with the discovery of the polytetrafluorethylene (PTFE) by Dr. Plunkett at DuPont in 1938[22].

Since their discovery, fluorinated polymers are still in growing and providing new solution and possibilities to various areas such as energy, storage, optical data transmission and transformation, besides the well-known applications as coating, piping, membrane, wire and cable. Fluoropolymers possess excellent properties such as outstanding chemical resistance and stability, low coefficient of friction and low dielectric constant. The physical and chemical properties of this class of polymers come from the presence of fluorine. Firstly, fluorine atoms form the strongest bond among the single bonds involving carbon. The C-F bond has high ionic character and is strongly polarized by the most electronegative element, but has extremely low degree of polarizability. These evidences are directly connected to the weak intermolecular forces between fluorinated molecules responsible of the reduced cohesive energy of the materials.

Moreover, the presence of fluorine, with its high electronegativity and relatively small size, ensures the absence to steric problems, leading to a possible substitution of hydrogen in a molecule, and the chemical resistance, due to the protective shield of fluorine atoms over the carbon skeleton.

Besides fluoropolymers, fluorinated polymers with functional groups are of much more interest because they combine the merits of perfluorinated materials and functional groups. Such materials can be used as ion exchange resins membranes for fuel cells, gas separations membranes, solid polymeric superacid catalysts and polymeric reagents for various organic reactions and chemical sensors[23]. Of course, fully fluorinated materials are exceptionally inert and stable, but at the same time are less workable.

The introduction of partially or totally non-fluorinated co-monomers, on one hand, improves particularly the physic-mechanical properties of the final polymer, thanks to the interactions increased between C-F and C-H bonds and groups. On the other hand, the presence of C-H bond reduces some of the properties about chemical and thermal stability of the final material. For this reason, the development and formulation of various fluorinated polymers are strongly influenced by the purpose of use. For example, PTFE, since its development, was subjected to changes in order to create a more ductile material. The first studies were focused on the production of copolymers of TFE with lower crystallinity, such as the Teflon FEP, which is the copolymer composed by tetrafluorethylene and hexafluoropropylene monomers. This particular material is more ductile with respect to the pure Teflon, but it is less thermal resistant. With the aim to improve the thermal stability of the copolymers, the use of perfluorovinylethers as comonomers, has assumed more and more importance allowing to decrease the very high crystallinity of the fully fluorinated polymers and at the same time improving the thermal properties. Teflon PFA can be an example of this type of copolymers, being composed by tetrafluorethylene and perfluormethylvinylether as monomers.

1.2.2 HDC reaction

The hydrodechlorination (HDC) reaction is one of the most important CFC conversion method. These environmental harmful compounds, through the reaction with hydrogen, are converted mainly in HFC (when chlorine is replaced by hydrogen) or fluorinated unsaturated compounds (when chlorine is eliminated). This last type of compounds are monomers of a strong industrial interest for the production of highly technological fluoropolymers[24].

The selective removal of chlorine atoms against fluorine atoms is due to the weaker bond C-Cl with respect to the stronger C-F bond; consequently, the fluorine atoms are not involved in the HDC reaction, if not in negligible percentage. The values of the energy of C-F bond in CFCs ranging from 500 to 540 KJ/mol, while the values for the C-Cl bond in the same molecules are reported to be around 320 KJ/mol[25].

The hydrodechlorination reaction is generally carried out at temperatures between 200 and 300 °C, at atmospheric pressure, and allows to obtain mixture of compounds in which chlorine has been eliminated (unsaturated) or substituted by hydrogen[26]. The use of suitable catalyst leads to significant yields even at moderate temperatures and the choice of the active phase plays an important role in obtaining mixtures of mono- and poly-hydrogenated compounds. The best catalyst's active phase has been identified in metals of VIII transition group, which give the best activity and selectivity. In particular, Pd finds great applicability thanks to its Cl/H exchange high selectivity and to its good resistance to deactivation induced by acids produced during the reaction[27]. Other metals, such as Pt, Ni, Ru and Rh, showed interesting catalytic properties due to their ability in promoting adsorption of hydrogen for homolytic rupture of covalent bond[28]. Moreover bimetallic active phase gave very good results in this type of reaction; in particular, bimetallic Pd/Cu catalysts are used in hydrodechlorination reactions since the combination of both metals gives rise to catalysts capable of anchoring chlorinated reagents with a tailored hydrogenating activity[29]. Concerning the type of support, the mainly used ones are silica, active carbon and inorganic fluorides; they have to resist to HCl and HF released during the reaction.

The reaction mechanism can be divided into two steps: the first stage is the CFC molecule adsorption on the catalyst surface through C-Cl bond cleavage with the formation of metal-carbon and metal-chlorine bonds. Then these species react with the activated hydrogen chemisorbed on the active phase leading to hydrofluorocarbon and HCl formation. In the case of the formation of fluorinated unsaturated molecules, the mechanism provides an adsorption of CFC molecule through two carbon atoms. The desorption of the molecule of interest is no longer due to hydrogenolysis, but to a rearrangement of the substrate with the formation of a double bond. In this case, the hydrogen adsorbed has the only function of eliminating the halogen from the surface of the catalyst, forming the corresponding hydrogen halide[28].

Nowadays, the trifluoromethyltrifluorovinyl ether ($CF_3OCF=CF_2$) commercial production process is based on hydrodechlorination of $CF_3OCFClCF_2Cl$ precursor[30]. This reaction is performed in liquid phase using dimethylformamide as solvent and stoichiometric amount of Zn, producing large quantities of co-product as $ZnCl_2$ and exhausted solvent. This particular process is characterized by significant costs of waste disposal and purification of the solvent. With the aim of searching new solutions for a more sustainable process, this work deals with the design of a metal-supported catalyst for the gas-phase hydrodechlorination reaction for the production of $CF_3OCF=CF_2$ product which is an important monomer for the production of fluorinated polymers (**Figure *8***).

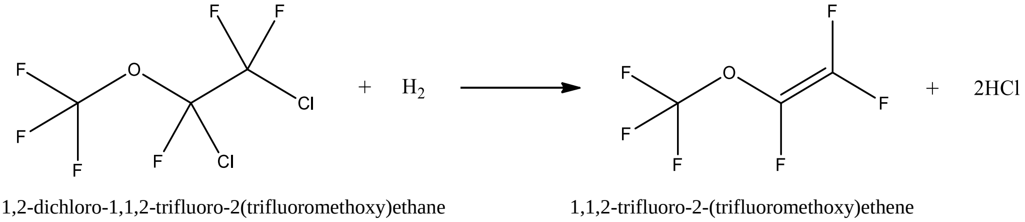

Figure 8 HDC reaction to the fluorinated monomer of interest.

In previous work[31], it has been demonstrated that PdCu active phase supported on active carbon can performed the HDC of the considered substrate with a high selectivity in the product of interest, but the microporous features of the support can restrict the possible application with larger molecules. In this way, the study of alternative catalysts with larger pores, such as mesoporous silica, can reach great interest.

1.3 Materials and methods

MCM-41 material was obtained through sol-gel synthesis, starting from sodium silicate as silica source and CTAB (cetyltrimethylammonium bromide) as templating agent, as proposed by Beck et al.[2]. The PdCu bimetallic phase was directly inserted during the synthesis of the support itself, starting from different precursor, chlorides and preformed nanoparticles. The choice to incorporate the active phase directly during the formation of the support came from previous works where impregnation of the support was studied[32]; this type of introduction of the active phase led to pore occlusion and segregation of the metallic species.

In this work, the procedure for the synthesis of MCM-41 support was also optimized in term of templating agent amount, in order to design a more sustainable synthetic process, also because the templating agent has to be removed to obtain the desired material. Moreover, the procedure for the templating agent removal was also changed with the aim to obtain, on the final catalyst, an active phase with better characteristic in terms of distribution on the support and particles size.

1.3.1 MCM-41 synthesis

The MCM-41 synthetic procedure was composed by different steps; it started from the solubilisation of the templating agent, followed by the addition of the silica source. Then the pH of the synthetic mixture was adjusted near 10.5 value with H_2SO_4, for preventing the formation of a less ordinated structure due to a fast condensation of the silica. The composition of the sol-gel was: 1.0 SiO_2:0.55 CTAB:0.14 H_2SO_4:73H_2O for the “classic” synthetic route. The material obtained through this procedure was then hydrothermally treated at 125°C for 7 h in a Milestone StartSYNTH microwave oven, filtered, washed, and dried. Finally, the templating agent was removed at 540°C for 6 h in static air. The final material was labelled as M1.

During the work, the M1 synthetic route was optimized decreasing the amount of the templating agent needed for the formation of the typical hexagonal structure and using an alternative method for its removal. In particular, the templating agent amount was divided in half, without changing the other synthetic parameter and steps. As a consequence, the composition of the sol-gel obtained with the optimized route was: 1.0 SiO_2:0.275 CTAB:0.14 H_2SO_4:73H_2O. The material was then hydrothermally treated at 125°C for 3 h in a Milestone StartSYNTH microwave oven, filtered, washed, and dried. Finally, the templating agent was removed through calcination at 540°C (M1) and an ionic exchange using ammonium nitrate at 60°C in ethanol, as reported by Lang et al.[33], obtaining the final material labelled as M2. The original procedure for the ionic exchanged was optimized for a less ethanol consumption; in particular, the amount of ethanol was divided in half and the exchange was performed on the same solid for two times and not for three time, as initially proposed by Lang et al.. Anyway, the molar ratio between ammonium nitrate and CTAB was 2, the same as the original procedure.

All the steps and the differences between the synthetic procedures are summarized in **Figure** *9*.

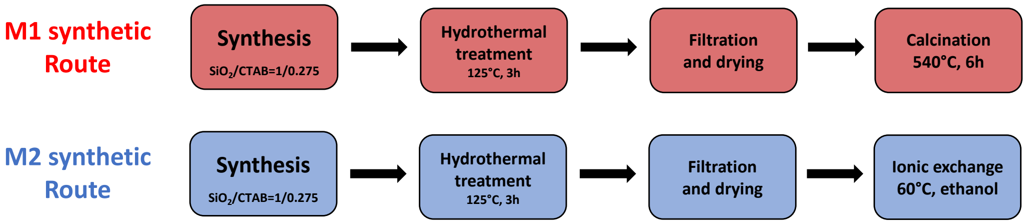

Figure 9 Different steps for the M1 and M2 synthetic routes.

1.3.2 PdCu/MCM-41 synthesis

The bimetallic active phase, composed by palladium and copper with a molar ratio of 1:1 and total amount of 2.4% wt, was supported on MCM-41 by the addition of metallic precursors directly during the synthesis of the support, in the form of chlorides and preformed nanoparticles, following the M1 and M2 optimized routes.

In the case of metallic chlorides ($PdCl_2$ and $CuCl_2 \cdot 2H_2O$), the precursors were dissolved in an acidic solution and then added to the CTAB solution. Before adding the sodium silicate, the pH of the solution composed by CTAB and metallic chlorides was adjusted at 6.80 with NaOH. Then the synthesis proceeded as reported before for the MCM-41 alone. In particular, on the dried solid the two type of templating agent removal, calcination at 540°C (M1) and ionic exchange at 60°C (M2), were performed. After the templating agent removal and before the catalytic tests in the HDC reaction, the catalysts both from M1 and M2 procedures, were reduced in flow of H_2 at 320°C for 3 h with the aim to obtain the active phase in the fundamental oxidation state.

In the case of bimetallic preformed nanoparticles, in the suspension of preformed nanoparticles was added and dissolved CTAB. Then the synthetic procedure was maintained the same as in the case of the other precursors. Also in this case, the dried solid was treated in two ways for the removal of the templating agent (M1 and M2). In particular, after the removal of templating agent through the ionic exchange (M2), a calcination treatment at 250°C was needed to remove the stabilizing agent of the nanoparticles (PVP).

The PdCu bimetallic nanoparticles were synthesized following the procedure reported elsewhere[32,34], starting from $PdCl_2$ and $CuSO_4 \cdot 5H_2O$, as metallic precursors, using polyvinylpyrrolidone (PVP) as stabilizing agent and water as solvent; moreover, glucose was employed as a mild, renewable and non-toxic reducing agent.

Finally, before the catalytic tests, the catalysts obtained from preformed nanoparticles were not reduced because the obtained nanoparticles showed already the reduced metals. Although, after many hours of reactivity, these catalysts were reduced directly in the plant in the same conditions as reported before.

In **Figure *10*** the different synthetic routes M1 and M2, followed for the preparation of the final catalysts are represented with the respectively metallic precursors.

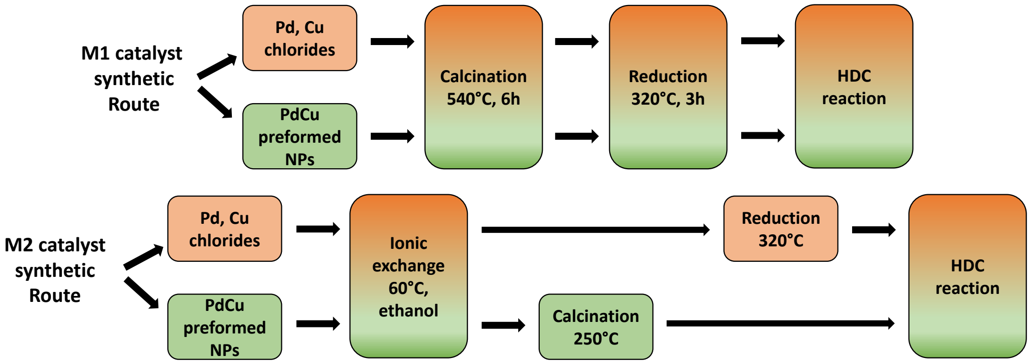

Figure 10 Different preparation routes for PdCu/MCM-41 catalysts.

In **Table *2*** the prepared catalysts obtained with several synthetic procedures and starting from different metallic precursors are reported with the main characteristics.

Sample name	**Metallic precursors**	**CTAB removal procedure**
M1	-	Calcination at 540°C
PdCu-M1	Chlorides	Calcination at 540°C
NPsPdCu-M1	Bimetallic preformed nanoparticles	Calcination at 540°C
M2	-	Ionic exchange at 60°C
PdCu-M2	Chlorides	Ionic exchange at 60°C
NPsPdCu-M2	Bimetallic preformed nanoparticles	Ionic exchange at 60°C

Table 2 Support and catalysts synthesized with different procedure and metallic precursors.

1.3.3 Characterization methods

Many different characterization techniques were employed on the support alone, the fresh catalysts and the used ones with the aim to follow the evolution of the catalysts features from the synthesis to the catalytic tests.

X-ray diffraction analysis

Powder X-ray diffraction analysis (XRPD) were used for investigate the evolution of the active phase and for acquire morphological information about MCMC-41 support.

Bragg’s law provides a relation between diffraction angle and the spacing of the crystalline planes, like a fingerprint for crystalline phases.

$$n\lambda=2d\mathrm{sen}\Theta$$

where:

n=diffraction order

λ=wavelength of the incident beam d=spacing of crystalline planes

ϴ=incident radiation angle

The XRPD analysis on the catalysts were carried out in a Bragg-Brentano geometry based diffractometer (Philips PW1710) using a Ni-filtered CuKα radiation (λ=1.5418Å) at 40mA and 40kV. The diffraction patterns were collected with a step size of 0.1° and time for step of 10 seconds. The angle range were different depending on the desired information; in particular, low angle range (1.6-15°2ϴ) was used for investigate the presence of the hexagonal phase in the MCM-41 support, and the medium angle (25-50°2ϴ), for searching information about the active phase and the size of the metallic crystallites.

The XRPD analysis were also performed also on the nanoparticles suspensions, using a different instrument (Bragg-Brentano X'PertPro Panalytical) in 39-45°2ϴ range, with a step size of 0.01° and time for step of 1500 seconds.

The size of metallic crystallites (D) was derived from the Scherrer equation:

$$D=K\lambda/\beta\cos\Theta$$

where:

K=0.9

λ=wavelength of the incident beam

ϴ=incident radiation angle

$\beta=(B^2-b^2)^{1/2}$ with B=FWHM and $b=3.49*10^{-3}$ rad

Nitrogen adsorption analysis

A typical adsorption/desorption measurement versus relative pressure p/p^0 over a solid provides several information about the morphological properties of the samples.

Through this kind of analysis are obtained isotherms of adsorption and desorption from which is possible to understand the type of porosity of the analysed material. The isotherms are elaborated with specific mathematic models to obtain information about morphology and surface properties of the sample. In particular, for the pores size and its distribution, DFT (Density Functional Theory) model was employed, while the specific surface area values were obtained by multi-point BET equation in the 0.05–0.2 p/p^0 range and total pore volume values were calculated at 0.995 p/p^0. The mesopore size distribution was calculated through the NLDFT-statistic method.

N_2 adsorption/desorption isotherms (-196°C) were performed in a Micromeritics ASAP 2020 instrument on the samples after the template removal. Samples were previously outgassed for 30 minutes at 150°C and 30 µmHg and then heated for 120 minutes at 350°C.

Transmission electron microscope analysis

Transmission electron microscope (TEM) analysis could provide information about particle distribution, composition, dimension and shape, through the interaction between the sample and an electrons beam.

The TEM analysis were performed on the nanoparticles suspension and on the supported catalysts, with the aim to understand the morphology of the mesoporous MCM-41 support, the distribution and dimension of the metallic particles and their composition which was investigated through the EDS probe.

The analysis were performed with TEM/STEM FEI TECNAI F20 operating at 200 kV; the samples were prepared by dispersion in ethanol and deposition in holey-carbon film supported with a titanium grid.

Dynamic light scattering analysis

The bimetallic nanoparticles were characterized through the Dynamic Light Scattering (DLS) analysis for determining the hydrodynamic radius of the nanoparticles in the suspension. This technique is based on the scattering of a laser beam caused by the presence of the nanoparticles in the suspension. The intensity of the diffused beam depends on the nanoparticles size. The hydrodynamic radius involved not only the metallic particles but also the species coordinated with them, as PVP.

The analysis were performed with a Zetasizer Nanoseries Malvern instrument with a laser source of 663 nm. The NIBS (Non Invasive Back Scattered) detector was placed at 173° with respect to the incident beam.

1. Mesoporous silica based materials

The nanoparticles suspensions were diluted adding 1-2 drops in 1 ml of water; then the solution was placed in a cuvette. The refraction index of the metals particles were: $R.I_{Pd}=1.77$, $R.I_{Cu}=0.583$ and $R.I_{PdCu}=1.328$.

Thermogravimetric analysis

The thermogravimetric analysis (TGA) follows the variation of the sample mass in function of the temperature. The weight loss can be due to different phenomena, as evolution of adsorbed compounds or decomposition of the sample itself. Through this type of analysis, only events which cause a variation of the sample mass, are detected while phase transition cannot be revealed.

The analysis were performed with TA Instrument Q600 under an air flow, from RT to 540°C at 10°C/min. The sample amount was around 8-10 mg. The analysis were performed on the dried samples, to follow the decomposition of the templating agent, and on the samples after the template removal, to investigate the efficiency of the treatment.

Infrared spectroscopy analysis

The infrared spectroscopy is based on the interaction between the matter and infrared radiation, which is referred to a determined region of the electromagnetic spectra, comprised between 4000 and 400 cm^{-1}. When an infrared radiation interacts with a molecule, it can cause different types of vibration, such as stretching and bending.

The energy necessary for provoking the vibrations depends on the bond energy and atoms mass. The infrared spectroscopy provides information about the bond strength and molecule geometry, from which the type of functional groups can be recognized.

The infrared spectroscopy was employed to detect the presence of the templating agent on the catalyst after its removal.

The analysis were performed with a FTIR Perkin Elmer ONE in a range of 400 to 4000 cm^{-1} and with a resolution of 2 cm^{-1}. The solid samples were mixed with KBr (1g of KBr and 5 mg of sample) and pressed using a pressure of 10 ton/cm^2.

Another characterization employed for the detection of the presence of the templating agent was ATR-IR. This technique is based on the Attenuated Total Reflection (ATR) and exploits the evanescent wave generated by the total reflection of the IR radiation and transmitted through a diamond crystal in contact with the sample. Indeed this characterization method deals with the infrared radiation and provides information similar to the one get from FT-IR analysis. The advantage of ATR-IR analysis is that the sample can be analysed as it is, placing it on the diamond crystal, without mixing and pressing it with KBr.

The analysis were performed with IR Brucker Alpha platinum ATR instrument on the solid sample between 400 and 4000 cm^{-1}.

Temperature programmed reduction

The Temperature Programmed Reduction (TPR) analysis is useful to understand characteristics of the active phase, such interaction between metals, their particle sizes and distribution. The sample, placed in a fixed bed reactor in an oven, is pre-treated in an inert gas to eliminate contaminants and water. Then the sample is reduce in H_2 flow with increasing temperature and the H_2 consuming is detected usually by a thermal conductivity detector (TCD).

The TPR analysis were performed on the catalysts before the reduction steps, in order to have information about the oxidation state of the metals and their interaction with each other and with the support.

The TPR analysis were performed on a TPD/R/O 1100 Catalytic Surface Analyzer ThermoQuest equipped with a TCD. Moreover, the pre-treatment was performed with 20 ml/min of He from RT to 120 °C, reached with 20°C/min ramp and maintained for 30 minutes. Then the reduction began from 60 °C with 20 ml/min of H_2 (5% H_2 in Ar) to 550°C, reached with 10 °C/min ramp and maintained for 30 minutes.

1.3.4 Catalytic tests in HDC reaction

The PdCu/MCM-41 catalysts were tested in the hydrodechlorination (HDC) reaction of $CF_3OCFClCF_2Cl$ (AM) to $CF_3OCF=CF_2$ (MVE) in a laboratory scale plant. Before the catalytic tests, the chlorides derived catalyst and NpsPdCu-M1 were reduced in H_2 flow for 3 hours at 330°C, reached with 10°C/min ramp. 2.7g of catalysts were loaded in a tubular Hastelloy steel down-flow reactor with a 60-80 mesh. The reaction mixture was composed by 20 ml/min of N_2, 7 ml/min of H_2 and 5.6 ml/min of AM. The contact time was around 10 seconds and the reaction temperature was 250°C. The gas flow coming out from the reactor, was purified from HCl and HF acids with an aqueous scrubber and the stripped water was adsorbed through a $CaSO_4$ trap, before reaching the analysis system. The products and not converted reagent were analysed with a gas chromatographer equipped with a TCD and a DVB Varian CP-Porabond Q column, following this method:

- 40°C, 3 minutes,
- 175°C, reached with a 10°C/min ramp,
- 250°C, reached with a 20°C/min ramp,
- 250°C, 9 minutes.

1.4 Results and discussion

The aim of this work was to search and study different synthetic strategies for the preparation of PdCu catalysts supported on mesoporous siliceous materials.

The optimization of the synthetic route involved many changes in the different steps of the catalyst preparation and the effect of the preparation methods on the catalytic properties in hydrodechlorination of $CF_3OCFClCF_2Cl$ (AM) to $CF_3OCF=CF_2$ (MVE) was studied.

Bimetallic Pd/Cu species supported on several materials, such as Al_2O_3, SiO_2 and active carbon, have been reported to be active catalysts in the hydrodechlorination of chlorofluoro- and chloro-carbons [35, 36, 37]. Palladium has a high hydrogenating activity, due to its ability to dissociate H_2, and fully hydrogenated compounds are obtained [38]. The presence of copper decreases the hydrogenating activity of noble metal and increases, therefore, the olefin selectivity [37]. The role of copper in bimetallic Pd/Cu and Pt/Cu catalysts has been studied by several authors. Copper can anchor chlorofluorinated reagents but is less active in mild reaction conditions and can deactivate at a relative high temperature during time-on-stream [39]. Moreover, it was reported to change the electronic properties of the noble metal [35] or just have a geometric effect, namely copper dilutes the noble metal ensembles [39]. Whatever the role of copper is, the adsorption and activation for reactants is modulated, enabling the progress of the dechlorination reaction. The properties can be modulated by the dispersion of metallic particles, the Pd/Cu ratio and the support. However, the control of the synthesis procedure is essential to determine the Pd–Cu interaction and therefore its activity.

It has already been demonstrated that Pd/Cu on carbon are optimal catalysts for the hydrogen assisted gas phase dechlorination of AM to produce MVE [40]. Nevertheless, the microporous texture of the activated carbon support can significantly limit possible applications of this catalytic system, because of reduced mass transfer. Supports with larger pores can overcome the drawbacks; in particular, MCM-41 silicate mesoporous materials can be used as alternative. SiO_2 has been used as support for hydrodechlorination processes[28] since it seems to be suitable in terms of inertness against HCl [35]. MCM-41 materials, constituted by a hexagonal arrangement of silica mesopores, display higher surface area than conventional SiO_2 and appreciable resistance to strong acids, hence, they could be an interesting alternative to conventional supports. The inclusion of monometallic Pd or Cu active species on MCM-41 structure can be performed by impregnation, ion-exchange, anchoring or direct inclusion of the ions of the metal into the MCM-41 framework. The synthesis, metal loading, metallic precursors, template removal procedure determine the location of active species (within or extra-framework)[41].

In our recent work [29, 32], we observed that the synthetic procedure, impregnation or incorporation of Pd and Cu active species during the MCM-41 synthesis, as well as the nature of the silica source (sodium silicate or TEOS), modified the composition and size distribution of metallic particles and therefore the catalytic activity. In particular, incorporation of Pd and Cu in the course of MCM-41 synthesis, due to the calcination for the removal of the template provoked the segregation of oxides and large Pd/Cu bimetallic particles were obtained after reduction. The Pd/Cu-MCM-41 preparation by impregnation led to pore-occlusion, and after reduction, both isolated monometallic Cu particles and large bimetallic Pd/Cu particles were present on the external surface of the support.

Accordingly, hereby a deep study was performed to optimized the synthesis of MCM-41 support in terms of reagent amount employed and to control the composition and particle size of the Pd/Cu species. Firstly, the amount of the templating agent and the time of hydrothermal treatment were reduced in order to have a less reagent and time consuming synthesis, maintaining the typical hexagonal features of MCM-41. Then the research work was focused on the PdCu/MCM-41 catalysts which were obtained by incorporation of Pd and Cu during the synthesis of MCM-41. The control of Pd and Cu particles size and composition was of great importance; consequently, to avoid the segregation of the oxides during template removal the ionic exchange was used rather than calcination. Furthermore, bimetallic species were introduced as preformed Pd/Cu nanoparticles into the MCM-41 structure to control the composition of the active phase.

During the PhD period, many catalysts were prepared, characterized and tested in the reaction of interest; the most significant are reported in **Table *3***.

Sample name	**Metallic precursors**	**CTAB removal procedure**
M1	-	Calcination at 540°C
PdCu-M1	Chlorides	Calcination at 540°C
NPsPdCu-M1	Bimetallic preformed nanoparticles	Calcination at 540°C
M2	-	Ionic exchange at 60°C
PdCu-M2	Chlorides	Ionic exchange at 60°C
NPsPdCu-M2	Bimetallic preformed nanoparticles	Ionic exchange at 60°C

Table 3 Most significant catalysts prepared during the PhD period.

1.4.1 Optimization of the MCM-41 synthetic route

The MCM-41 synthesis is composed by two main parts: the first one consists in the condensation of the siliceous precursor, while the second one is made up of many treatments done for the formation and stabilization of the hexagonal phase characteristic of the desired material.

The obtained materials were subjected to X-ray diffraction (XRD) and porosimetric analysis to discover the morphological features and structural characteristics derived from different synthetic routes. The mainly difference between M1 and M2 route is represents by the template removal method: calcination at 540°C for M1 route and ionic exchange at 60°C for M2 route.

In **Figure *11*** the typical XRD pattern of MCM-41 is reported and the signals typical of the hexagonal phase can be observed.

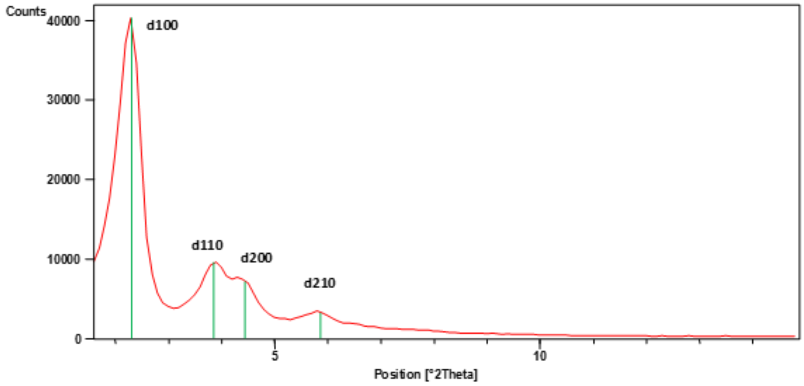

Figure 11 XRD patter typical of MCM-41 material.

The d(100) peak represents the space between the planes parallel to the channels section, as showed in ***Figure 12.*** This parameter is useful for evaluate the cell parameter a_0 which represents the distance between the centre of two adjacent pores.

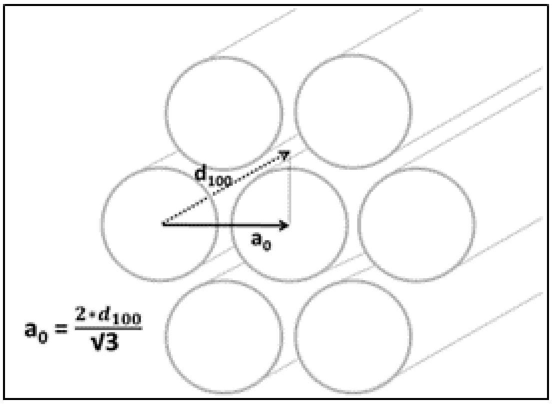

Figure 12 d(100) and a_0 parameters and their correlation.

The porosimetric analysis on the MCM-41 obtained through the M1 route revealed that the prepared material is highly mesoporous with a high surface area, as reported in **Table *4***.

Sample	Surface area (m^2/g)	Mesopores surface area (m^2/g)	Pore diameter (Å)	Mesopores diameter (Å)
M1	1109	639	44	46

Table 4 Porosimetric data of MCM-41 supports obtained from M1 synthetic routes.

In addition, the isotherm displayed in **Figure *13*** showed the characteristic features of Type IV isotherms of MCM-41 materials and a narrow pore sizes distribution.

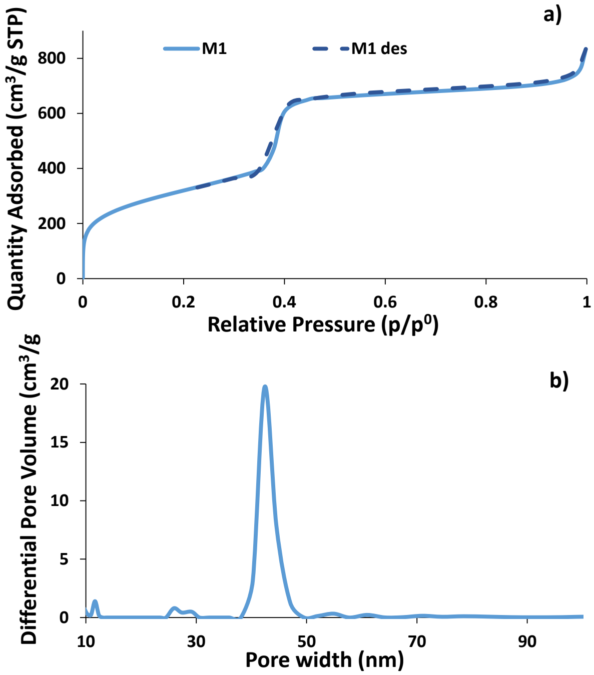

Figure 13 a) N_2 Adsorption-desorption isotherms of M1 sample. b) DFT pore size distribution of M1 sample.

With the aim to optimize the synthetic procedure in terms of time and reagents amount, the influence due to the change of some parameters was investigated.

First of all, the effect of the time of the hydrothermal treatment, essential for the formation of the desired structure, on the MCM-41 features was investigated. In particular, the hydrothermal treatment in the not modified synthesis was performed at 125°C in microwave oven for 7 hours. The same treatment was performed in the same conditions, but for 3 and 1 hours, trying to verify if the material could be treated for less than 7 hours. In **Figure *14***, the diffraction patterns of the calcined samples after being hydrothermally treated for different time are displayed.

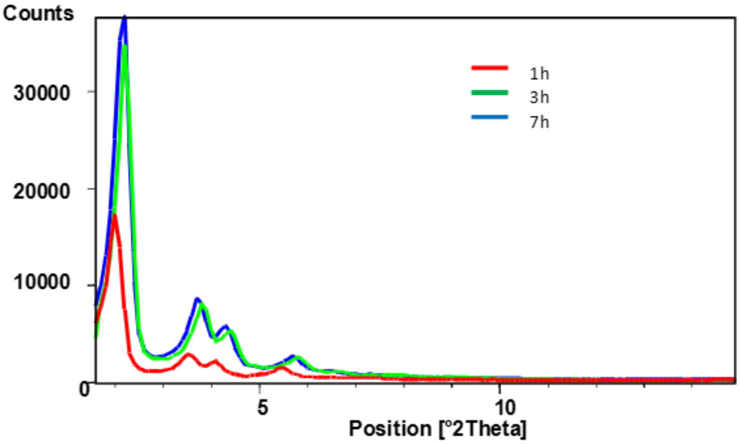

Figure 14 XRD patterns of the MCM-41 samples hydrothermally treated for different time.

The order degree of the MCM-41 structure can be evaluated from the intensity of the main peaks, the d(100). From the reported patterns, the typical peaks of MCM-41 appeared already after 1 hours of microwave treatment and they became more intense with increasing the time of the treatment. Comparing the XRD patterns related to the 7 and 3 hours hydrothermally treated samples, it was decided to perform the hydrothermal treatment for 3 hours, because the two samples showed the same order degree and crystallinity. In this way the synthetic procedure became less time consuming.

The step following the hydrothermal treatment was the removal of the templating agent, necessary to obtain the desired porosity. Usually, this step was performed through calcination at 540°C, temperature chosen on the base of the TG analysis made on the dried sample and reported in **Figure *15***.

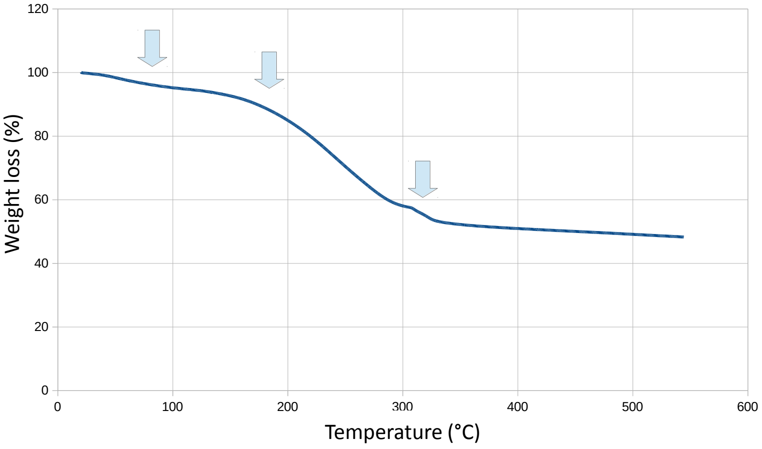

Figure 15 TGA results of the dried material obtained from M1 route.

From the TG analysis, it can be deduced that the decomposition of the templating agent was completed at near 500°C. In this figure, three main weight losses are indicated. In particular, at 100°C the sample lost the water and moisture adsorbed on its surface; then, from 160 to 290°C, the most important weight loss corresponds to the degradation of the templating agent. Finally, near 300°C, carbonaceous residuals were removed.

The complete removal of the templating agent was also proved by the comparison of the FT-IR spectra of the dried and the calcined samples, as showed in **Figure *16***.

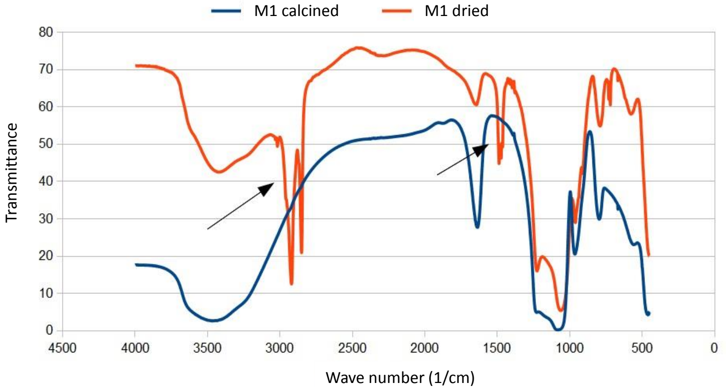

Figure 16 FT-IR spectra of MCM-41 dried and calcined at 540°C from M1 route.

In this figure, the bands related to the presence of the templating agent are indicated, and after the calcination, they disappeared. In particular, the bands characteristic of the templating agent are located at near 2900 cm^{-1} (C-H stretching) and 1450 cm^{-1} (C-H bending), both related to the aliphatic chain of CTAB. The other bands are due to the siliceous matrix of the samples and they are not considered for the evaluation of the effectiveness of the calcination.

From these analyses, it can be concluded that the template removal is already completed at 540°C, temperature at which the calcination has been performed. Nevertheless, the removal process is very delicate because during the calcination the support, generated by the template micelles, of the siliceous framework is removed, causing possible collapse and loss of porosity. With the aim to avoid this phenomenon and optimize the synthesis, the CTAB amount used during the MCM-41 synthesis was decreased searching the minimum amount of CTAB, which ensured the formation of the desired structure. It was decided to cut in half the original CTAB amount suggested by Beck et al.[2], passing from CTAB/Si=0.55 to 0.275 molar ratio.

In **Figure *17***, the comparison of the XRD patterns obtained from MCM-41 prepared with different CTAB amount and then calcined is reported.

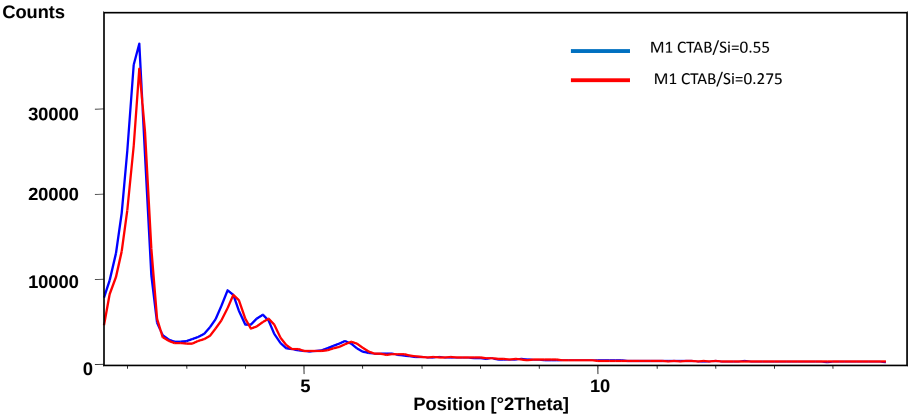

Figure 17 XRD patterns obtained from MCM-41 prepared with different CTAB amount.

From this comparison is clear that using less CTAB the desired hexagonal structure can be obtained with the same order degree and crystallinity of the material prepared with more CTAB. For the synthesis of these systems, the templating agent amount suggested by Beck can be damaging because the material with more organic loading will have a bigger weight loss, increasing the possibility of structural collapse.

Always with the aim to decrease the negative impact of the template removal on the MCM-41 structure, an alternative procedure was studied (M2 route). In particular, this new method for the template removal consisted in an ionic exchange and not in a thermal treatment, as in the case of calcination. This procedure was performed employing ammonium nitrate in ethanol at 60°C and, during the exchange, the ammonium ion substitutes CTAB$^+$ ion, removing the template, which was dissolved in the ethanol solution. The ionic exchange was performed on the dried material for three times, in the case of the MCM-41 prepared with the original CTAB amount, and for two times in the case of the optimized synthesis. During the ionic exchange, the degree of the template removal was followed by ATR analysis on the treated samples after each exchange. The comparison of the ATR spectra during the template removal from MCM-41 obtained from the optimized route is showed in **Figure *18*** with the spectra related to CTAB.

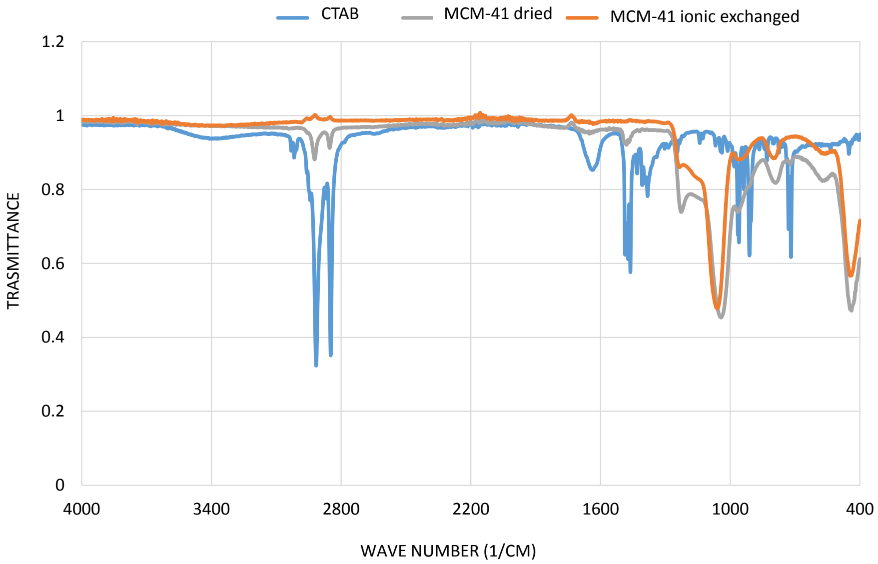

Figure 18 ATR spectra related to CTAB, MCM-41 dried and subjected to ionic exchange.

From this comparison it can be deduced that also through the ionic exchange, even if it was not a thermal treatment, the templating agent could be removed with a high efficiency. This fact can be confirmed by the TG analysis performed on the ionic exchanged sample and compared to the dried and the calcined materials (**Figure *19***).

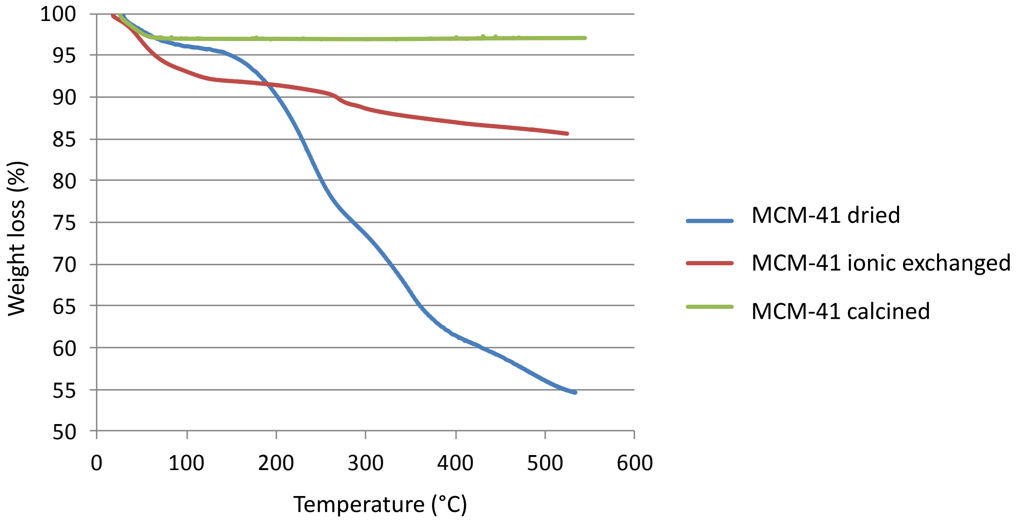

Figure 19 TG analysis related to MCM-41 samples dried, calcined and ionic exchanged.

The thermogravimetric analysis on the ionic exchanged sample revealed a weight loss in the range between 200 and 400 °C, which was not so different from the one observed for the calcined sample (more or less 10% of difference).

Moreover, through the porosimetric data was possible to understand if there were some differences due to the template removal method (**Table *5***).

Sample	**Surface area (m^2/g)**	**Mesopores surface area (m^2/g)**	**Pore diameter (Å)**	**Mesopores diameter (Å)**
M1	1109	639	44	46
M2	872	538	49	45

Table 5 Porosimetric data of MCM-41 supports obtained from different synthetic routes.

The M2 sample showed a slightly lower surface area respect to M1 sample; this was probably due to the presence of residual templating agent.

Also the comparison between the N_2 adsorption/desorption isotherms of the materials prepared following M1 and M2 synthetic route, can be useful to understand possible difference due to the different template removal procedure (**Figure *20***).

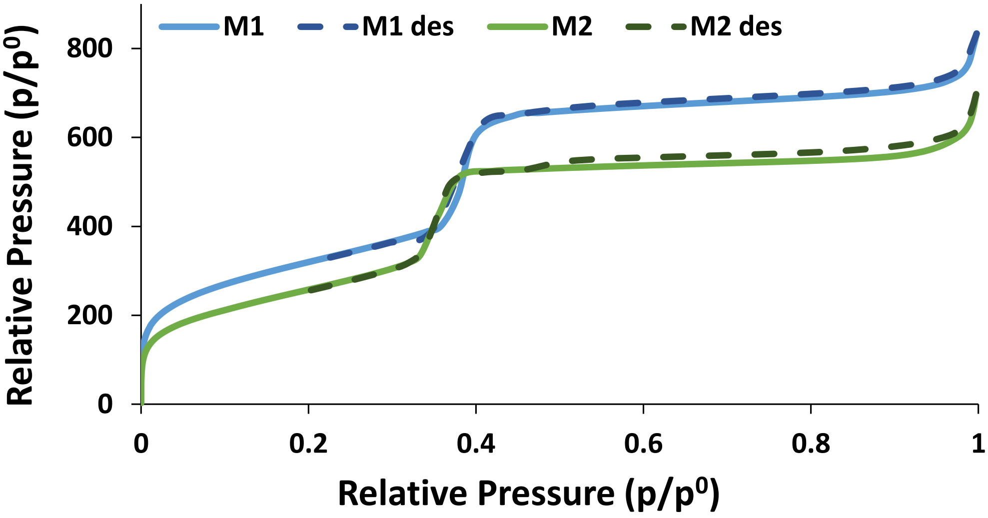

Figure 20 Adsorption-desorption isotherms of M1 and M2 samples.

The displayed isotherms, regardless of the treatment to remove the templating agent, showed the characteristics features of Type IV isotherms of MCM-41 materials. The differences in the quantity of N_2 adsorbed and the height of the capillary condensation step indicated that specific surface area depended on the synthesis procedure. Indeed, samples submitted to thermal treatment to remove the template showed high surface area with respect to the ionic exchanged one. This feature suggested that probably the M2 sample had a lower order degree.

Moreover, the XRD patterns of the samples obtained from M1 and M2 route through the optimized synthesis are compared in **Figure *21***.

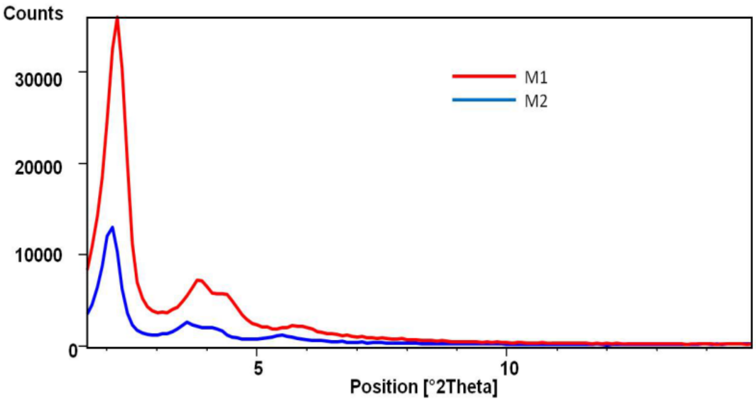

Figure 21 XRD patterns of the MCM-41 samples obtained from M1 and M2 routes.

From this analysis, it can be deduced that even through the ionic exchange was possible to obtain the structure typical of MCM-41. Nevertheless, the peaks were less intense with respect to the calcined sample, suggesting a lower crystallinity degree.

In conclusion, through this work of optimization of the synthetic route, it was possible to use less CTAB and find an alternative and efficient template removal method. For all the catalyst PdCu/MCM-41 prepared and studied during the PhD period, the procedure followed was the optimized one; in particular, 3 hours of hydrothermal treatment, less CTAB and two ionic exchange treatment for the M2 route.

1.4.2 PdCu/MCM-41 catalysts from chloride

Initially, the Pd and Cu precursors used for the catalysts preparation were their respective chlorides ($PdCl_2$ and $CuCl_2 \cdot 2H_2O$) added directly during the synthesis of the MCM-41 support and, in particular, before the silica precursor condensation.

First of all, the effect of the insertion of the metals in the siliceous framework on the MCM-41 structure was studied. The XRD patterns of the pure MCM-41 and PdCu/MCM-41 samples prepared through M1 route are showed in **Figure** *22*.

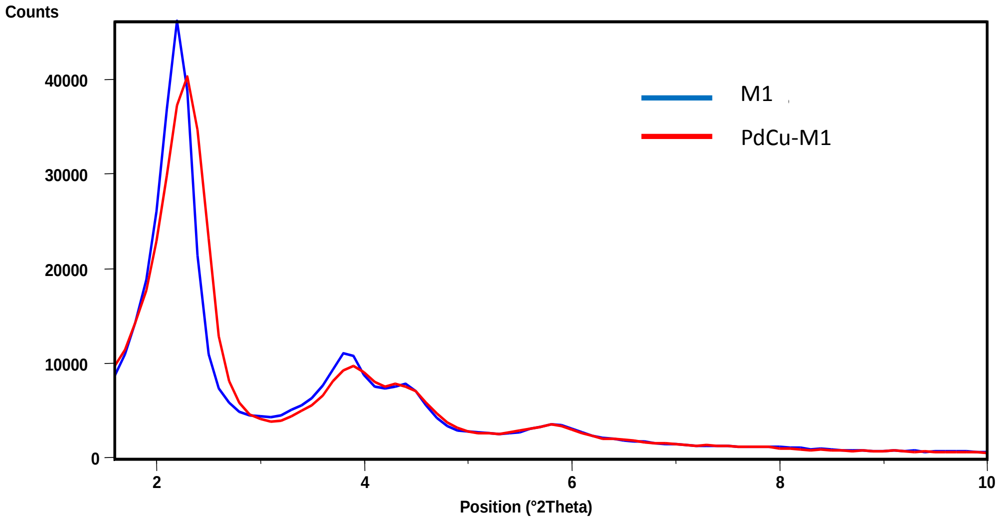

Figure 22 XRD patterns of support alone (M1) and catalyst obtained from chloride (PdCu-M1).

1. Mesoporous silica based materials

The insertion of the metals in the siliceous framework did not affect the structural features of the MCM-41, as demonstrated by the XRD patterns where the typical peaks of the hexagonal structure were present also in the case of the PdCu catalyst.

This behaviour is confirmed also from the porosimetric data, reported in **Table *6***, where the morphological features were not modified by the insertion of the metals.

Sample	**Surface area (m^2/g)**	**Mesopores surface area (m^2/g)**	**Pore diameter (Å)**	**Mesopores diameter (Å)**
M1	1109	639	44	46
PdCu-M1	1097	656	49	40

Table 6 Porosimetric data of MCM-41 supports and PdCu/MCM-41 catalyst obtained from route M1.

Moreover, the XRD analysis performed at wide angle was useful to discover the characteristics of the metallic active phase and to follow its evolution during the different synthetic steps.

First of all the evolution of the active phase was studied on the PdCu-M1 sample and the XRD patterns obtained are reported in ***Figure 23***, in comparison with the monometallic catalysts (Pd-M1 and Cu-M1 both reduced).

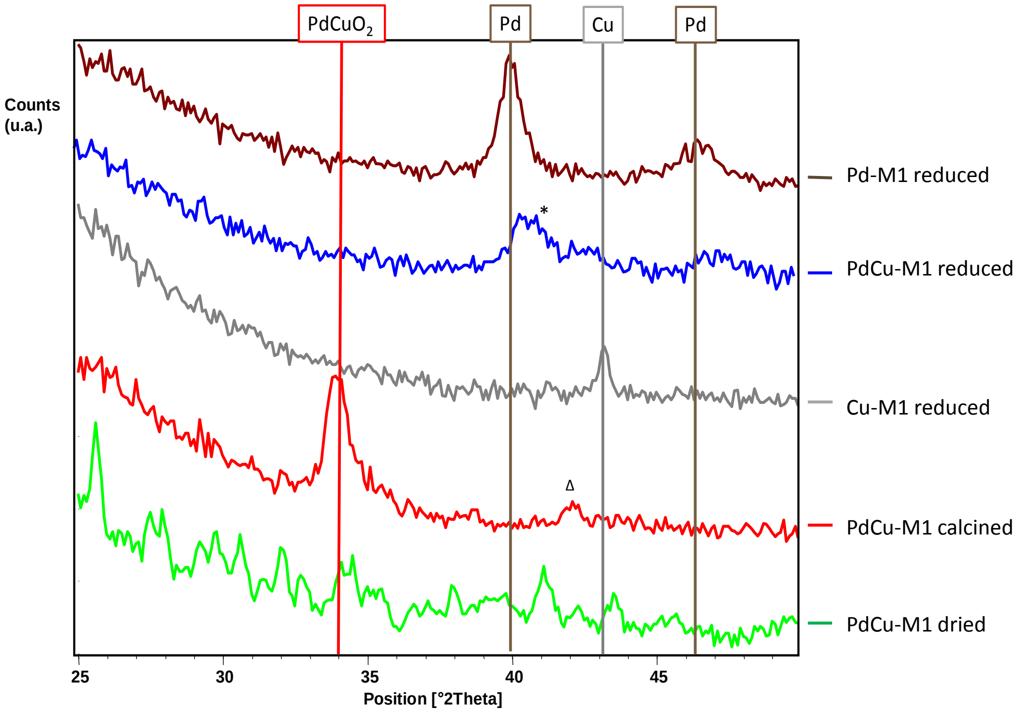

Figure 23 XRD patterns of PdCu-M1 catalyst acquired after each synthetic steps and compared with monometallic catalyst. Δ PdO phase (Reference Code 00-002-1432). * PdCu phase (00-048-1551).

The PdCu-M1 catalysts showed the presence of different phases for each synthetic steps. In particular, in the dried sample, peaks due to the active phase can not be observed probably due the presence of the templating agent, but a homogeneous distribution of the metallic species can be supposed. After the template removal through calcination, segregated species can be observed, such as the mixed oxides phase ($PdCuO_2$, ref. code 00-044-0185) and the Pd oxide phase. The reduction performed at 320°C caused a partial re-dispersion of the metallic aggregates, which were in the form of mixed reduced PdCu phase. Indeed, the peak related to this mixed phase is located between Pd and Cu single reduced phase peaks, indicating the insertion of one metal in the framework of the other one, which causes the shift of the peaks of the single metal.
Moreover, through the Scherrer equation, the particle size were calculated to be 10 nm for PdCu-M1 calcined sample and 6 nm for the reduced one. This behaviour can be confirmed by the TEM images (**Figure *24***).

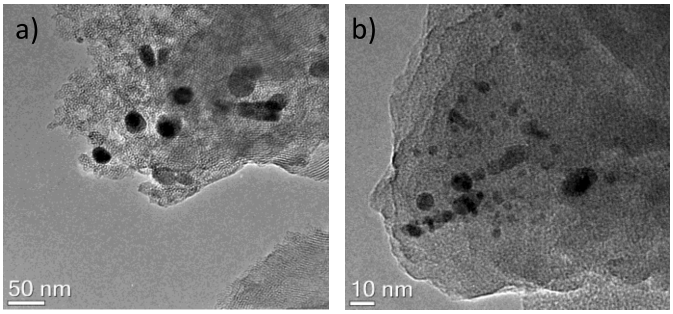

Figure 24 TEM images of PdCu-M1 catalyst a) calcined and b) reduced.

From the TEM analysis the metal particle sizes were deduce to be about 27 nm in the calcined sample and about 7 nm for the reduced one, confirming the re-dispersion effect of the reduction treatment.

The different characterization performed on the material for each synthetic steps evidenced that through the M1 route was possible to insert Pd and Cu in the siliceous framework in the form of mixed phase without altering the MCM-41 structure. Nevertheless, the calcination led to the formation of metallic aggregates with an inhomogeneous distribution, probably due to the high temperature used for the template removal. For this reason, an alternative method for the template removal (M2 route) was performed on the same catalyst, the one obtained from Pd and Cu chloride, through the ionic exchange. Thanks to the lower temperature of this alternative treatment (60 °C, in ethanol) the particle size would be smaller and the active phase distribution could be more homogeneous. This hypothesis was confirmed by the TEM images related to sample obtained after the ionic exchange and the reduction (**Figure *25***).

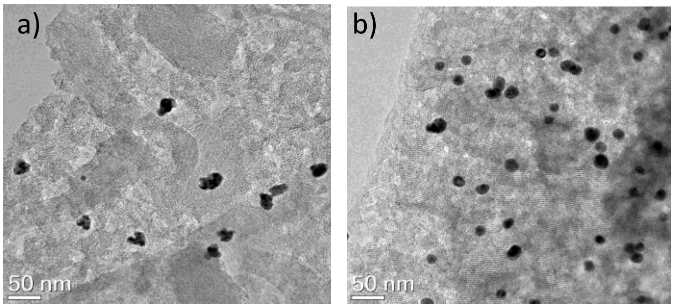

Figure 25 TEM images related to the PdCu-M2 catalysts a) after the ionic exchange and b) reduced.

Through the M2 route, after the template removal were obtained metal particle sizes smaller (around 17 nm) than in the calcined sample (around 27 nm). Nevertheless the re-distribution of the active phase during the reduction did not happen, contrary to the case of the M1 route. Indeed, after the reduction, the metal particles showed dimensions (around 16 nm) more or less similar to the pristine one (around 17 nm).

Trying to obtain more information about the composition of the active phase, TPR analysis were performed on PdCu-M1 and M2 catalysts (**Figure** *26*).

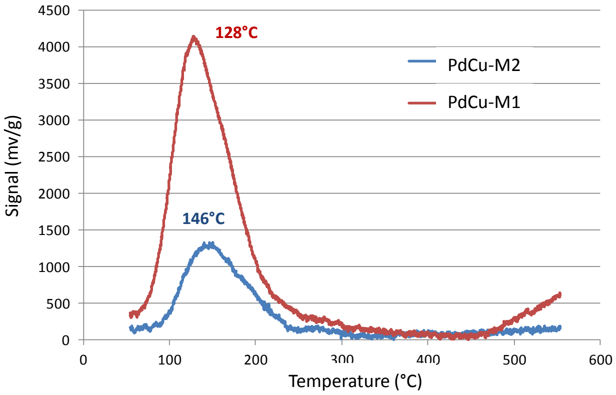

Figure 26 TPR profile of PdCu-M1 and PdCu-M2 catalysts.

In this analysis, the interaction between the two metals is of great importance because it influences the way the metals react with H_2 and consequently the reduction temperature of the active phase. The Pd, being highly affine to H_2, was reduced before the analysis started. As a consequence, the signal acquired was due only to the Cu reduction, which happened at lower temperature with respect to Cu alone that could be reduced also above 300°C. This phenomena was observed for both the type of catalysts, so in both samples Cu was in deep contact with Pd, being the reduction temperature an half of the pure Cu one. From this analysis, it seems that in both catalysts a similar active phase in terms of composition and distribution was present. This feature can be confirmed by the XRD analysis performed on the reduced samples (**Figure** *27*).

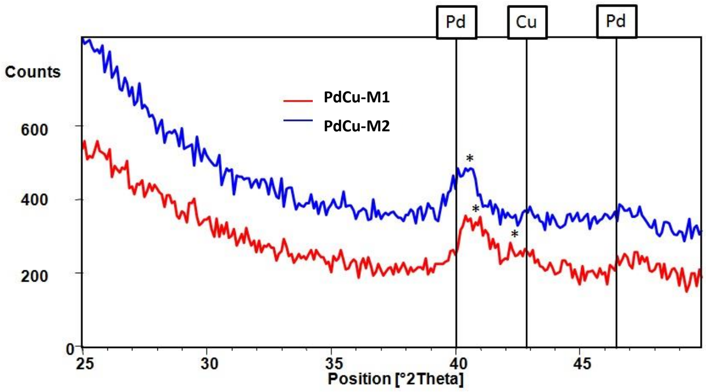

Figure 27 XRD patterns of PdCu-M1 and PdCu-M2 catalysts. * PdCu phase (Reference code 00-048-1551)

The XRD pattern relative to PdCu-M1 catalyst showed the presence of the PdCu mixed phase, which was present also in the PdCu-M2 catalyst but with a less deep contact between the two metals. In fact, in this case, the peaks of the mixed phase was shifted toward the position of the single phase.

Consequently, the calcination seemed to be an essential step for obtaining a deeper contact between the two metals, but, at the same time, it led to the formation of big aggregates. The ionic exchange could avoid the formation of big aggregates, but without guarantee the presence of the two metal in deep contact. Moreover, although the lower temperature of the ionic exchange, the metal particles showed relatively lower dimension, but they were still too big. This could mean that the metallic aggregates were formed during the synthesis and before the template removal; for this reason, PdCu preformed nanoparticles would be employed as metal precursors, instead of chlorides, with the aim to control better the dimension and composition of the active phase.

1.4.3 PdCu/MCM-41 from nanoparticles

After the study of PdCu/MCM-41 catalysts obtained from chlorides, the attention was focused on the PdCu/MCM-41 catalysts prepared using bimetallic preformed nanoparticles. Following the same two procedures (M1 and M2) seen for the chlorides derived catalysts, the catalytic systems prepared with nanoparticles were: NPsPdCu-M1 and NPsPdCu-M2, where M1 and M2 referred always to the procedure employed for the template removal (M1 for calcination and M2 for ionic exchange).

As in the case of chlorides precursors, also the preformed nanoparticles were introduced during the formation of the MCM-41 support, but the sol of nanoparticles was used directly as batch for the catalyst synthesis in which the CTAB were then dissolved. Also the synthesis of the bimetallic nanoparticles was the result of a study for obtaining the desired composition and dimensions. In particular, the nanoparticles dimensions were deduced from the DLS analysis, which provided the value of the hydrodynamic radius. In **Figure *28***, the comparison between the hydrodynamic radius of the nanoparticles sol as synthesized and after the addition of CTAB is reported.

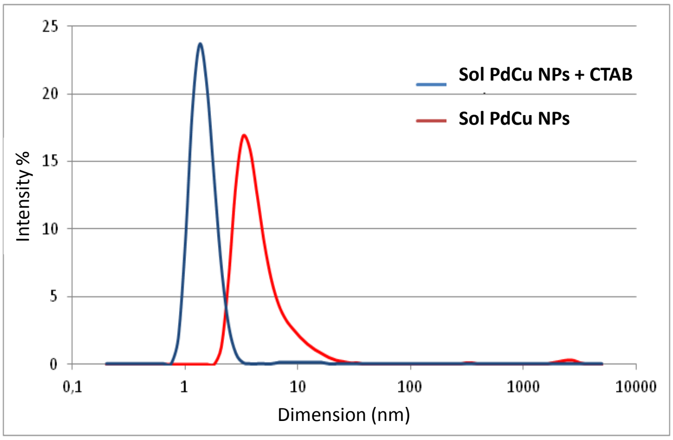

Figure 28 DLS analysis of NPs suspension as synthesized and after the CTAB addition.

From this comparison, it appears clearly that the CTAB decreased further the nanoparticles dimensions, enhancing the stabilization effect of PVP.

After the drying steps, the samples were subjected to the template removal, which was performed into two ways (M1 and M2). The calcination at 540°C removed both the CTAB and the PVP, the nanoparticles stabilizing agent which decomposed near 300°C [34]. Also in the case of the ionic exchange, it seemed that even the PVP was efficiently removed, together with the CTAB, as confirmed by TG and ATR analysis.

Moreover, the active phase of these catalysts was characterized through XRD analysis (**Figure *29***). It should be reminded that the preformed nanoparticles were composed by metals already reduced before the addition of CTAB.

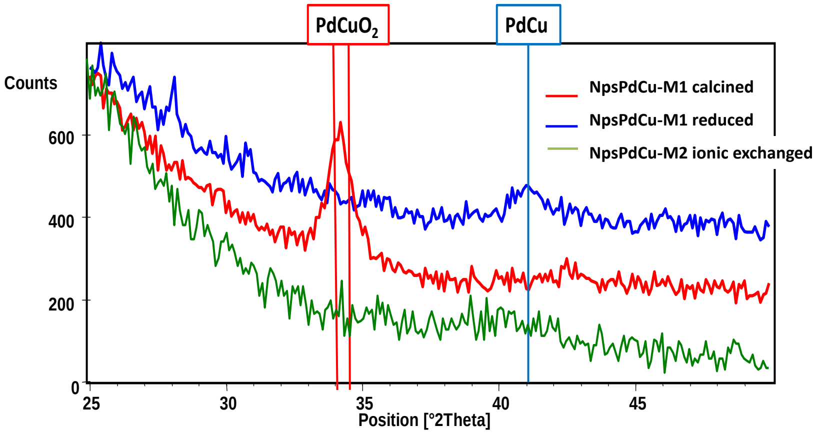

Figure 29 XRD patterns of NpsPdCu-M1 calcined, reduced and NpsPdCu-M2 after the ionic exchange.

The NpsPdCu-M1 sample after the calcination showed the presence of aggregates composed by $PdCuO_2$ mixed phase (ref. code 00-044-0185) due to the oxidation of the nanoparticles, which, at 540°C, lost the stabilizing agent and oxidized. After the reduction, essential before the catalytic test, the active phase of the NpsPdCu-M1 catalyst completely changed with the formation of a PdCu mixed phase with a better dispersion on the support.

Concerning the NpsPdCu-M2 catalyst after the ionic exchange, the XRD patterns did not show the presence of significant peaks. This was probably due to the fact that the material was not subjected to treatments at high temperatures, avoiding the formation of metallic aggregates. This behaviour could suggest that through the use of preformed nanoparticles was possible to control the dimension of the active phase particles during the synthesis and the two template removal methods led to the formation of catalysts with two different active phase distributions.

To get more information about the interaction between Pd and Cu, TPR analysis was employed (**Figure** ***30***).

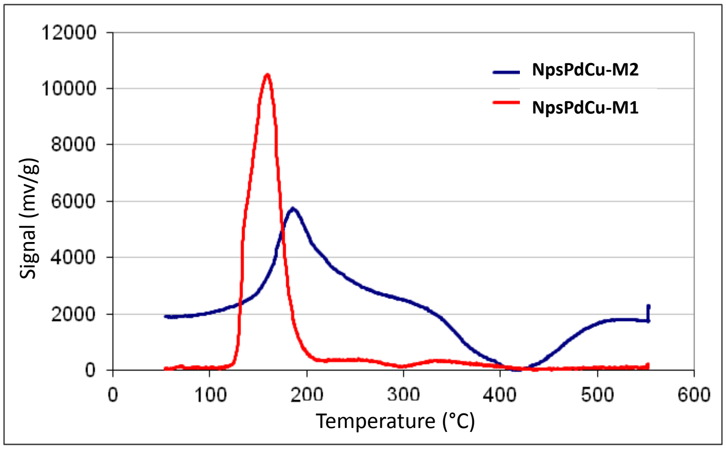

Figure 30 TPR analysis of the NpsPdCu-M1 and NpsPdCu-M2 samples after the template removal.

The calcined sample, as expected, showed an H_2 consumption at 170°C, suggesting that the active phase was oxidized during the calcination and that the Cu was in deep contact with Pd because it was reduced at relatively low temperature during the analysis. Concerning the ionic exchanged sample, it showed a smaller H_2 consumption near 200°C. This signal was of a difficult attribution; it could be due to decomposition of organic residue, taking into account that the preformed nanoparticles were already reduced during their synthesis and that they were not subjected to air mediated treatment at high temperature. Moreover, this sample showed also a negative signal at 400°C, which could be due to decomposition of templating agent residuals.

In conclusion, the TPR analysis suggested, as the other characterization, that the catalysts obtained through the different preparation routes showed different behaviour in presence of H_2. Although, for the NpsPdCu-M2 sample was not possible to define the type of active species because the signal acquired during the TPR analysis could not be attributed with certainty to the active phase or to organic residues. As a consequence, another characterization was employed for understand better the characteristics of the active phase, in particular TEM analysis. The reported images (**Figure *31***) are related to the dried sample already containing the nanoparticles and still CTAB and PVP. From this catalyst precursor were originated the NpsPdCu-M1 and NpsPdCu-M2 through the template removal and their TEM images are reported too with the aim to follow the evolution of the particles dimensions during the different treatments.

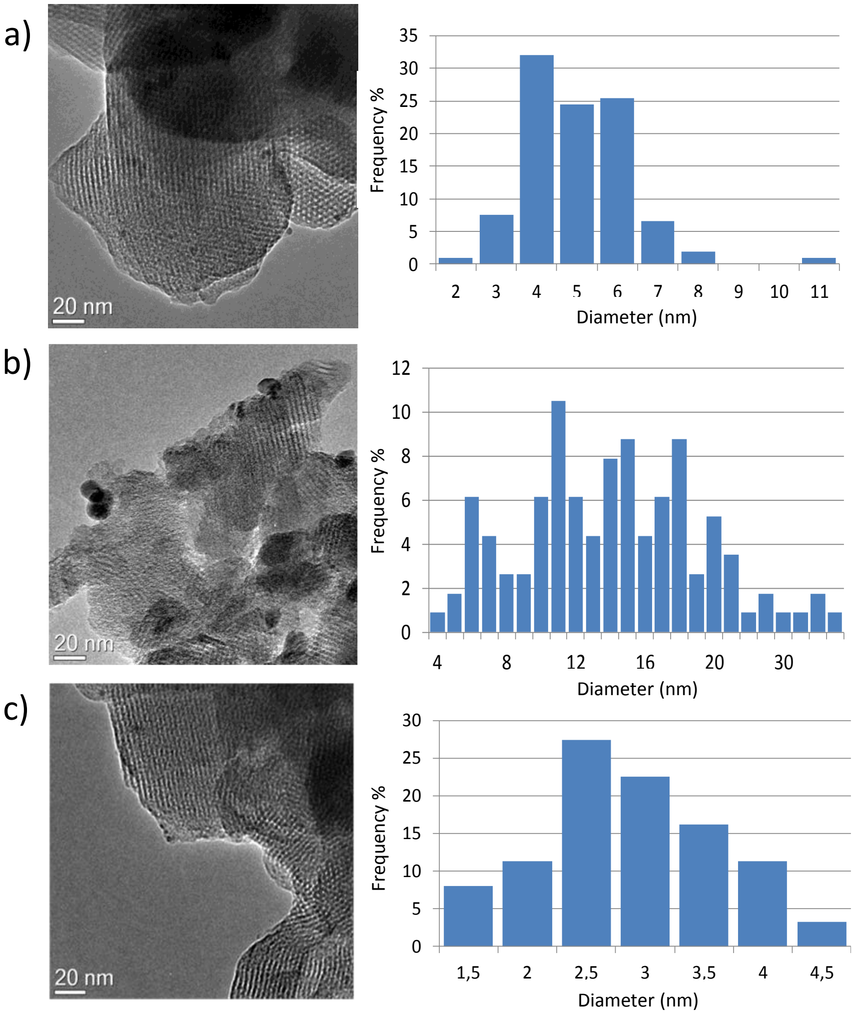

Figure 31 TEM images with particle size distributions of a) NpsPdCu dried sample, b) NpsPdCu-M1 and c) NpsPdCu-M2 samples.

First of all, from this images the typical hexagonal structure of MCM-41 can be recognized in both catalysts, independently from the template removal route. In addition, from the comparison between the dimension distributions, it can be deuced that the ionic exchange, contrarily to the calcination, let the control of dimension of the metallic particles which maintained sizes similar to the dried sample (2.5-4 nm).

Moreover, the metallic particles can be easier observed in the calcined sample; this could be due probably to the residual PVP on the nanoparticle in the ionic exchanged sample which partially hid the nanoparticles (**Figure** *32*).

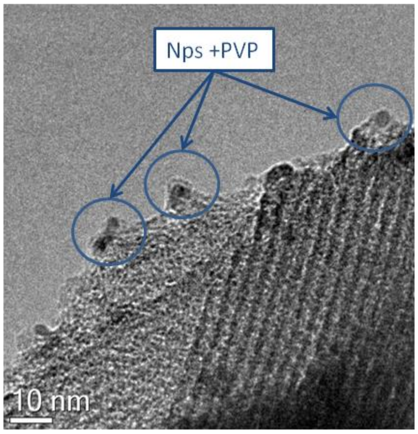

Figure 32 TEM images of NpsPdCu-M2 sample.

As observed before, the calcination, beside increasing the particle size, let the oxidation of the metals, indeed the reduction at 320°C was needed before the catalytic tests and the effect of this treatment was followed through the TEM analysis (**Figure** ***33***).

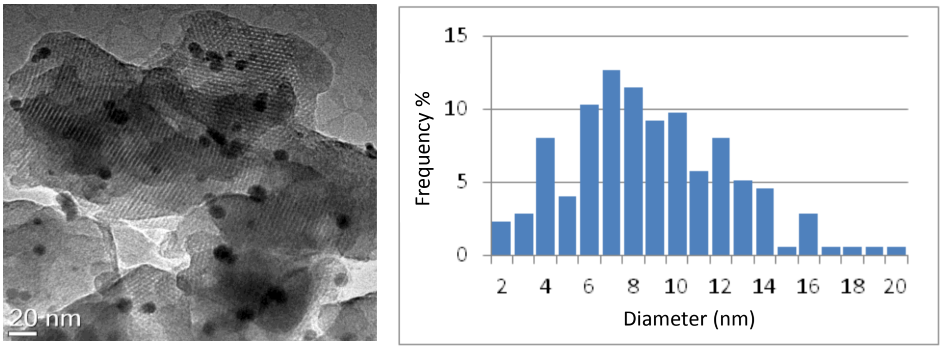

Figure 33 TEM images with size distribution of NpsPdCu-M1 reduced.

As already observed in the case of chlorides precursors, the reduction treatment caused a re-distribution of the active phase. Indeed, comparing the particle size of the sample before and after the reduction, a general decrease of the particles dimensions can be observed. Although, the metal particles in the reduced sample were not smaller than in the ionic exchange catalyst.

With the aim to complete the removal of the organic residue detected in the ionic exchanged sample, the catalyst was subjected to two different treatments: 250°C in H_2 or 250°C in air, obtaining respectively NpsPdCu-M2 A and NpsPdCu-M2 B samples. Then the TPR analysis was performed on the differently treated catalysts (**Figure** ***34***).

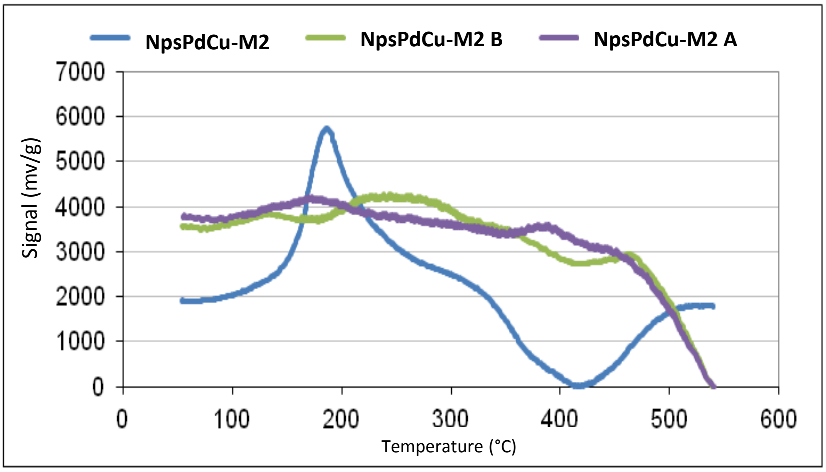

Figure 34 TPR analysis of NpsPdCu-M2, NpsPdCu-M2 A (after calcination) and NpsPdCu-M2 B (after reduction) samples.

From this analysis, it clearly appears that the metallic species after the reduction and the calcination at 250°C were already reduced because there was no consumption of H_2 for both treated samples. Moreover, being no signals due to organic residues, both the treatment were able to remove them. With the aim to understand better the nature of the active species after these treatments, XRD analysis were performed on the differently treated samples (**Figure** *35*).

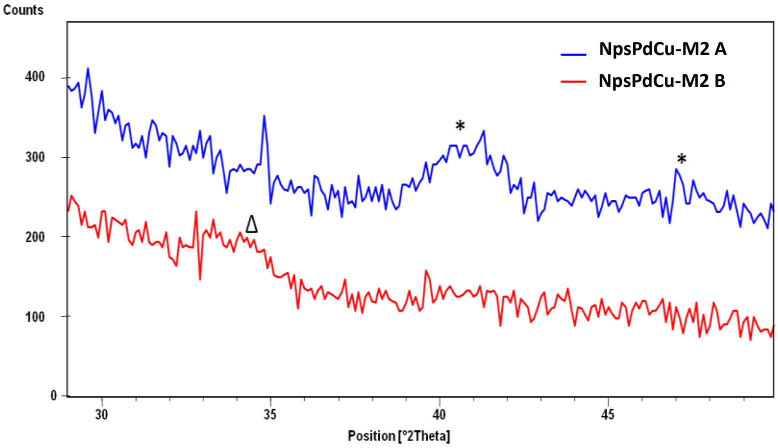

Figure 35 XRD patterns of NpsPdCu-M2 A and NpsPdCu-M2 B catalysts. * PdCu mixed phase, Δ $CuPdO_2$ mixed oxides phase.

The patterns showed the presence of signals for both samples (A and B), contrarily to the not treated sample. In particular, the active phase of the H_2 treated sample, was in the form of reduced and mixed phase; while, the calcined sample showed only traces of a mixed oxides phase, confirming the TPR results where no H_2 consume was detected because the metallic phase was almost reduced.

The effect of these different treatments on the particle size was studied through the TEM analysis (**Figure** *36*).

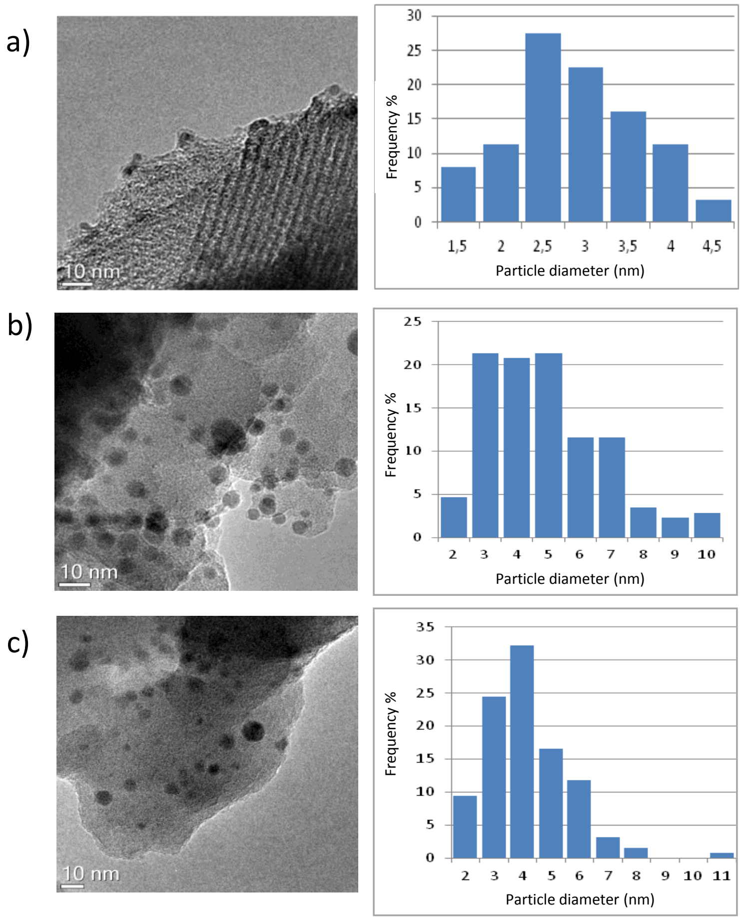

Figure 36 TEM images with particle diameter distribution of a) NpsPdCu-M2, b) NpsPdCu-M2A, treated in air and b) NpsPdCu-M2B, treated in air samples.

From these images emerged that the particles sizes were maintained also after both treatments in hydrogen and in air and that there were no aggregation phenomena. Indeed, in the treated samples, the metal particles were no more surrounded by PVP, as was observed for the sample before the treatments.

1.4.4 Catalytic performances in the HDC reaction

The prepared catalysts were tested in the reaction of hydrodechlorination of $CF_3OCFClCF_2Cl$ (AM) to $CF_3OCF=CF_2$ (MVE) with the aim to understand the effect of the various synthetic procedures and template removal methods on the catalytic properties. The supposed reaction scheme is reported in ***Figure 37***.

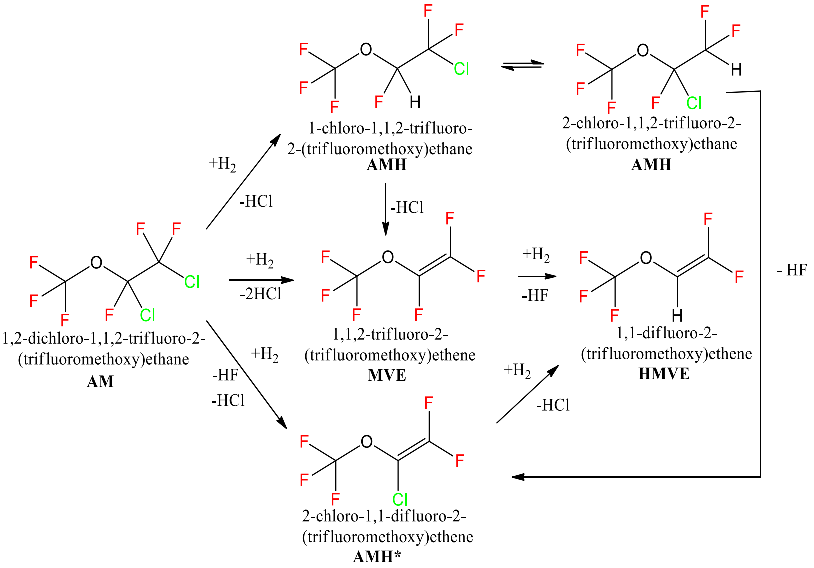

Figure 37 Reaction scheme for the HDC reaction of $CF_3OCFClCF_2Cl$ (AM) to $CF_3OCF=CF_2$ (MVE).

In particular, besides the desired product (MVE), HMVE can be obtained through two ways: from halogen-hydrogen exchange on MVE or on AMH*. Probably, the favoured path is the one passing through AMH* because the dissociation energy of C-Cl bond is lower than the C-F one.

Firstly, the effect of the metallic precursors was studied, comparing the catalytic performances of the catalyst both calcined but prepared with chlorides (PdCu-M1) or preformed nanoparticles (NpsPdCu-M1).

In **Figure** ***38***, the catalytic performances of PdCu-M1, the calcined catalyst obtained from Pd and Cu chlorides, are reported in function of time.

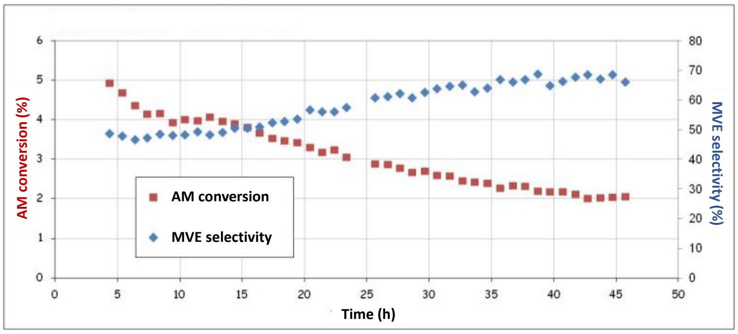

Figure 38 AM conversion and MVE selectivity of PdCu-M1 catalyst.

Concerning the AM conversion, it decreased with time on stream, suggesting deactivation phenomena. Contrarily, the MVE selectivity increased with time on stream; moreover, the selectivity in HMVE decreased, while the selectivity in the other products did not evidently change, as reported in **Figure** *39*.

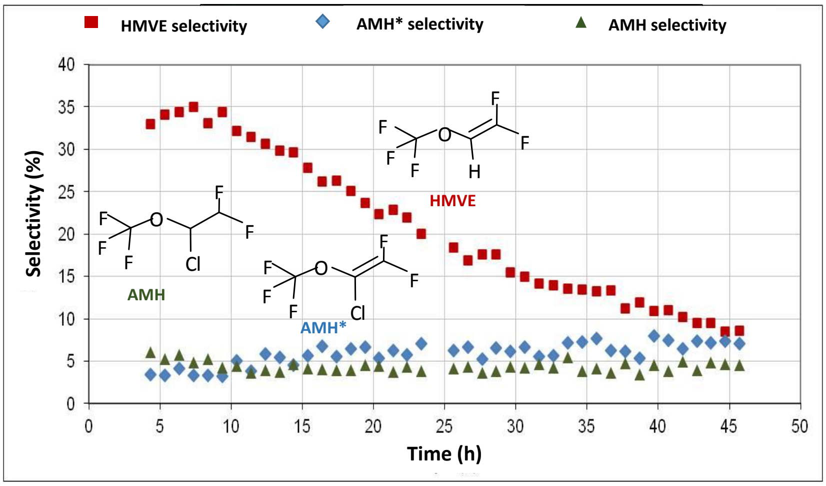

Figure 39 Selectivity in HMVE, AMH and AMH* provided by PdCu-M1 catalyst.

The trends of MVE and HMVE selectivity probably demonstrated how the formation of these products was linked at two different catalytic active sites, confirming the possible change of the active phase and, consequently of the catalytic sites, during the reaction.

This interesting behaviour could be explained also considering HMVE as a consecutive product of MVE. Unfortunately, this hypothesis should be discharged on the basis of the bond energy of C-Cl and C-F, from which HMVE could be more favourably formed from AMH* than from MVE.

Indeed, the possible changes in the catalytic system during the time on stream, due to H_2 and HCl reach environment, could be a more sustainable hypothesis for explaining the selectivity and conversion trends. The modifications of the active phase emerged from the XRD and TEM analysis performed on the used catalyst (**Figure** ***40***).

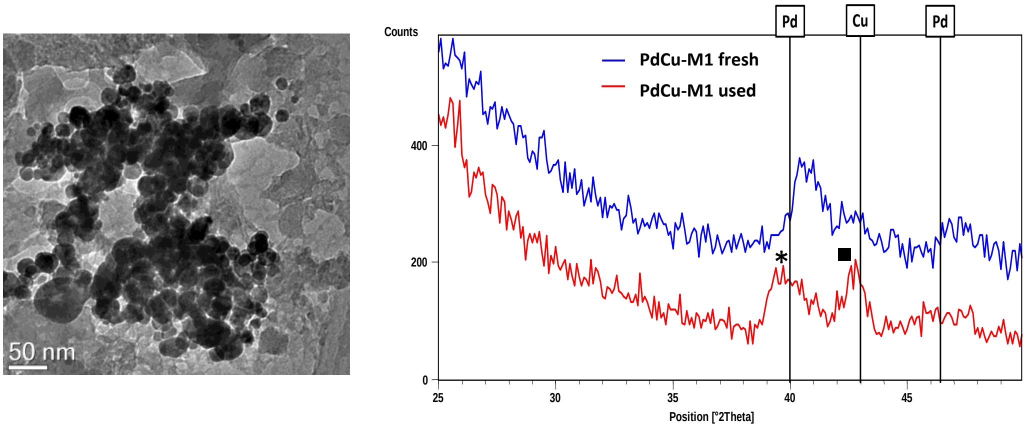

Figure 40 TEM images and XRD analysis, compared with fresh catalyst, of PdCu-M1 used catalyst. * Pd phase (ref. code 01-087-0643) ■ Cu phase (ref. code 01-070-3038).

The TEM images evidenced that, after the reaction, the particles size increased: from 7 nm, on the fresh catalyst, to 15 nm in the used one. Moreover, during the reaction, segregation of the active metals happened, as showed from the XRD patterns, where peaks due to the presence of single metals can be observed.

In conclusion, the trends of the selectivity of MVE and HMVE seem to be due to modifications of the active species passing from sites, which favoured the formation of HMVE to those which favoured the MVE production.

To understand the effect of the type of the metals precursors on catalytic performances, a comparison between the catalytic data related to the two different systems is necessary. In **Figure** ***41***, AM conversion trends provided by the calcined catalysts obtained from chlorides and preformed nanoparticles are reported. Moreover, trying to enhance its activity, the nanoparticles derived catalyst was reduced in situ, during the reaction, because the TPR analysis (**Figure** ***30***) and the XRD pattern (**Figure** ***29***) showed that the active phase, after the calcination, was oxidized.

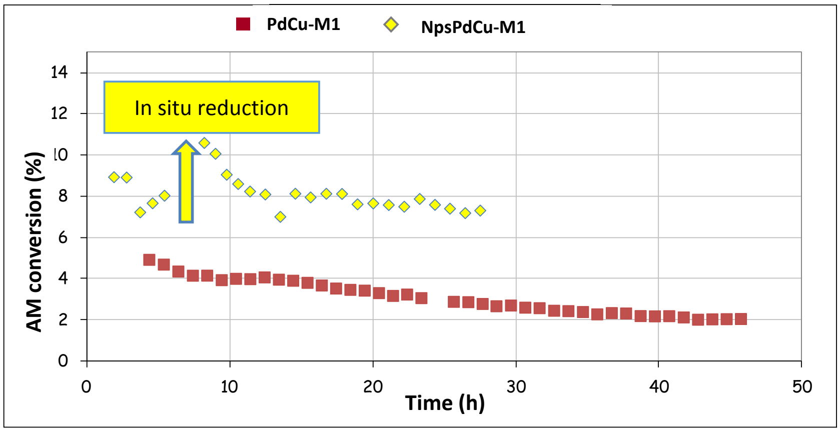

Figure 41 Comparison of AM conversion trends provided by PdCu-M1 (from chlorides) and NpsPdCu-M1 (from nanoparticles) catalysts.

The nanoparticles derived system (NpsPdCu-M1) showed a higher AM conversion than the chlorides derived one (PdCu-M1); moreover, the catalytic activity was enhanced after the in situ reduction. Although, after some hours the AM conversion values became similar to the pristine ones, but remaining always higher than the catalyst obtained from chlorides.

In **Figure *42***, the selectivity of the other products is reported in function of the time on stream.

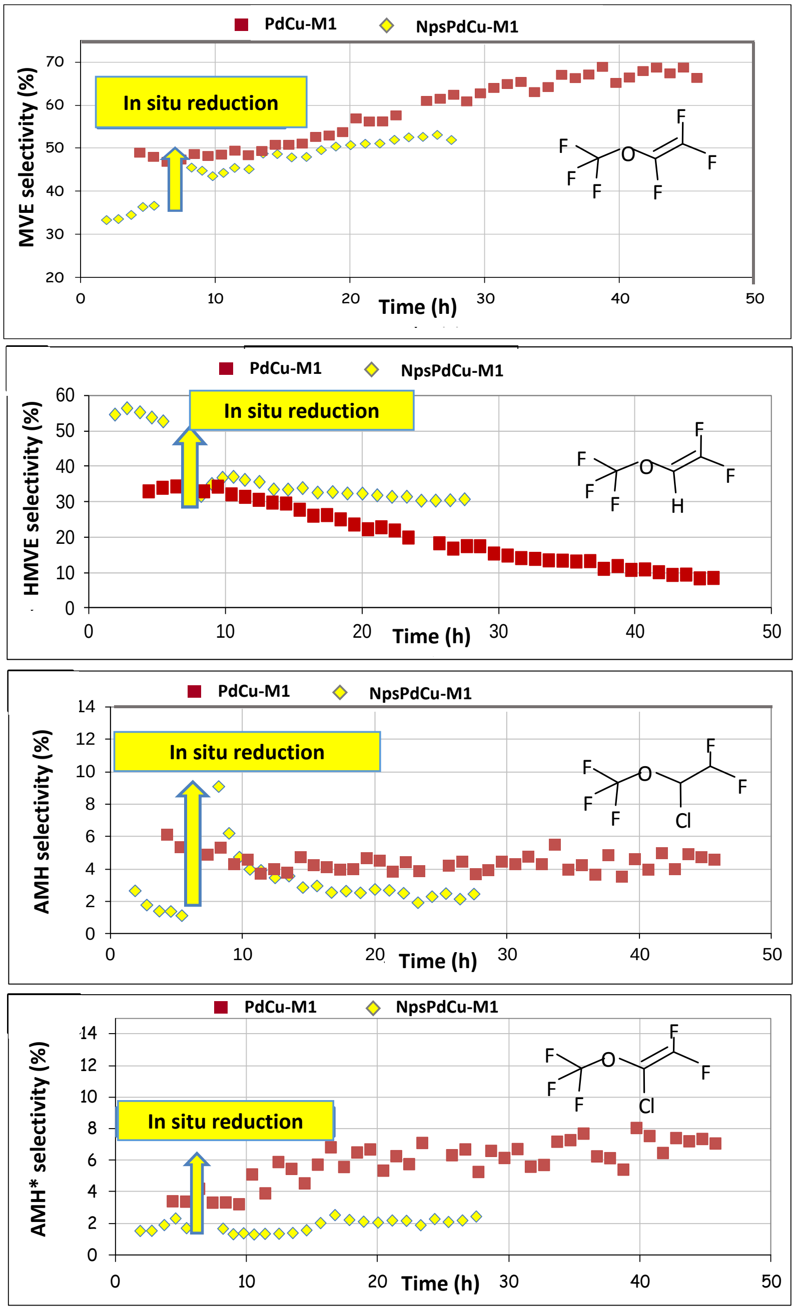

Figure 42 Selectivity in MVE, HMVE, AMH and AMH* provided by PdCu-M1 and NpsPdCu-M1 catalysts.

The MVE selectivity provided by NpsPdCu-M1 catalyst was lower than the chlorides derived catalyst, but after the in situ reduction, it was considerably enhanced. Moreover, for both catalysts the trend of the HMVE selectivity was the opposite of the

MVE selectivity. Indeed the former decreased with time on stream while the latter increased.

In addition, the AMH selectivity of NpsPdCu-M1 increased after the in situ reduction, suggesting that the formation of this product, which is partially hydrogenated and saturated, was favoured by the H_2 adsorbed in higher amount after the reduction, as also observed in previous work[31].

In conclusion, after many hours of reaction, the catalytic performance provided by NpsPdCu-M1 catalyst were better than PdCu-M1 catalyst only in terms of AM conversion, while looking at the formation of the desired product (MVE), the chlorides derived catalyst gave higher selectivity. Moreover, the higher AM conversion was probably due to a smaller size of the metal particles, while the lower MVE selectivity was probably caused by the presence of partially oxidized species.

Although the different values of conversion and selectivity, the differences were smoothed as the reaction proceeded, suggesting that the active phases were modified leading to similar active species. The XRD of the used catalysts can demonstrate these phenomena (**Figure *43***).

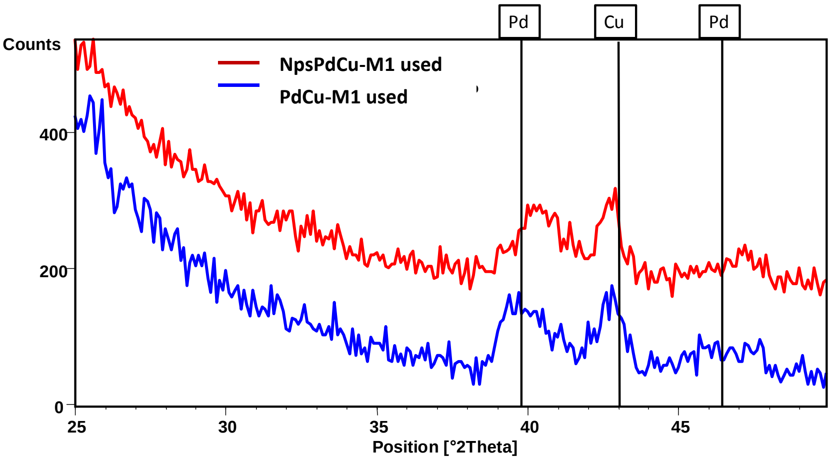

Figure 43 XRD patterns of the used PdCu-M1 and NpsPdCu-M1 catalysts.

Indeed, the XRD patterns showed similar peaks, which can be attributed to the presence of segregated Pd and Cu metallic species for both used catalysts.

To understand the effect of the template removal method on catalytic performances, a comparison between the catalytic data related to the two differently treated systems is necessary. In particular, the comparison could be done for the preformed nanoparticles catalysts and, in particular, between the calcined system (NpsPdCu-M1) and the ionic exchanged sample after the air mediated treatment at 250°C (NpsPdCu-M2B). Only the NpsPdCu-M1 sample was reduced in situ, during the reaction.

In **Figure *44*** the AM conversion provided by the two different systems is reported.

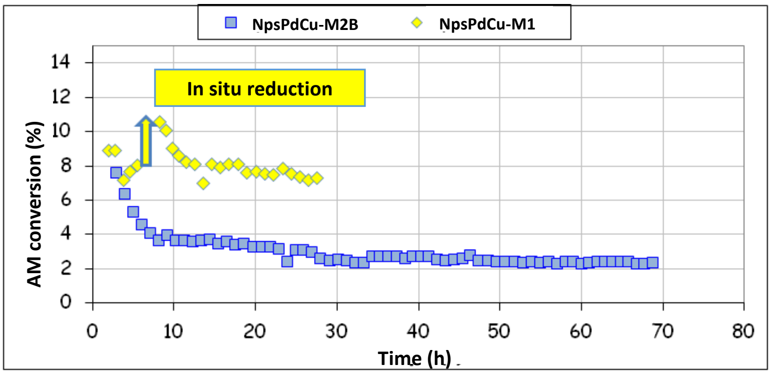

Figure 44 AM conversion provided by NpsPdCu-M2B and NpsPdCu-M1 catalysts.

The calcined catalyst gave a higher AM conversion, before and after the in situ reduction, while the ionic exchanged one showed very low AM conversion.

The effect of the template removal method on the selectivity in the different products can be observed in **Figure *45***.

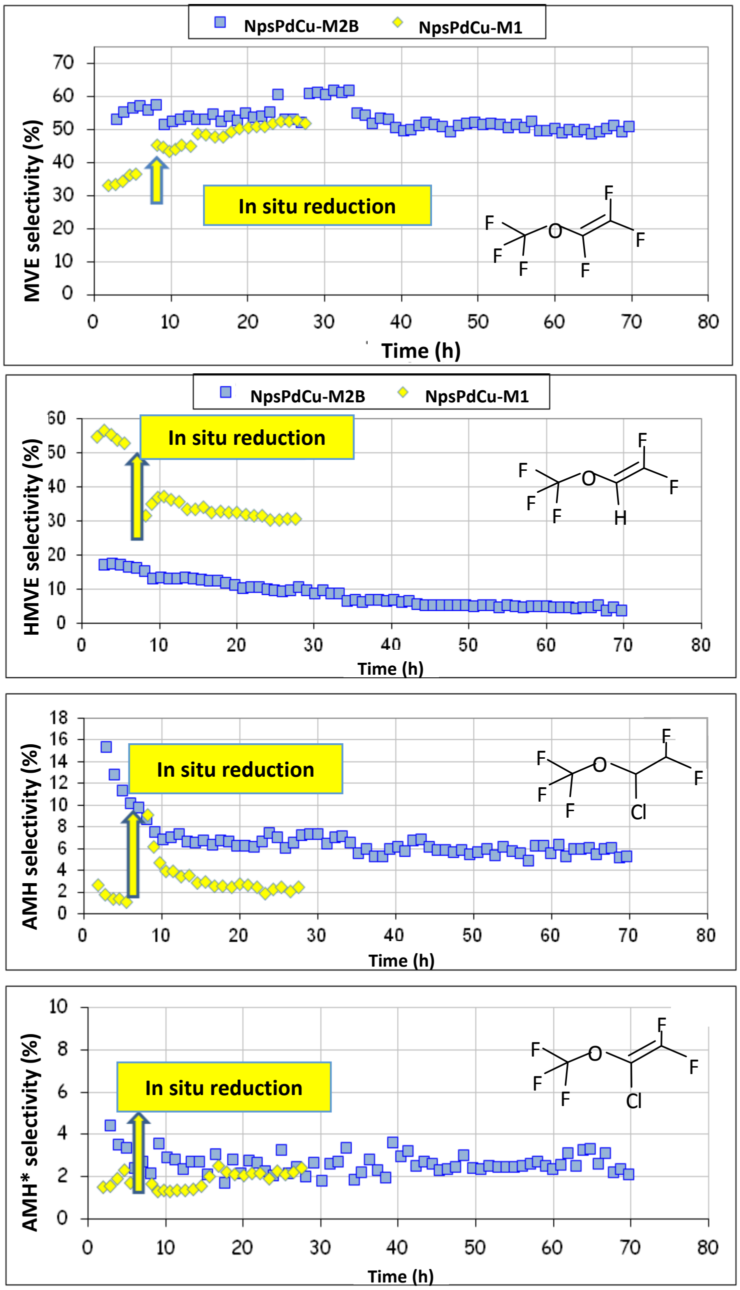

Figure 45 Selectivity in MVE, HMVE, AMH and AMH* provided by NpsPdCu-M1 and NpsPdCu-M2B catalysts.

Concerning the MVE selectivity, at the beginning the two catalysts showed very different values; in particular, for the ionic exchanged sample the MVE selectivity was higher than 50%, while for the calcined one, it was around 33-35%. The in situ reduction, changed completely the behaviour of the NpsPdCu-M1, enhancing its MVE selectivity which was similar to the other catalyst. From these differences, it would be concluded that the active species at the beginning of the reaction were different and only after the in situ reduction became similar. Looking at the selectivity in the other products, the main differences can be noted for the HMVE selectivity, while the other products (AMH* and AMH) were formed with similar selectivity. In particular, the ionic exchanged catalyst gave a lower HMVE selectivity, while the calcined system showed at the beginning a higher HMVE selectivity which dramatically decreased after the in situ reduction. This behaviour suggests that the HMVE formation is linked to the presence of Cu particles not totally reduced.

In addition, the HDC reaction had the same effect already observed for the previous catalytic system; in particular, the used ionic exchanged catalyst, as the calcined one, showed the presence of segregated metallic particles (**Figure *46***).

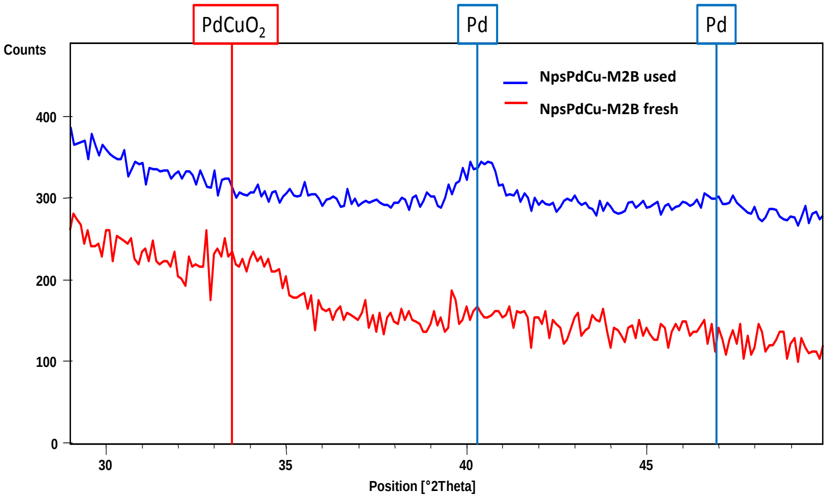

Figure 46 XRD patterns of the NpsPdCu-M2B used and fresh catalysts.

In conclusion, the type of the template removal method influenced the AM conversion and the HMVE selectivity. Indeed, for the ionic exchanged catalyst (NpsPdCu-M2B) lower AM conversion and HMVE selectivity were obtained. This particular behaviour was probably caused by a low active phase exposition, which, although the more controlled particle size, did not show a relevant catalytic activity.

Moreover, the calcination, as template removal method, seemed to be essential for creating a particular interaction between Pd and Cu and a more available active phase, which ensured higher AM conversion and MVE selectivity.

1.5 Conclusions

This study demonstrated that through the sol-gel method and the insertion of the metallic precursor directly during the synthesis of the MCM-41 support, it was possible to obtain PdCu/MCM-41 catalysts with ordinated structure high surface area and interesting hydrodechlorinating activity.

First of all, the attention was focused on the effect of the metals insertion on the mesoporous structure of MCM-41; the particular features of the support were not modified by the presence of metals. Moreover, the optimization of the synthetic route, in particular, the less amount of template and the shorter microwave mediated hydrothermal treatment, led to the formation of a material with properties similar to the one obtained from the original procedure.

The template removal was preformed through calcination at 540°C or ionic exchange at 60° in ethanol. Both methods were efficient in removing the templating agent; although through the ionic exchange less crystalline material was obtained. On the other hand the ionic exchange let a slight control of metals particle size which otherwise increased after the calcination. Indeed, with ionic exchange it was possible to avoid the growth of metals particles, but on the final material metallic aggregates were found. This meant that the aggregation of metal particles happened during the synthesis of the catalyst, before the template removal. With the aim to avoid the aggregation of metals, preformed nanoparticles were used as metals precursors instead of chlorides and their combination with the ionic exchange for the template removal were also tested. Moreover, another advantage deriving by the use of preformed nanoparticles, was that the metals were already reduced before their insertion in the MCM-41 support. Starting from preformed nanoparticles and using calcination as template removal method, the size of the metals particles increased forming oxides mixed aggregates. For this reason, an in situ reduction during the catalytic test was necessary. Through the ionic exchange, the nanoparticles sizes were maintained similar to the pristine, but some organic residues were already present on the nanoparticles. Consequently, a calcination at 250°C was necessary to remove all the residues and increase the active phase accessibility, without oxidizing the metals and increasing their particle sizes.

Finally, through the ionic exchange and the use of preformed nanoparticles, the control of the metals particles sizes was possible. Consequently the attention could be focused on the effect of all these treatments and synthetic parameters on the catalytic activity in the HDC reaction of $CF_3OCFClCF_2Cl$ (AM) to $CF_3OCF{=}CF_2$ (MVE). The chlorides derived systems showed a low AM conversion and an opposite trend between MVE and HMVE selectivity with time on stream. Indeed, during the reaction the former increased while the latter decreased. This behaviour was observed also for all the other catalytic systems and two hypothesis were proposed: consecutive relationship between the two products or modification of the active phase due to the reaction environment. The latter hypothesis was sustained by characterization of the used catalysts which showed a segregation of the bimetallic phase in the single metals. Concerning the effect of the metallic precursor, in the case of preformed nanoparticles in the calcined system, the AM conversion was, at the beginning, similar to the chlorides derived catalyst, while, after the in situ reduction, it was greatly enhanced. The MVE selectivity was lower for the nanoparticles containing catalyst and, as for the conversion, after the in situ reduction it was enhanced, becoming similar to the chlorides derived catalyst. Indeed, the reaction smoothed the possible differences that could derive from the use of different metallic precursors, as demonstrated by the characterization performed on the used catalysts, which showed the presence of a similar active phases, although at the beginning they were different in terms of particles size and oxidation state.

The effect of the template removal method was studied in the nanoparticles derived catalyst. The calcined catalyst gave higher AM conversion and HMVE selectivity, while the ionic exchanged catalyst provided a better MVE selectivity.

Even if the PdCu/MCM-41 catalysts synthetic route was optimized in terms of metallic particles size and distribution, the catalytic activity seemed to be not so enhanced. Moreover, the reduced metal particles size and their high dispersion obtained through preformed nanoparticles and ionic exchange, were not enough to ensure a better catalytic activity in the reaction of interest.

References

---

[1] IUPAC Manual of Symbols and Terminology, *Pure appl. Chem.* **31** (1972) 578.

[2] J. S. Beck, J. C. Vartuli, W. J. Roth, M. E. Leonowicz, C. T. Kresge, K. D. Schmitt, C. T-W. Chu, D. H. Olson, E. W. Shepperd, S. B. McCullen, J. B. Higgins, J. L. Schlenkert, *J. Am. Chem. Soc.* **114** (1992) 10834-10843.

[3] J. S. Beck, J. C. Vartuli, G. J. Kennedy, C. T. Kresge, W. J. Roth, S. E. Schrammt,, *Chem. Mater.* **6** (1994) 1816-1821.

[4] X. S. Zhao, G. Q. Lu, G. J. Millar, *Ind. En. Chem. Res.* **35** (1996) 2075-2090.

[5] A. Corma, *Topics in Catalysis* **4** (1997) 249-260.

[6] C. T. Kresge, M. E. Leonowicz, W. J. Roth, J. C. Vartuli, J. S. Beck, *Nature* **359** (1992) 710-712.

[7] J. C. Vartuli, K. D. Schmitt, C. T. Kresge, W. J. Roth, M. E. Leonowics, S. B: McCullen, S. D. Hellring, J. S. Beck, J. L. Schlenker, D. H. Olson, E. W. Sheppard, *Chem. Mater.* **6** (1994) 2317-2326.

[8] J. Y. Ying, C. P. Mehnert, M. S. Wong, *Angew. Chem. Int. Ed.* **38** (1999) 56-77.

[9] R. Ryoo, C. H. Ko, R. F. Howe, *Chem. Mater.* **9** (1997) 1607-1613.

[10] Z. Luan, C. F. Cheng, W. Zhou, J. Klinowski, *J. Phys. Chem.* **99** (1995) 1018-1024.

[11] Q. Huo, D. Margolese, U. Ciesla, P. Feng, T. E. Gier, P. Sieger, R. Leon, P. M. Petroff, F. Schuth, G. D. Stucky, *Nature* **368** (1994) 317-321.

[12] K. M. Reddy, C. Song, *Catal. Lett.* **36** (1996) 103-109.

[13] K. M. Reddy, C. Song, *Catal. Today* **31** (1996) 137-144.

[14] J. S. Beck, J. C. Vartuli, *Curr. Opin. Solid State Mater. Sci.* **1** (1996) 76-87.

[15] C. Y. Chen, S. L. Burkett,, H. X. Li, M. E. Davis, *Microporous Mater.* **2** (1993) 27-34.

[16] A. Steel, S. W. Carr, M. W. Anderson, *J. Chem. Soc. Chem. Comm.* (1994) 1571-1572.

[17] A. Monnier, F. Schuth, Q. Huo, D. Kumar, D. Margolese, R. S. Maxwell, G. D. Stucky, M. Krishnamurthy, P. Petroff, A. Firouzi, M. Janicke, B. F. Chmelka, *Science* **261** (1993) 1299-1303.

[18] Q. Hou, D. Margolese, U. Ciesla, D. G. Demuth, P. Feng, T. E. Gier, P. Sieger, A. Firouzi, B. F. Chmelka, F. Schuth, G. D. Stucky, *Chem. Mater.* **84** (1994) 1176-1191.

[19] P. T. Tanev, T. J. Pinnavaia, *Science* **267** (1995) 865-867.

[20] P. T. Tanev, M. Chibwe, T. J. Pinnavaia, *Nature* **368** (1994) 321.

[21] P. T. Tanev, T. J. Pinnavaia, *Chem. Mater.* **8** (1996) 2068-2079.

---

[22] H. Teng, *Appl. Sci.* **2** (2012) 496-512.

[23] G. Hougham, P. E. Cassidy, K. Johns, T. Davidson, *Fluorpolymer 1: Synthesis, (Topics in Applied Chemistry)*, **1**, Springer, 1999.

[24] R. Ohnishi, W. L. Wang, M. Ichikawa, *Appl. Catal., A* **113** (1994) 29-41.

[25] C. D. Thomson, R. M. Rioux, N. Chen, F. H. Ribeiro, *J. Phys. Chem.* **104** (2000) 3067-3077.

[26] E. J. Shin, A. Spiller, G. Tavolaris, M. A. Keane, *Phys. Chem. Chem. Phys.* **1** (1999) 3173-3181.

[27] A. Weirsma, A. T. Cate, E. J. A. X. Van de Sandt, M. Makkee, *Ind. Eng. Chem. Res.* **46** (2007) 4158-4165.

[28] T. Mori, J. Kubo, Y. Morikawa, *Appl. Catal., A: General* **271** (2004) 69-76.

[29] P. Benito, M. Gregori, S. Andreoli, G. Fornasari, F. Ospitali, S. Millefanti, M. S. Avila, T. F. Garetto, S. Albonetti, *Catal. Today* **246** (2015) 108-115.

[30] V. Tortelli, P. Calini, A. Zompatori, E. Antenucci, **US Patent 203368** (2007) assigned to Solvay Solexis Spa [IT/IT].

[31] M. Gregori, G. Fornasari, G. Marchionni, V. Tortelli, S. Millefanti, S. Albonetti, *Appl. Catal. A: General* **470** (2014) 123-131.

[32] P. Benito, M. Gregori, S. Andreoli, G. Fornasari, S. Millefanti, F. Ospitali, S. Albonetti, *Catal. Today* **235** (2014) 134-143.

[33] N. Lang, A. Tuel, *Chem. Mater.* **16** (2004) 1961-1966.

[34] M. Blosi, S. Albonetti, S. Ortelli, A. L. Costa, L. Ortolani, M. Dondi, *New J. Chem.* **38** (2014) 1401-1409.

[35] A. Srebowata, W. Lisowski, J. W. Sobczak, Z. Karpinski, *Catal. Today* **175** (2011) 576-584.

[36] M. A. Keane, ChemCatChem 3 (2011) 800-821.

[37] B. T. Meshesha, N. Barrabes, J. Llorca, A. Dafinov, F. Medina, K. Fottinger, *Appl. Catal. A: General* **453** (2013) 130-141.

[38] V. I. Kovalchuk, J. L. d’Itri, *Appl. Catal. A: General* **271** (2004) 13-25.

[39] L.S. Vadlamannati, V. I. Kovalchuk, J. L. d’Itri, *Catal. Lett.* **58** (1999) 173-178.

[40] M. Gregori, P. Benito, G. Fornasari, M. Migani, S. Millefanti, F. Ospitali, S. Albonetti, *Microporous Mesoporous Mater.* **190** (2014) 1-9.

[41] N. Koizumi, X. Jiang, J. Kugai, C. Song, *Catal. Today* **194** (2012) 16-24.

Chapter 2: Mesoporous carbon based materials

2.1 Introduction

In the recent years, the preparation and the characterization of nanocarbon have reached great attention due to the large field of applications of these materials and their attracting properties, such as electrical and thermal conductivity, mechanical strength and chemical inertness that conventional materials cannot match [1]. Nanocarbon is a term used to indicate the broad range of carbon materials having a tailored nanoscale dimension and functional properties that significantly depend on their nanoscale features. Carbon nanotubes (CNT) and graphene belong to this class of materials comprising many more types of carbon materials, such as nanofibers, fullerene and ordered mesoporous carbon (OMC).

This kind of material find increasing relevance for the development of advanced, sometimes radically new, catalysts, even if carbons (mainly in the form of active carbons) are already extensive applied as support for catalysts. In particular, nanocarbon materials have potential advantages also in comparison to active carbon, such as tailored pore structure, reduced microporosity, reduced number of defects and impurities and, finally, specific active sites. In catalysis, carbon based materials can be used as support for active phase or directly as metal-free catalysts; their catalytic activity is due to the presence of surface functional groups, edge sites, defects and heteroatoms.

The OMC are carbon materials with high surface area, pore dimensions between 2 and 50 nm and an ordered structure. Moreover, the OMC can be synthesized through mainly two kinds of methods: hard-templating and soft-templating, both employing a sacrificial templating agent that controls the order degree and the formation of mesopores.

2.1.1 Mesoporous carbon synthesis via soft and hard-templating method

The synthesis of porous carbon with high surface area can be achieved by various methods, such as catalytic activation of carbon precursors, carbonization of polymer blends containing thermally decomposable components or the carbonization of resorcinol-formaldehyde aerogels[1]. However these materials often possess a broad pore size distribution.

One suitable strategy, to obtain material with narrow and controlled pore size distribution, is the replication of a rigid template material which already possesses controlled mesoporosity. Using this hard templating method approach and mesoporous silica as template, Ryoo et al.[2, 3] and Hyeon et al.[4] pioneered the synthesis of ordered mesoporous carbon (OMC). The synthesis procedure involves infiltration of the pores of the template with appropriate carbon precursor, its carbonization, and subsequent template removal. Then the hard-templating has been improved using a variety of mesoporous oxides, but it also inherits severe drawbacks. In particular, the necessity of removing the inorganic template employing hazardous chemicals such as HF or NaOH is a drawback in industrial applications. Moreover, facile control over the pore size and structure of the classic hard-templated OMCs is obstructed by the fact that the carbon pore system represents the inverse structure of the template porosity; consequently, the wall thickness of the mesoporous oxide determines the pore size of the carbon material. In addition, other limitations have already emerged for the hard templating strategy, such as the high number of experimental steps[5]: (a) preparation of ordered mesoporous silica/surfactant composites; (b) removal of surfactant molecules by calcination, extraction, or other techniques; (c) filling of suitable carbon precursors into the template pores; (d) carbonization of the carbon precursors inside the pore system of mesoporous silica; (e) removal of silica template (**Figure *47***).

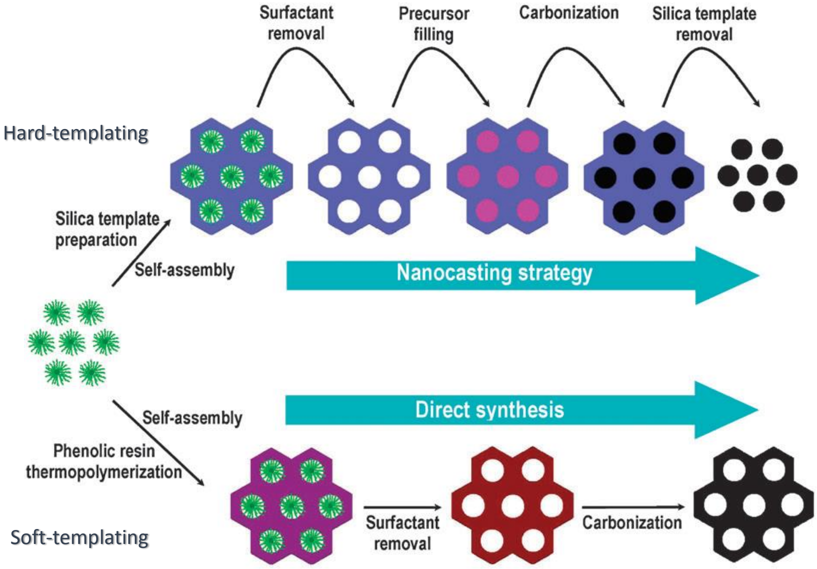

Figure 47 Two typical strategies for the preparation of OMCs (adapted from Ma et al.[5]).

In conclusion, the hard-templating strategy is an expensive, complicated and time-consuming process, consequently is not suitable for large-scale production and industrial applications.

Meanwhile, much progress has been achieved on soft-templating method by self-assembly of copolymer molecular arrays and carbon precursors. This new method for the OMCs preparation shows many advantages compared with the previous one. First, fewer steps are needed in the preparation process (**Figure *47***): (a) self-assembly of phenolic resin and block copolymer surfactants into three-dimensional ordered mesostructures according to corresponding symmetries; (b) removal of the surfactants leaving the mesoporous polymers and opened pores with the dimension and shape depending on the size and structure of the supramolecular aggregates; (c) carbonization of the mesoporous polymers to give the final mesoporous carbon materials.

The soft-templated carbon materials are more varied and mechanically stable due to the continuous framework. Their formation is dependent on the temperature, type of solvent and ionic strength, which makes the pore structure and surface propertied easy to adjust[5]. The entire procedure is low-cost, simple, convenient and suitable for large-scale industrial production. Due to these many advantages and the resultant materials, the attention will be focused on the different procedures, which are based on the soft-templating strategy.

In general, the synthetic procedure requires a phenolic resin, as carbon precursor, and a block-copolymer, such as PEO-PPO-PEO, as templating agent and acidic or basic conditions[6]. Once the carbon precursor is isolated, a curing treatment is performed for the reticulation of the resin. In order to provide a stable framework that withstands the template removal, carbon precursor must undergo a stabilization process, which can be achieved by the curing treatment[1]. Lastly, a pyrolysis step is needed for templating agent removal and transformation of the resin into carbon.

The synthesis mechanism is based on the hydrogen-bonding interaction between templates and precursors, in particular between the PEO-containing block-copolymers and the hydroxyl-groups-containing organic precursors. Indeed, in order to form a mesostructured phase from a structure-directing agent and precursor, a driving force must exist for microphase separation. The driving force for micelle formation and self-assembly of the structure-directing agent, usually a block-copolymer, is based on the constituent blocks of the polymer possessing different affinities to the precursor resin than the other blocks. This can be achieved by selecting carbon precursors containing a large number of hydroxyl groups (-OH), which can strongly interact with the polar parts of the structure-directing agent block-copolymers[1]. Furthermore, precursor aggregates should be small enough to enable assembly around micelles. The most commonly employed mechanism for self-assembly is the I^0S^0 mechanism, where I represents –OH or –NH moieties of the carbon precursor and S represent hydrophilic blocks of block-copolymers, respectively[1]. Indeed, the mechanism relies on hydrogen bonding between template polymer blocks and precursor resin. In general, the I^0S^0 mechanism involves both the neutral polymer blocks and precursor molecules in the absence of electrostatic interactions. However, Dai et al. recently reported that under highly acidic conditions the self-assembly of polymeric precursor can also be driven by $I^+X^-S^+$, mechanism; where X represents counter ions (Cl^- in this case), along with the normal I^0S^0 mechanism[7]. The acidic conditions induce protonation of phenol molecules (or their derivatives) and of cross-linked phenols. Moreover the EO blocks of PEO-containing block-copolymers (Pluronic) are also protonated. Using Cl^- as a mediator, coulombic interaction can then facilitate the $I^+X^-S^+$ mechanism and enable the self-assembly of surfactant-polymer nanocomposites[7].

Ordered mesoporous carbon materials can be successfully synthesized through different pathways, always based on soft-templating method:

- EISA (Evaporation Induced Self Assembly) method
- Dilute aqueous route
- Macroscopic phase separation

The EISA method avoids the cooperative assembling process between the precursor and the surfactant template. Indeed the resols assembly on the block-copolymer is driven by the increasing concentration of template due to the evaporation of the solvent. Then the obtained solid has to be cured and pyrolysed to have the carbon material. The obtained carbons exhibit well-structured porosity with high surface area, large pore volume and uniform pore size.

EISA is a facile method under wide synthetic conditions and since the mesostructures are formed on the surface, it meets the demands of preparing mesostructured films. Ethanol and other organic solvents, such as methanol, acetone and THF, can be used as a solvent, but water is not adopted because the evaporation is too slow.

The dilute aqueous route consists in a surfactant induced self-assembly method in aqueous solution, which has been widely used in the synthesis of many ordered mesoporous siliceous materials and it can be an alternative path to prepare mesoporous carbons. The ordered mesostructures derived from this method have advantages of few defects, easily tailored pore sizes, and well-controlled morphologies. Compared with EISA method, the aqueous route exhibits better reproducibility and an unlimited fabrication batch size, which is suitable for industrial production.

Concerning the macroscopic phase separation, when resorcinol or phloroglucinol is used as the precursor to polymerize with formaldehyde in an acidic system, it undergoes a macroscopic phase separation process during the generation of ordered mesoporous carbons[7,8]. For example, Zhang and co-workers synthesized ordered mesoporous carbons through the self-assembly of resorcinol/formaldehyde and surfactant F127 in the mixed solution of ethanol and water [9,10]. The synthesis was performed in a strong acidic system with hydrochloric acid as the catalyst. After adding the precursors, F127 and hydrochloric acid, into the ethanol/water solution, the mixture turned cloudy and began to separate into two phases. The upper phase (consisting mainly of water/ethanol) was discarded, whereas the composite of resorcinol/formaldehyde oligomers and F127 was formed in the lower polymer-rich phase. After aging, curing and carbonization, mesoporous carbons could be obtained. The phase separation of the polymer-rich phase from the ethanol/water solvent is the key step in their synthesis. Resorcinol and formaldehyde first polymerized slowly to ethanol-soluble resol oligomers with a low polymerization degree, which would interact with the PEO segments of the self-assembled triblock copolymers through hydrogen bonds. When the linear resols further polymerized to each other to achieve a relatively large molecular weight, a glue-like polymer product began to separate from the solvent, resulting in macroscopic phase separation.

The larger amount of resorcinol would lead to stronger hydrogen-bonding interactions and the longer aging time would lead to less defects. The resultant mesoporous carbons possessed high surface areas and large pore volumes. The same macroscopic phase separation phenomenon was also observed when Dai and co-workers performed the synthesis of ordered mesoporous carbons in the acidic solution by using phloroglucinol[8] or resorcinol[7] as the monomer.

The structure and properties of soft-templated OMCs depends on:

- Carbon precursor
- Templating agent
- Swelling agent
- Catalyst
- Solvent
- Reticulation time
- Pyrolysis temperature

The modifications of these parameters lead to the formation of carbon materials with different features and properties. In particular, the choice of carbon precursor is critical to the formation of mesoporous carbons. Typically, the carbon precursors employed for mesoporous carbon formation are phenolic resins, having a very good affinity with PEO-containing block-copolymers.

Precursor molecules typically employed in the resin formation, that precedes the synthesis of soft-templated mesoporous carbon, are phenol, resorcinol and phloroglucinol (**Figure** ***48***).

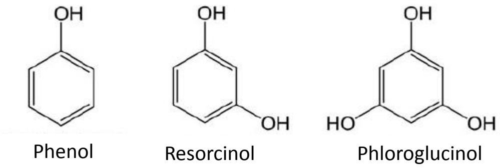

Figure 48 Chemical structure of precursor molecules commonly used in the preparation of the precursor resin for the soft-templating of mesoporous carbon materials.

Chemical cross-linking of these molecules, often with formaldehyde acting as a linker, forms oligomers that co-assemble with the template micelles. The reactivity of the different monomers with formaldehyde follows a trend of phloroglucinol >> resorcinol >> phenol[5]. Under acidic conditions, the reaction and polymerization of these monomers with formaldehyde involves the protonation of hydrated formaldehyde and electrophilic aromatic substitution reaction of phenols[11]. Therefore, the concentration acid and the reactivity of the different phenols are two key factors in determining the polymerization rate of phenolic resins.

There are also some illustrations of replacing formaldehyde in order to have more green synthetic route. As mentioned above, phloroglucinol reacts faster than resorcinol and phenol with formaldehyde. To obtain an ordered porous carbon, the fast reactivity of phloroglucinol must be countered by a low acid concentration or a slower reacting aldehyde than formaldehyde. Glyoxal is a slow reacting aldehyde and a potential substitute of formaldehyde.

Concerning the templating agent, it should interact strongly with both resin precursor and be easily removed. The PEO-PPO-PEO type amphiphilic triblock copolymers, such as F127, F108 and P123, are most widely used. The organic-organic self-assembly is driven by the hydrogen-bonding interaction, and the PEO-PPO-PEO templates can be easily removed at low temperature without destroying the resin framework, because they contain many oxygen atoms and have a low glass transition temperature. Although cationic quaternary ammonium and non-ionic alkyl PEO oligomeric surfactants were also used to prepare mesostructured resin-surfactant composites, these templates were difficult to remove.

The type of templating agent and its ratio with phenols influence the structure of the final carbon and the pore size[12].

Swelling agents can be also used for increasing the pore size. They are added during the formation of the micelles and, interacting with the hydrophobic part of the block-copolymer, they increase the volume of the micelles and consequently the dimension of the pores. Examples of swelling agent can be hydrocarbon, as decane[5].

The polymerization of phenolic resin can be performed in either acidic or basic systems. The most commonly used catalyst are HCl and NaOH. The acidic conditions lead to a more time-consuming synthesis, but more controllable and guarantee a better solubilisation of the templating agent. Alternative catalysts have been studied[5], such as glutamic acid, citric acid; while for basic conditions, amino acid, such as lysine or ammines, can be employed.

For the mesoporous carbon synthesis, the most commonly used solvents are ethanol, THF, water or a mix of them.

The reticulation can be performed through a catalytic or thermic (curing) way. The latter strategy is usually employed for phenolic resin, which have a reticulation temperature around 100°C. The time of curing treatment influences the structure stability and the order degree of the final material. Indeed, the curing treatment is necessary for stabilizing the resin framework, before the template removal[1].

The pyrolysis represents the last step of the soft-templating synthesis and it is necessary for the removal of the templating agent and for the carbonization of the resin. In order to obtain mesoporous carbons, the templating agent should decompose at a lower temperature than the resin carbonization one. Usually, the pyrolysis is performed in an inert atmosphere; although in some cases mix with oxidant agent is also used. Typically, the pyrolysis temperature ranged between 350 and 2600°C, but for the most common carbon precursor, temperatures higher than 600°C are necessary for a complete carbonization. Moreover, with increasing the pyrolysis temperature, the carbonization degree increases together with the possibility of structure collapse. Consequently, the choice of the pyrolysis temperature is a key factor for having at the same time a good carbonization degree and a material with high surface area and stable structure.

2.1.2 Carbon material as catalyst

Due to their unique properties, such as chemical stability, electronic conductivity, defined pore size, large surface area and high pore volume, ordered mesoporous carbons are increasingly applied in fields such as sorption, catalysis, energy storage and biomedicine.

In the catalysis field, the carbon materials have been used mostly as support for active phases; although, in the last years, their application directly as catalyst is increasing.

In particular, in heterogeneous catalysis carbon materials attract a growing interest due to their specific characteristics, which are mainly: (i) resistance to acid/basic media, (ii) possibility to control, up to certain limits, the porosity and surface chemistry and (iii) easy recovery of precious metals by support burning resulting in a low environmental impact[13].

In general, they can be used in gas and liquid phase; the only limitations for this application are the hydrogenation and oxidation reactions. In the former case, temperature higher than 300 °C cannot be used, while in the latter case 400°C should not be overcome[14].

The most used carbon materials in catalysis are active carbons due to their high surface area, chemical inertness and mechanical stability. Recently, thanks to also a better understanding of the surface chemistry of carbons, the range of industrial use of active carbons as support in catalysis has been extended to new areas, such as environmental protection (VOC oxidation, dehalogenation and oxidation reactions), selective oxidation and hydrogenation and synthesis of fine chemicals[15]. Although active carbon surface area and porosity can be tuned within some range by controlling the preparation method, in large part their high surface area is due to micropores that can be a dramatic drawbacks in various catalytic reactions.

The carbon-based nanomaterials have not yet found industrial applications in large scale. The main reason can be the higher cost to performance ratio of these materials with respect to active carbon, but with actual possibility of mass production, the cost could become well comparable to other alternative materials, increasing also the possible catalytic applications[15].

Among all the different catalytic applications of nanocarbons, their direct use as metal-free catalyst is one of the most interesting, but a deep understanding of their catalytic activity is fundamental.

In general, the carbon-based materials have numerous types of catalytic sites, depending on the kind of material, the structure and the possible treatment done on the material itself[16].

Some examples of type of active sites are:

- Surface functional groups
- Defects and edges
- Dopant heteroatoms (such as N, O, B)

Concerning the surface functional groups, they can be composed by heteroatoms such as O, N, S, P and halogen and they can be acid, basic or neutral groups[17](**Figure *49***).

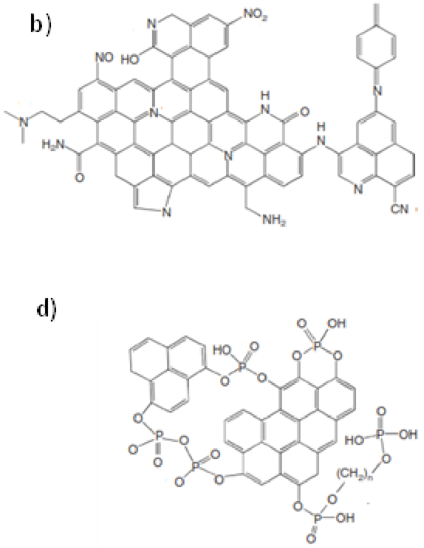

Figure 49 Surface functional groups in carbon material containing (a) oxygen, (b) nitrogen, (c) sulphur and (d) phosphorous[17].

The O-containing surface functional groups are the most common functionalities present on the carbon surface.

Oxygen-containing functionalities are for example carboxylic, phenolic groups and ketones. Generally, oxygen-containing functionalities are considered as acidic or basic. Acidic surface groups are formed when the carbon surface is exposed to oxygen via reactions with oxidizing agents from solutions or gas phase, either at room or high temperatures. Oxidative treatments have been designed to produce acidic carbon surfaces with different distributions of oxygen-containing groups. On the other hand, basic groups are formed when an oxidized surface is reduced by heating in an inert atmosphere at high temperature. The decomposition of acidic groups (e.g., carboxylic acid, lactone, phenol groups) results in active sites at the edges of the graphene layers, which upon cooling in an inert atmosphere and re-exposure to air, attract oxygen, forming basic functional groups[17].

Besides the O-containing surface functional groups, N and S-containing functionalities are the most studied. For example, amines increase the basic character of the material and become important in some types of reactions such as transesterification of triglyceride[18] and Knoevenagel condensation reactions[6]. Concerning the S-containing functionalities, they are important in esterification and condensation reactions[16].

Concerning the edges and defects, the carbon atom in an ideal graphene sheet, or in the derived nanostructure, is formally inactive, because it has no possibility to coordinate molecules, except through delocalized electrons. The electronic structure in an ideal CNT, for example, has π-electrons delocalized across the whole cylindrical structure. However, at the end of the nanotube, the equivalence of the bond is broken and the degree of the π-electron delocalization decreases. Several resonance structures are possible and, due to the easy change of hybridization, many possible defects are also present in the basal plane. There are topological defects, which lead to re-hybridization (C5 and C7 instead of C6 lead to re-hybridization between sp^2 and sp^3) and incomplete bonding defects (vacancies, dislocation). These defects influence not only the nanostructure, but also functional and catalytic behaviour. Indeed, edge sites and defects in basal plane are the starting point to create functional groups. However, they can play a direct role as catalytic centres in some reactions, although this aspect of their reactivity was studied in much less detail than the catalytic behaviour of functional groups. It should be remarked that defects and disordered local structures influence many properties of nanocarbons, from electronic and heat transport to semiconducting behaviour, surface mobility of adsorbed species and adsorption properties. They thus may also influence the catalytic behaviour. An interesting study on the direct role of the edge sites and defects in determining the catalytic behaviour of nanocarbons was made by Zhong at al.[19] that investigated the behaviour of nanodiamond in the decomposition of methane. They found that the initial rate is linearly dependent on the number of –CH=CH– defective sites. Thermal treatment improves the ordering of surface atoms, resulting in a lower activity.

Both the nature and the amount of nanocarbon active centres, related to the defects in basal planes or dandling bonds at the edge sites and the species formed by interaction of these sites with heteroatoms, are greatly depending on the of nanocarbon, the preparation procedure and post-treatment as well[16]. However, the different active centres have also a different thermal stability as well as stability during the catalytic reaction. It is necessary not only to have specific active centres, but especially centres stable during the reaction.

It should be clarified that functionalization means that heteroatom is introduced in the carbon material associated with covalently bonded functional groups on carbon basal surfaces or edge planes. Doping instead does not necessarily incorporate foreign atoms in the sp^2 network of graphitic carbon, while substitution means replacing a sp^2 bonded carbon atom with a heteroatom. However, there are not clear proofs that elements such as S and P can really substitute carbon, differently from N, B and O. The substitution alters significantly the electronic properties of nanocarbons, in addition to create functional and catalytic sites. N and O are electronegative with respect to C; consequently, substitution of C with these heteroatoms breaks the charge neutrality of atoms in sp^2 carbon lattice and form reactive sites. While there are many papers showing that doping with heteroatoms improves the catalytic behaviour of nanocarbons, demonstration of the direct catalytic role of substitutional heteroatoms are more limited. For example in the ORR (Oxygen Reduction Reaction) electrodes doping with N, O, B, P, S atoms changes the catalytic reactivity by facilitating the O_2 adsorption, increasing the total number of active sites and improving the surface hydrophilicity[20].

Moreover there is a general agreement that the role of substitutional nitrogen is to modify the properties of near carbon atoms. For example, the N-doped CNTs for acetylene hydrochlorination show a linear relationship between quaternary N content and activity. The presence of N increases not only the catalytic activity, but also the adsorption capacity; for example, the insertion of N in the carbon increases the basic character and consequently the CO_2 adsorption capacity[21].

2.2 Materials and methods

The OMC samples were synthesized through the soft-templating method, with the macroscopic phase separation strategy. The synthetic procedure started from a phenolic resin obtained through the reticulation of phloroglucinol and glyoxal in acidic environmental, while Pluronic F127, a PPO-PEO-PPO block-copolymer, was used as templating agent. After the phase separation, the gel obtained was cured and finally pyrolysed for the template removal and the carbonization of the carbon precursors. In this work, the synthesis followed for the OMC preparation was firstly proposed by Mayes et al.[22], where the formaldehyde was substituted with glyoxal and phenol by phloroglucinol, in order to have a more green synthesis.

With the aim to generate O-containing surface functional groups, some OMC samples were treated after the synthesis in liquid phase with HNO_3 or H_2O_2 and in gas phase with N_2O. Moreover, N heteroatoms were added during the synthesis of the carbon material. In this case, the soft-templating synthesis was performed in basic conditions, using an amine and starting from the same carbon precursors, to obtain N-containing carbon and the curing treatment was made in autoclave for short time, giving a carbon monolith[21].

Lastly, functionalized carbon materials were tested in the oxidation of benzyl alcohol to benzyl aldehyde [23, 24]. to understand the effect of the surface functional groups on the catalytic behaviour.

2.2.1 Mesoporous carbon synthesis

For the synthesis of mesoporous carbon in acidic conditions, Phloroglucinol, Pluronic F-127, Glyoxal (40% w/w in water), ethanol (≥ 99.8%) and HCl (37% w/w) from Sigma-Aldrich were used as chemicals.

The synthesis of the mesoporous carbon was performed as reported elsewhere[22], increasing the amount of reagents with the aim to obtain a greater quantity of the desired material.

In a typical experiment, 11,17 g of Pluronic F-127 were solubilized in a solution of ethanol (43,8 ml) and HCl (44,3 ml, 3M). Under stirring at room temperature, 11,17 g of Phloroglucinol were added to the solution; once dissolved, 12,6 ml of glyoxal solution were added and the solution was stirred for 20 minutes, until a phase separation was observed. Then the mixture was stirred for 30 minutes. The gel was separated from the solvent by centrifugation at 4000 RPM for 15 minutes, then the solvent was decanted off the gel layer. 4,9 ml of THF and 24,3 ml of ethanol were added to the gel and the mixture was put into glass Petri dishes and allowed to dry in a fume hood for 24 hours. The dried material was cured for 24 or 36 hours at 80°C in an oven. After the curing treatment, the resin obtained was pyrolysed at 850°C, heating rate 3°C/min, for 2 hours under N_2 flow. The samples cured for 24 and 36 hours were referred to MC24 and MC36, respectively.

2.2.2 Post-synthesis functionalization treatments

The post-synthesis functionalization was performed in liquid phase with HNO_3 or H_2O_2 and in gas phase with N_2O on the mesoporous carbon obtained with 24 hours curing treatment (MC24).

Functionalization with HNO_3: For 1 g of carbon 10 ml of 6,34 M HNO_3 (Sigma-Aldrich, 65% w/w) solution were used; the mixture was stirred at 50°C for 3 hours[25]. Then the solid was filtered, washed with water and dried in an oven at 110 °C overnight. The sample prepared was named HNO3MC24.

Functionalization with H_2O_2: For 1 g of carbon 10 ml of 8,82 M H_2O_2 (Sigma-Aldrich, 30% w/w) solution were added and the mixture was kept under stirring at room temperature for 2 hours; then the solid was filtered and dried in an oven at 60°C for 24 hours [26]. The sample prepared was named H2O2MC24.

Functionalization with N_2O: The carbon, in the form of pellet (mesh 40-60), was placed in a glass reactor and then heated at 400°C for 7 hours with a 10°C/min heating ramp under a N_2O/N_2 gas mixture (50/50 v/v). The sample prepared was named N2OMC24.

2.2.3 Nitrogen insertion

The N-containing carbon was obtained using Phloroglucinol, Pluronic F-127, Glyoxal (40% w/w in water), ethanol (≥ 99.8%) and 1,6-diaminohexane (98%), also named DAH, from Sigma-Aldrich.

The procedure followed for the synthesis of the N-containing carbon was slightly modified with respect to the original one[21]. In particular, the steps were maintained the same, only the carbon precursors were changed; resorcinol and formaldehyde, added as formalin, were substituted by phloroglucinol and glyoxal.

In a typical experiment[21], 1,25 g of Pluronic F-127 were solubilized in a solution of 11,4 ml of ethanol and 8,21 ml of water; then under stirring 3,43 g of Phloroglucinol were added. Once dissolved, 0,08 g of DAH (1,6-Diaminohexane) were added and the mixture was kept under stirring for 30 minutes, when the solution became light yellow. Then 4,7 ml of glyoxal solution were added under stirring and after 10 minutes a white emulsion was obtained. The mixture was transferred in an autoclave and placed in an oven for 4 hours at 90°C; at the end of the curing treatment a monolith was obtained which was dried at 50°C in air for 24 hours and then pyrolysed at 850 °C, reached with 3°C/min ramp, for 2 hours under N_2 flow. The sample obtained in the form of monolith was named N-MC.

A brief scheme of the different synthetic routes of mesoporous carbons is shown in **Figure *50***.

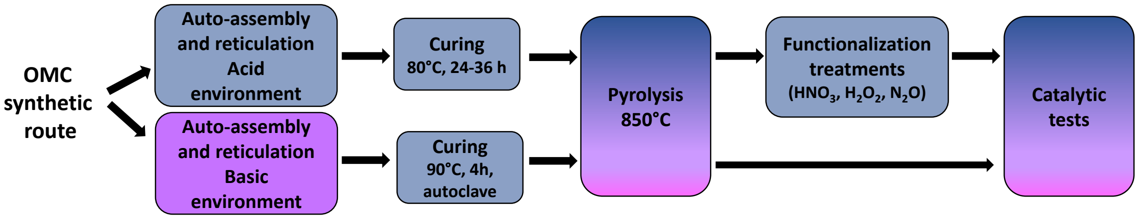

Figure 50 Scheme of the different synthetic route of mesoporous carbons.

All the synthesized samples are reported in **Table *7*** with the main differences.

Sample name	Synthetic environmental	Curing time (h)	Post-synthesis treatments
MC24	Acid	24	-
MC36	Acid	36	-
HNO3MC24	Acid	24	6.34M HNO_3, 3h, 50°C
H2O2MC24	Acid	24	8.82M H_2O_2, 2h, RT
N2OMC24	Acid	24	N_2O/N_2 (50/50 v/v) 7h, 400°C
N-MC	Basic	4	-

Table 7 Summary of the carbon samples prepared in this work.

2.2.4 Characterization methods

Many different characterization techniques were employed on the prepared samples with the aim to discover their structure, features, composition and the degree of functionalization.

Raman spectra were obtained in a Reinshaw RM 1000 micro Raman spectrometer with an excitation wavelength of 514 nm, in a range of acquisition between 4000 and 200 cm^{-1}.

XRD measurements were carried out at room temperature with a Bragg/Brentano diffractometer (X'pertPro PANalytical) equipped with a fast X'Celerator detector, using a Cu anode as the X-ray source (Kα, $\lambda = 1.5418$ Å). The diffractograms were collected at two different 2θ angle range: low angle, from 0.5 to 15 °2θ counting every 0.02 step for 15 s, and medium angle, from 10 to 90 °2θ counting every 0.1 step for 10 s.

N_2 adsorption/desorption isotherms (77 K) were performed in a Micromeritics ASAP 2020 instrument. Samples were previously outgassed for 2 hours at 150°C and 10 µmHg, and then heated for 4 hours at 350°C. Specific surface area values were obtained by multi-point BET equation 0.005–0.01 p/p^0 range for mesoporous carbon and 0.005-

0.5 p/p^0 range for N-containing carbon. The pore size distribution was calculated from the adsorption branch using NLDFT.

TEM images were acquired by a TEM/STEM FEI Tecnai F20 working at 200 kV. The samples were prepared by dispersion of the powder in ethanol and deposition in a holey-carbon film supported with a copper grid.

Temperature programmed desorption (TPD) analysis were performed using a Micromeritics Autochem II 2920 instrument coupled with MKS Cirrus MS analyser. The samples were heated in He flow (20 ml/min), at 100°C, 5°C/min, for 20 minutes, then the temperature was raised to 800°C, 5°C/min and maintained for 20 minutes.

The C, H and N contents were measured on an Elemental Analyser FLASH 2000 instrument.

The behaviour of the material during the pyrolysis was followed through thermogravimetric analysis (TGA) performed in a TA Instrument Q600 coupled with a FT-IR spectrometer. For studying the pyrolysis of the resin the samples were heated at 850°C, 5°C/min, under nitrogen flow (100 ml/min) and then kept at 850°C for 30 minutes. For the study of the combustion of the N-containing carbon (N-MC), the samples were heated at 850°C, 5°C/min, under air flow (100 ml/min) and then kept at 850°C for 30 minutes.

2.2.5 Catalytic tests with benzyl alcohol oxidation

The liquid phase oxidation of benzyl alcohol over the prepared carbon materials was carried out using a 100 ml autoclave (Parr Instruments) reactor, equipped with a mechanical stirrer (0–600 rpm) and temperature and pressure gauges. The reactor was charged with 25 ml of CH_3CN containing 0.03 g of carbon catalyst and 0.12 g of benzyl alcohol.

The autoclave was purged three times with O_2 and then pressurized at 10 bar. The temperature was increased to 160°C and the reaction mixture was stirred at approximately 400 rpm for 4 h. The initial time (time 0) for the reaction was taken when the set point temperature was reached. At the end of the reaction, the reactor was cooled down to room temperature and the solution was centrifuged for 20 minutes at 4000 rpm. Then the supernatant was filtered with a syringe equipped with a 0.45μm filter. Then 1 ml of the filtered solution was diluted 1:10 with CH_3CN before the analysis with an Agilent Infinity 1260 liquid chromatograph equipped with a DAD UV-Vis detector and an Agilent POROshell 120 C-18 column. The compound identification was achieved by calibration using reference commercial samples.

2.3 Results and discussion

The aim of this work was twofold: i) to prepare carbons with an optimized mesopore structure for catalytic applications using green chemicals; ii) to introduce surface functional groups and N heteroatoms without damaging the ordered structure giving rise to catalysts active in oxidation reactions.

In particular, the effect of the curing treatment on the mesoporous structure and textural properties of mesoporous carbon synthesized with Pluronic F127, as templating agent, and replacing formaldehyde by glyoxal and phenol by phloroglucinol, as reported by Mayes et al.[22] was investigated.

Then O-containing surface functional groups were generated through post-synthesis oxidative treatments with HNO_3, H_2O_2 and N_2O. While N heteroatoms were added during the synthesis of the carbon material, using an amine as nitrogen source and obtaining a carbon monolith through the curing in autoclave[21]. Lastly, functionalized carbon materials were tested in the oxidation of benzyl alcohol to benzyl aldehyde [23, 24]used as a model reaction to understand the effect of the surface functional groups on the catalytic behaviour.

2.3.1 Pyrolysis of the resin

The chemical composition and structural evolution of the carbon material are strongly dependent on the carbonization temperature[27] being the pyrolysis temperature a key parameter in the preparation procedure. Thus the pyrolysis temperature was firstly investigated. It was selected based on the TGA coupled with FT-IR analysis shown in **Figure *51***.

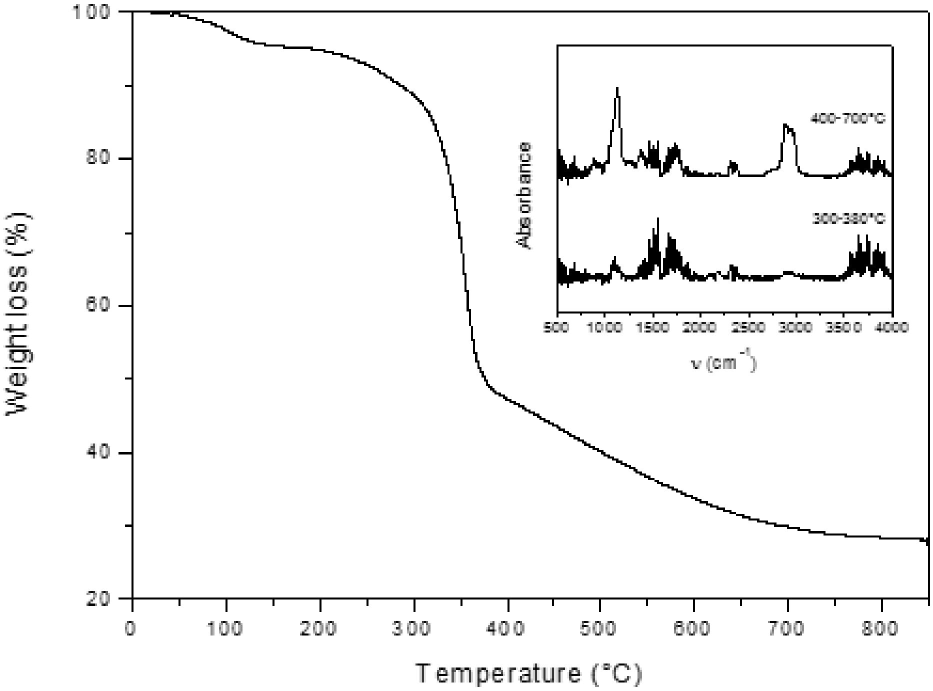

Figure 51 TGA analysis of precursor of MC24 sample. FT-IR spectra of the gases evolved in the 300-380 and 400-700 °C range during the observed weight losses.

Three weight losses were recorded in the TGA curve. The first one, till 120 °C, is due to the remove of physisorbed water. The weight loss, from 300 to 380 °C, is attributed to the templating agent decomposition. Indeed, FT-IR spectra of the evolved gases showed bands characteristics of ethers (**Figure** ***51***), which derive from the radicalic decomposition of the templating agent[28]. The decomposition of both residual templating agent and phenolic precursor occurred in the 400 and 700°C range accompanied by the removal of ethers, CO and CO_2, as shown in the FT-IR spectra of the evolved gases (**Figure** ***51***).

In conclusion, the TGA coupled with FT-IR analysis demonstrated that the carbonization of the resin is completed at a temperature above 700°C; on the other hand higher temperature causes a decrease of oxygen functionalities in the material[12]. Thus 850 °C was chosen in this work as pyrolysis temperature for all the prepared resins, as reported elsewhere[22].

2.3.2 Influence of the curing time

The influence of the curing time, 24 and 36 h, on the textural and structural properties of the carbon materials was firstly studied. XRD patterns recorder at low angle of MC24 and MC36 samples, recorded at low angle are reported in **Figure *52***.

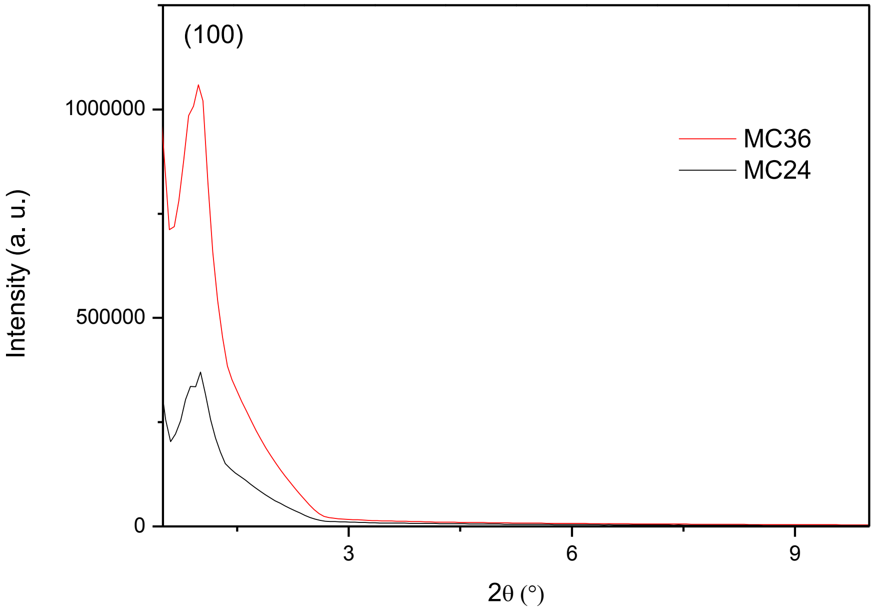

Figure 52 XRD patterns of MC24 and MC36 recorded at low angle.

For both samples, the (100) reflections were identified, suggesting a mesostructural order[29]. The estimated d-spacing values are typical of mesoporous carbon and around 88 Å for MC24 and 90 Å for MC36 sample. The reflection intensity is higher for MC36 sample, suggesting a higher long-range order. Indeed the curing treatment is needed to provide a sufficiently stable and rigid framework before the template removal[1]. Thus, with increasing the curing time a more stable structure can be obtained, leading to the improvement of long-range order.

N_2 adsorption/desorption isotherms at -196°C (**Figure *53***) show the plateau at high relative pressures and characteristic Type IV isotherm of mesoporous materials [12, 22].

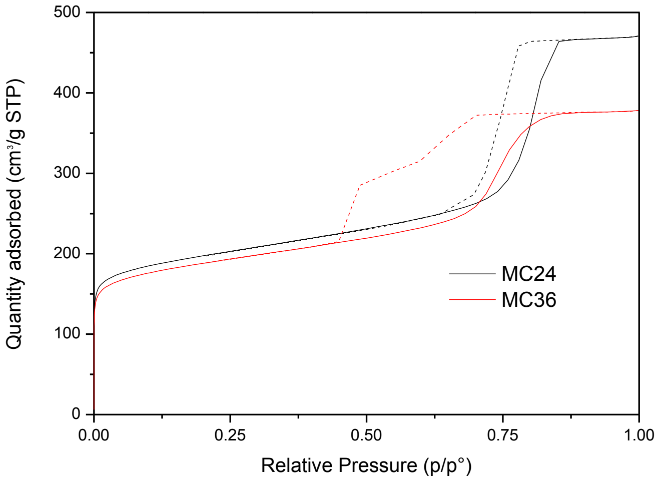

Figure 53 N_2 Adsorption-desorption isotherms of MC24 and MC36 samples.

Two different types of hysteresis and consequently pore system, were present: H1 hysteresis for MC24, which was indicative of open cylindrical pores, and H5 hysteresis for MC36, indicating the presence of plugs within the pores. H5 hysteresis can be considered as a combination, two steps desorption, of H1 and H2 hysteresis, as recently reported[30].

However, the adsorption taking place at low relative pressure also indicates the presence of micropores, which were generated inside the carbonaceous framework by solidification and gasification of the polymer[31].

The surface area of the samples prepared are summarized in **Table *8***; they are very similar to those previously reported for mesoporous carbon prepared by organic-organic self-assembly[12]. Although, the surface areas obtained in this case are higher than the one obtained by Mayes at al.[22].

Sample	**S BET (m²/g)**	**SA micro (m²/g)**	**V MICRO (cm³/g)**	**SA meso (m²/g)**	**V MESO (cm³/g)**
MC24	728	545	0.224	183	0.499
MC36	697	529	0.218	168	0.370

Table 8 Specific surface area (S_{BET}), surface area and pore volume due to micro- ($S_A$micro, Vmicro) and mesopores ($S_A$meso, Vmeso) of MC24 and MC36 samples.

The increase of the curing time slightly decreased the surface area of both meso and micropores due to an increased cross-linking within the resin[32].

As the time of curing treatment was increased, the same shape of isotherm was maintained, but the capillary condensation was shifted at lower pressure, suggesting the presence of smaller pores.

DFT pore size distributions in the 0.9-22 nm range confirmed the presence of a narrow mesopore distribution between 7.5 and 16 nm for the MC24 sample (**Figure *54***), which was shifted with respect to the pore size distribution obtained by Mayes at al.[22].

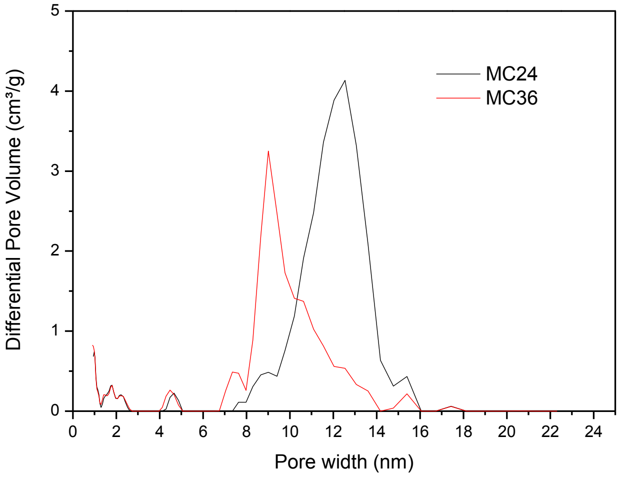

Figure 54 DFT pore size distributions of MC24 and MC36 samples.

The slightly narrower pore size distribution of MC36 sample (from 7 to 14 nm) was centred on 9 nm while, in the case of MC24 sample, the DFT maximum was found at 12 nm. On the other hand, a micropore average size of 0.69 nm was obtained by the HK method regardless of the curing time.

TEM images (**Figure *55***) show that both samples (MC24 and MC36) had an ordered pore distribution; in particular, a hexagonal pore arrangement with pore sizes around 6-7 nm can be observed for these samples, in accordance with the DFT distribution.

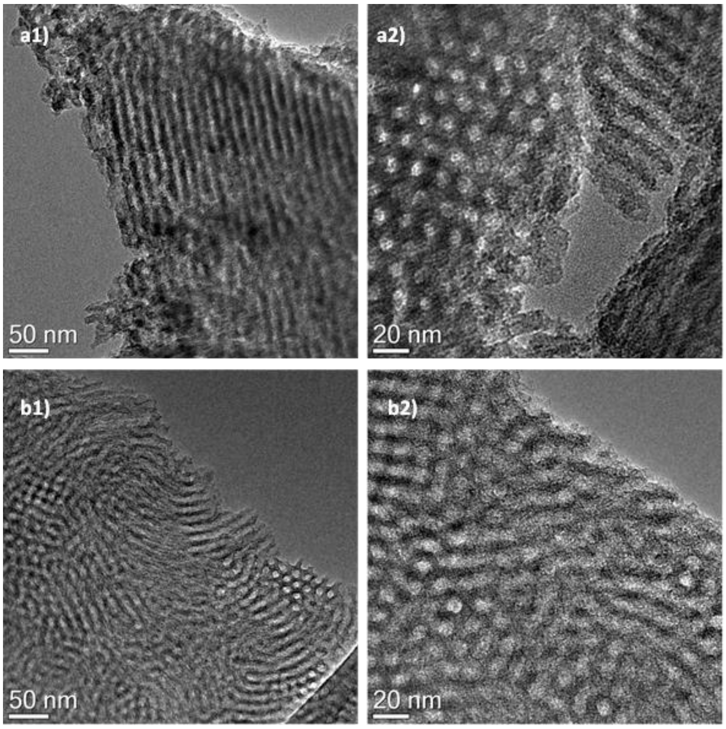

Figure 55 TEM images of a) MC24 and b) MC36 samples.

Wide angle XRD patterns show the characteristic reflections of graphitic carbon[33] (**Figure** ***56***).

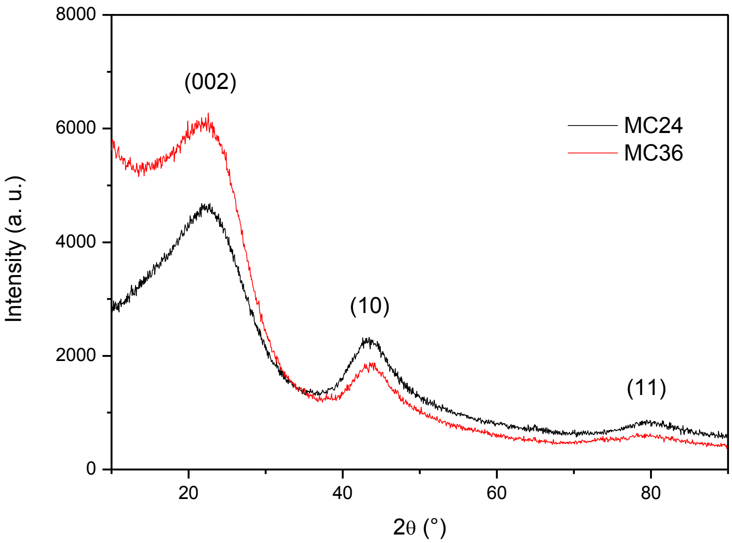

Figure 56 XRD patterns of MC24 and MC36 recorded at medium angle.

The (002) reflections at 22°2θ due to the 3D disposition of carbon planes shifted toward higher °2θ and became more intense by increasing the curing time, bearing out a better packing of the planes within the pore wall. The (10) and (11) reflections, at 44 and 79°2θ respectively, due to the 2D rearrangements of the carbon plane were slightly modified.

The Raman spectra of MC24 (**Figure *57***) and MC36 show the D band, attributed to amorphous carbon, and G band, due to graphitic carbon, at 1350 and 1590 cm^{-1} respectively, in accordance with the spectra obtained by Mayes at al.[22].

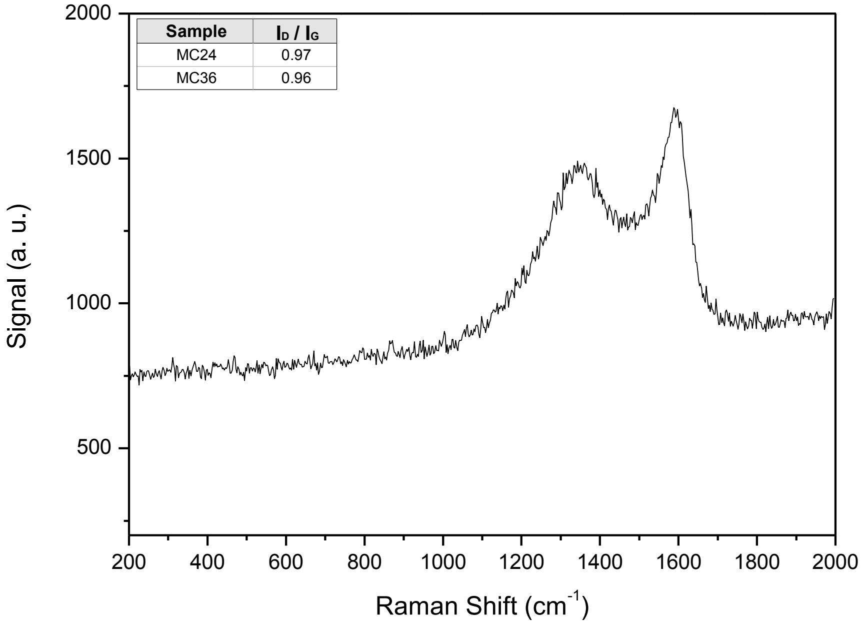

Sample	I_D / I_G
MC24	0.97
MC36	0.96

Figure 57 Raman spectra of MC24 and I_D/I_G ratio of MC24 and MC36 (Table).

A shoulder was also observed in the D band located near 1170 cm $^{-1}$, also due to disordered carbon structure.

The I_D/I_G ratios of both samples were very similar and typical of carbon materials with a structure between nanocrystals of graphite and amorphous carbon[34].

In conclusion, with 24 hours of curing treatment, a higher surface area was obtained; this meant that more surface area would be available for catalytic application. Although the curing time was shorter, an ordered mesostructured was obtained. Moreover, the synthetic procedure was shorter and the pores were larger.

Thus, the activation of the carbon to prepare metal-free catalysts for oxidation processes was performed on the resin cured for 24 h.

2.3.3 Post-synthesis functionalization treatments

The functionalization treatments were performed on the prepared carbon with the aim to enhance the catalytic activity, creating new surface functional groups and obtaining metal-free catalysts. The MC24 material was treated in liquid phase with HNO_3 or H_2O_2, and in gas phase with N_2O.

The composition of the different treated materials obtained by CHN analysis is reported in **Table *9***.

Sample	C content (wt %)	H content (wt %)	N content (wt %)	O content (wt %)
MC24	93	1	-	6
HNO_3MC24	82	1	1	16
H_2O_2MC24	87	1	-	12
N_2OMC24	92	1	-	7

Table 9 CHN analysis results of the synthesized and treated samples.

The carbon content of the as synthesized material (MC24) is over 90%, as previously reported for mesoporous carbon[35, 36].

In general, the oxidative treatments let the O-content increase[37], while the H-content was not modified. Moreover, in the HNO_3 treated sample and in N-MC sample N was also found[38].

The HNO_3 treatment caused the major modification in the composition of the mesoporous carbon, the C, O and H content of the HNO3MC24 was similar to the one reported in literature[39], followed by H_2O_2 and then N_2O treatment.

Surface functional groups are studied through thermal decomposition by MS-TPD analysis[39]. Surface oxygen groups on carbon material decompose upon heating, releasing CO and CO_2 at different temperatures. The assignment of TPD peaks to specific surface groups was challenging because the peak temperatures may be affected by the texture of the material, the heating rate and the geometry of the experimental system used[39, 40, 41].

However, it could be stated that a CO_2 peak at low temperatures results from decomposition of carboxylic acid, while at high temperatures it comes from lactones. On the other hand, thermal treatment of phenols, ethers, carbonyls and quinones originate a CO peak. Finally, carboxylic anhydrides originate both CO and CO_2 peaks around 500°C[39].

The MS-TPD results from the as-synthesized material (MC24) show the presence of some surface functional groups but in lower amount than in treated sample (**Figure *58***).

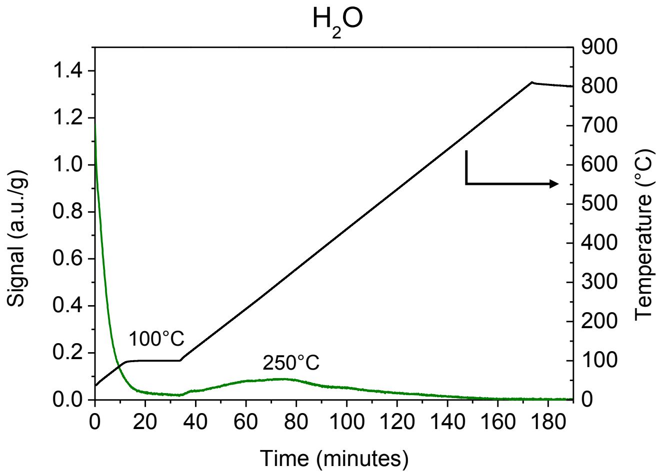

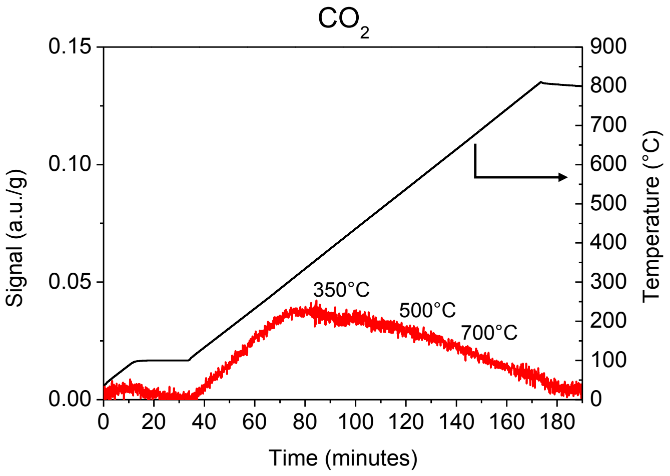

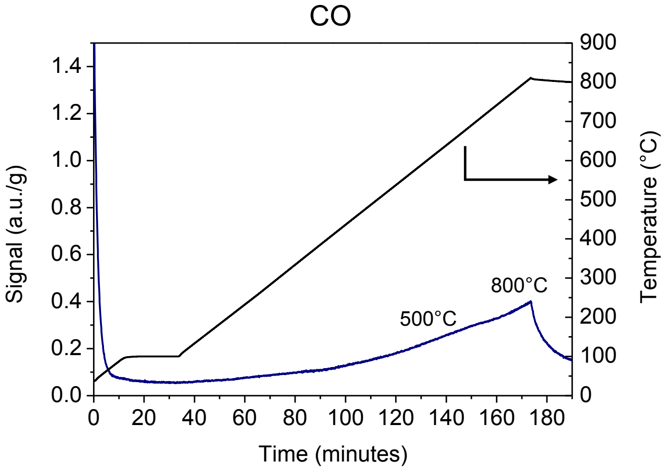

Figure 58 MS-TPD analysis of untreated MC24 sample.

During the analysis MC24 released H_2O at 100 °C, due to physisorbed water, and at 200-300 °C, due to the decomposition of phenol and hydroquinone groups[42]. Moreover, CO_2 was detected at around 350 °C, 500 °C and 700 °C due to the decomposition of carboxylic acid, anhydride and lactones, respectively. The first CO peak, around 500 °C, can be attributed to anhydride, while the one around 800 °C can be attributed to quinones, carbonyl and ether functional groups.

Some oxidative treatments increased the amount of functional groups (**Figure *59***) with respect to the as synthesized sample, which showed more or less the same kind of groups, in agreement with the CHN analysis.

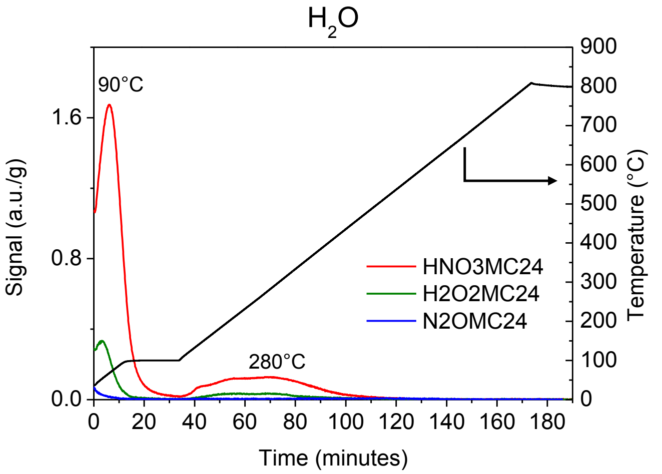

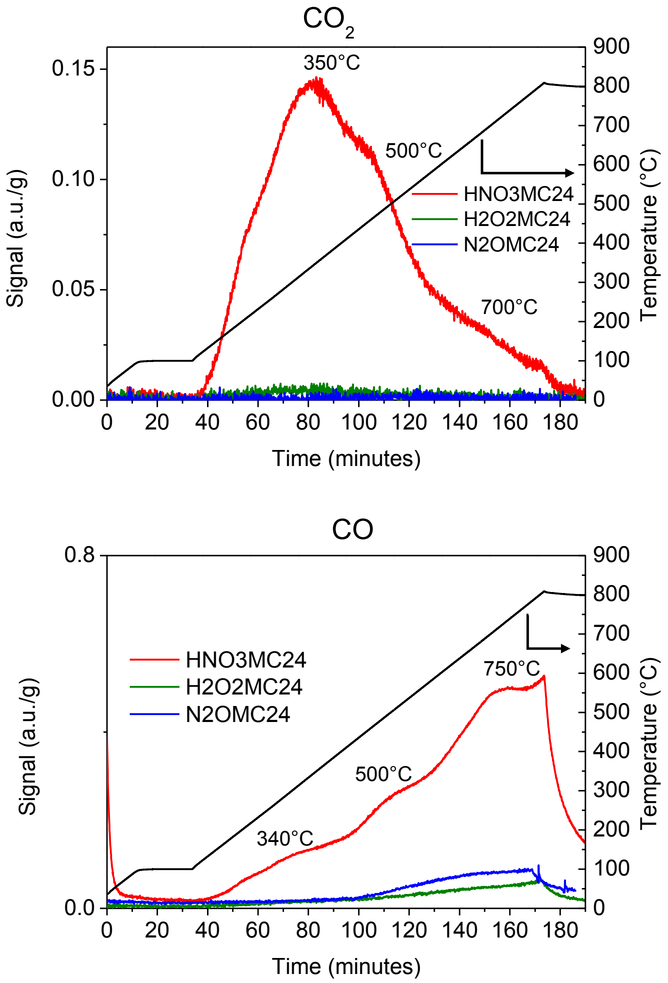

Figure 59 MS-TPD analysis of MC24 samples after post-synthesis oxidation treatment with HNO_3, H_2O_2 and N_2O.

The largest effect of the post-oxidative treatment was observed for the carbon treated with HNO_3[43]. Namely, the amount of released CO, CO_2 and H_2O became higher, suggesting the formation of a larger amount of the surface groups, as explained above for MC24 sample.

The quick decomposition of H_2O_2 and its lower oxidation capacity relative to that of HNO_3, may explain this behaviour[43].

However it should be taken into account that the presence of surface functional groups on the as-synthesized material can also modify the efficiency of the oxidative treatments[44].

The influence of surface functional groups on the reactivity of carbon may also explain the poor effect of the gas-phase N_2O oxidative treatment on the formation of new surface functional groups, conversely to what reported elsewhere[39].

The carbons submitted to oxidation treatments, were further characterized by XRD, N_2 adsorption/desorption and Raman analysis. Besides the surface characteristics, the HNO_3 treatment did not change significantly the texture of the carbon material[39,45].

Low angle XRD confirmed that the mesoporous structure of the carbon was kept after oxidative treatments, even with HNO_3 that generated the largest surface functionalities, as identified by **Figure *60*** where the (100) reflection can be still observed.

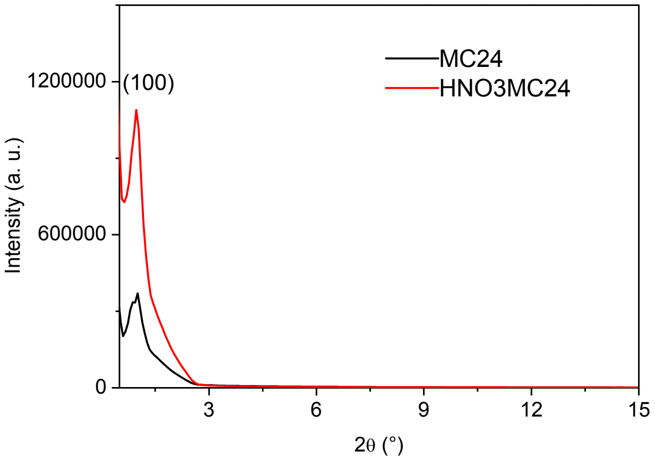

Figure 60 XRD pattern of MC24 and HNO3MC24 samples recorded at low angle.

This behaviour was confirmed also by the N_2 adsorption/desorption isotherms (**Figure *61***).

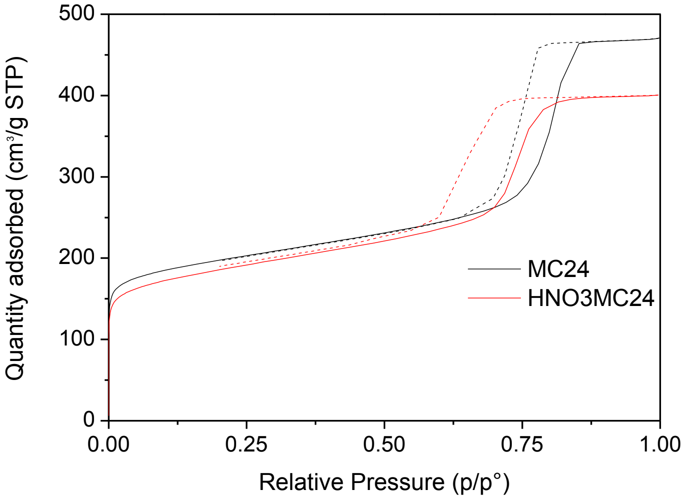

Figure 61 N_2 Adsorption-desorption isotherms of HNO3MC24 and MC24 samples.

The isotherm shape did not change, although the total amount of N_2 adsorbed and the desorption relative pressures were modified. Indeed, pore dimension, specific surface area and pore volume are slightly modified (**Table *10***).

Sample	**S BET (m²/g)**	**SA micro (m²/g)**	**V MICRO (cm³/g)**	**SA meso (m²/g)**	**V MESO (cm³/g)**
MC24	728	545	0.224	183	0.499
HNO_3MC24	681	481	0.200	200	0.419

Table 10 Specific surface area (S_{BET}), surface area and pore volume due to micro- ($S_A$micro, Vmicro) and mesopores ($S_A$meso, Vmeso) of HNO3MC24 and MC24 samples.

In particular, the surface area after the HNO_3 oxidative treatment decreased, but the relative amount of micro and mesopores was similar, as reported in **Table *10***.

Moreover, the pore size decreased, as shown in the DFT distribution (**Figure *62***) where the maximum was shifted at lower values and centred near 9 nm.

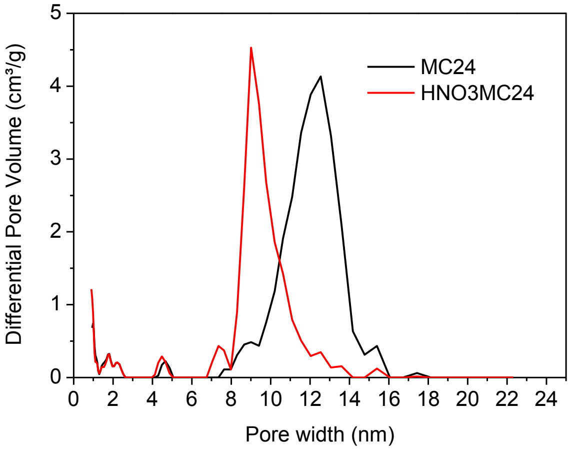

Figure 62 DFT pore size distributions of HNO3MC24 and MC24 samples.

The structure of the carbon within the walls did not change as revealed by Raman analysis; indeed the I_D/I_G ratio for HNO3MC24 sample was slightly lower than for MC24, due to a small increase of surface defects.

In conclusion, the mild oxidation conditions, concentration and time for the HNO_3 treatment, were able to generate surface functional groups, but without damaging the structure.

2.3.4 N-containing carbon

The N-containing carbon monolith (N-MC) was obtained through the addition of nitrogen, in the form of amine, during the synthesis in basic conditions.

The CHN analysis confirms the inclusion of a small amount of N into the material, similar to that in HNO_3MC24 (**Table *11***).

Sample	C content (%)	H content (%)	N content (%)	O content (%)
MC24	93	1	-	6
HNO_3MC24	82	1	1	16
N-MC	91	1	1	7

Table 11 CHN analysis of the synthesized and treated samples.

On the other hand, the O content was similar to the one in the as-prepared mesoporous carbon.

The presence of nitrogen within the carbon layers was also confirmed by the TGA in air coupled with FT-IR analysis (**Figure *63***).

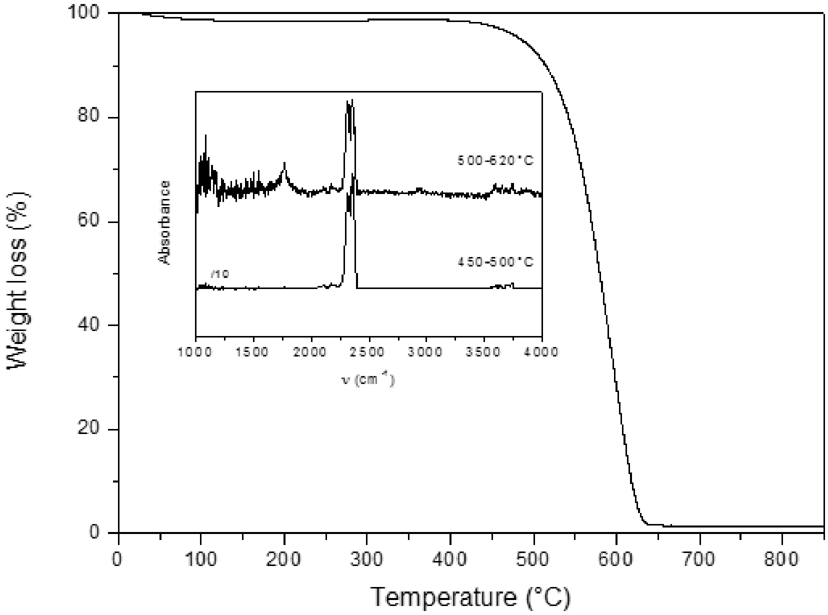

Figure 63 TGA analysis of N-MC and FT-IR spectra of the gases evolved in the 450-500 and 500-620°C ranges.

During the combustion of the material, the evolution of CO, CO_2 and NO_2 was detected in the gaseous stream. CO and CO_2 were evolved during the entire weight loss, from 450 to 650°C, while NO_2 could be detected from 500 to 620°C. The removal of NO_2 at this high temperature suggested the inclusion of nitrogen in the carbon framework.

N_2 adsorption/desorption analysis shows that the inclusion of N during the synthesis modified the porous structure (**Table *12***).

Sample	**S BET (m²/g)**	**SA micro (m²/g)**	**V MICRO (cm³/g)**	**SA meso (m²/g)**	**V MESO (cm³/g)**
MC24	728	545	0.224	183	0.499
N-MC	675	657	0.252	18	0.059

Table 12 Specific surface area (S_{BET}), surface area and pore volume due to micro- ($S_A$micro, Vmicro) and mesopores ($S_A$meso, Vmeso) of mesoporous carbons obtained in acid (MC24) and basic (N-MC) environment.

Adsorption/desorption isotherms is of type 1, characteristic of microporous materials[30] (**Figure** *64*).

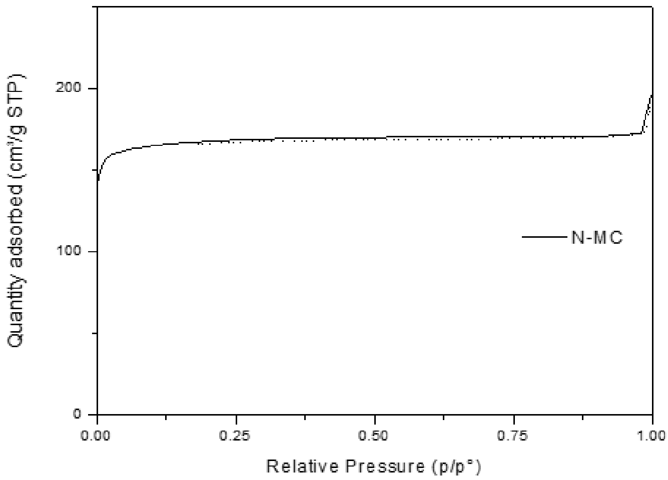

Figure 64 N2 Adsorption-desorption isotherm of N-MC sample.

The carbon monolith has a surface area of 675 m^2/g, similar to the carbon materials obtained from the acid synthesis, but the great part of the surface area is due to the presence of micropores with an average pore diameter of 3.5Å, while a very little part is correlated to the presence of larger pores. This behaviour may be related to the use of amine as N-source. It has been reported that the nature of the amine can be a crucial factor in determining the assembly of the mesostructured[21]; the amine can influence the interaction between the carbon precursors and the templating agent and consequently the type of structure obtained. Generally, the synthesis that involves the typically used reagents, such as resorcinol and formaldehyde, protic organic bases, i.e. DAH (1,6-Diaminohexane), EDA (ethylenediamine) and DMA (dimethylamine), seem to favour the formation of ordered mesoporous in carbon monoliths; while aprotic organic bases result in the formation of microporous carbons[21].

In our specific case, even if DAH base was used, microporosity was obtained; this could be due to the different reagents used as carbon precursor (phloroglucinol and glyoxal). The interaction between these precursors and the templating agent can be influenced in a different manner from the type of amine used as source of nitrogen[21].

In agreement with the N_2 adsorption/desorption analysis, TEM images of the N-containing carbon (**Figure *65***), confirmed the formation of a carbon material without the ordered pore disposition identified in the N-free sample prepared in acid media.

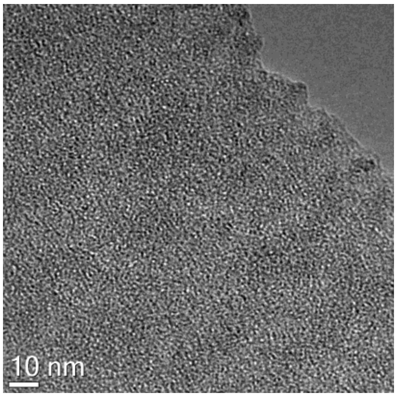

Figure 65 TEM image of N-MC sample.

The Raman spectra shows the typical features of a material with a structure between nanocrystalline graphite and amorphous carbon[34], as the I_D/I_G ratio, which is the same of the MC24 sample, can prove.

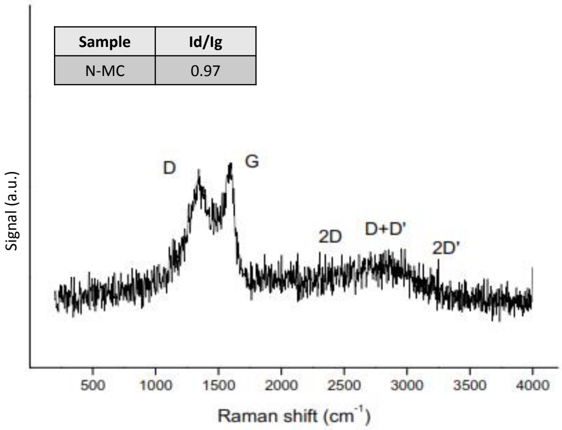

Sample	Id/Ig
N-MC	0.97

Figure 66 Raman spectra of N-MC and its I_D/I_G ratio (Table).

In conclusion, the N-containing carbon shows a surface area similar to the other synthesized carbon, but without mesoporous structure and with different composition.

2.3.5 Benzyl alcohol oxidation as model reaction

Under the reaction conditions investigated, in the oxidation of benzyl alcohol with the synthesized carbon samples the main detected product was benzaldehyde (**Figure *67***).

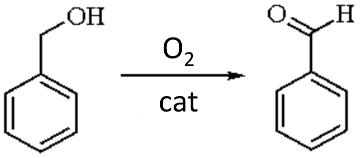

Figure 67 Benzyl alcohol oxidation to benzaldehyde.

The catalytic performances were influenced by the oxygen content on the catalyst surface, related to the amount of surface functional groups, as can be observed in the **Table *13***.

Sample	Benzyl alcohol conversion (%)	Benzaldehyde selectivity (%)	I_D/I_G
MC24	20	17	0.97
HNO3MC24	39	70	0.93
H2O2MC24	28	51	0.95
N-MC	11	40	0.97

Table 13 Catalytic performance and I_D/I_G of carbon samples.

The MC24 sample showed a low benzyl alcohol conversion and selectivity in benzaldehyde, while after the oxidation with H_2O_2 and HNO_3 (H2O2MC24 and HNO3MC24) the catalytic performances were clearly improved. In particular, the conversion of the alcohol and selectivity in benzaldehyde increased with increasing the surface functional groups content of the carbon. These results confirmed that the generated surface oxygen-containing groups were active in the oxidation reaction as previously reported for carbon materials[46,47,48,49].

The trend of the benzaldehyde selectivities was similar to the one reported by Luo at al. with carbon nanotubes[23]; the selectivities in benzaldehyde decreased with I_D/I_G ratio increasing. This behaviour suggested that the surface defects had a negative effect on benzaldehyde selectivity.

The N-containing carbon (N-MC) showed a lower alcohol conversion than the MC24 sample, but a higher selectivity in benzaldehyde, conversely to what reported in literature[50], where carbon with different porosity and composition were employed.

In conclusion, HNO3MC24 gave the best catalytic performance in terms of alcohol conversion and benzaldehyde selectivity; this behaviour could be due to the presence of O-containing surface functional groups.

2.4 Conclusions

Through the soft-template method it was possible to synthesized OMC samples with high surface area and different characteristics, depending on many parameters. The acid route let the formation of mesoporous and ordered structure with hexagon pores arrangement, moreover, the prepared material showed a structure between nanocrystal and amorphous carbon.

The time of curing treatment influenced the structure order degree; in particular, with 24 hours of curing treatment, a higher surface area was obtained with respect to the sample cured for 36 hours. This meant that for the 24 hours cured sample there was more surface area available for catalytic applications. Although the curing time was shorter, an ordered mesostructure was obtained. Moreover, the synthetic procedure was shorter, the pores were larger and with more homogeneous distribution, with respect to the 36 hours cured sample.

The post-synthesis functionalization treatments, performed through oxidations in liquid and gas phase, changed the composition of the materials, depending on the type and conditions of the treatments. Moreover, the treated samples showed the presence of new surface functional groups, maintaining characteristics similar to the untreated carbon. In particular, oxidation with HNO_3 was the more efficient in creating O-containing surface groups such as carboxylic acid, lactone and anhydride, but without damaging the structure.

Through the basic route, performed with the use of amine both for creating basic environmental and as N source, it was possible to change the composition of the material, inserting N in the carbon material. Nevertheless, the high surface area was mainly due to the presence of micropores; moreover, the order degree similar to the acid route synthesized material was not obtained.

Finally, through the catalytic tests in the model reaction of benzyl alcohol oxidation, it was demonstrate that changing the preparation route was possible to tune the properties of carbons, making them suitable for interesting catalytic applications.

References

---

[1] L. Chuenchom, R. Kraehnert, B. M. Smarsly, *Soft Matter* **8** (2012) 10801-10812.

[2] R. Ryoo, S. H. Joo, S. Jun, *J. Phys. Chem. B* **103** (1999) 7743-7746.

[3] R. Ryoo, S. H. Joo, M. Krunk, M. Jaroniec, Adv. Mater. **13** (2001) 677-681.

[4] J. Lee, S. Ham, T. Hyeon, *J. Mater. Chem.* **14** (2004) 478-486.

[5] T-Y Ma, L. Liu, Z-Y Yuan, *Chem. Soc. Rev.* **42** (2013) 3977-4003.

[6] N. Kan-nari, S. Okamura, S. Fujita, J. Ozaki, M. Arai, *Adv. Synth. Catal*. **352**, 1476-1484 (2010).

[7] X. Q. Wang, C. D. Liang, S. Dai, *Langmuir* **24** (2008) 7500-7505.

[8] C. Liang, S. Dai, *J. Am. Chem. Soc.* **128** (2006) 5316-5317.

[9] P. Gao, A. Wang, X. Wang, T. Zhang, *Chem. Mater.* **20** (2008) 1881-1888.

[10] X. Zhao, A. Wang, J. Yan, G. Sun, L. Sun, T. Zhang, Chem. Mater 22 (2010) 5463-5473.

[11] A. Gardziella, L. A. Pilato, A. Knop, *Phenolic Resins*, Springer, New York, 2000.

[12] Y. Meng, D. Gu, F. Q. Zhang, Y. F. Shi, L. Cheng, D. Feng, Z. X. Wu, Z. X. Chen, Y. Wan, A. Stein, D. Y. Zhao, *Chem. Mater.* **18** (2006) 4447-4464.

[13] P. Serp, M. Corrias, P. Kalck, *Appl. Catal. A* **253** (2003) 337-358.

[14] P. Serp, J. L. Figuereido, *Carbon Material for Catalysis*, Wiley, Hoboken, 131-156 (2009).

[15] D. S. Su, S. Perathoner, G. Centi, *Chem. Rev.* **113** (2013) 5782-5816.

[16] G. Centi, S. Perathoner, D. S. Su, *Catal. Surv. Asia* **18** (2014) 149-163.

[17] P. Serp, J. L. Figuereido, *Carbon Material for Catalysis*, Wiley, Hoboken, 45-92 (2009).

[18] A. Villa, J. P. Tessonier, O. Majoulet, D. S. Su, R. Schlogl, *Chem. Commun.* (2009) 4405-4407.

[19] B. Zhong, J. Zhang, B. Li, B. Zhang, C. Dai, X. Sun, R. Wang, D. S. Su, *Phys. Chem. Chem. Phys.* **16** (2014) 4488-4491.

[20] DW. Wang, DS. Su, *Energy & Env. Science* **7** (2014) 576-591.

[21] G. P. Hao, W. C. Li, D. Qian, G. H. Wang, W. P. Zhang, T. Zhang, A. Q. Wang, F. Schuth, H. J. Bongard, A. H. Lu, *J. Am. Soc.* **133** (2011) 11378-11388.

[22] R. T.Mayes, C. Tsouris, J. O. Kiggans, Jr., S. M. Mahurin, D. W. DePaoli, S. Dai, *J. Mater. Chem.* **20** (2010) 8674-8678.

[23] J. Luo, F. Peng, H. Yu, H. Wang; *Chem. Eng. J.* **204-206** (2012) 98-106.

[24] J. Luo, H. Yu, H. Wang, H. Wang, F. Peng; *Chem. Eng. J.* **240** (2014) 434-442.

---

[25] P. Janus, R. Janus, P. Kustrowski, S. Jarczewski, A. Wach, A. M. Silvestre-Albero, F. Rodriguez-Reinoso; *Catalysis Today* **235** (2014) 201-209.

[26] V. Gomez-Serrano, M. Acedo-Ramos, A. J. Lopez-Peinado, C. Valenzuela-Calahorro; *Fuel* **73** (1994) 387-395.

[27] A. H. Lu, W. C. Li, W. Schmidt, F. Schuth, *Microporous Mesoporous Mater.* **80** (2005) 117-128.

[28] A. Choukourov, A Grinevich, O. Polonskyi, J. Hanus, J. Kousal, D. Slavinska, H. Biederman; *J. Phys. Chem. B* **113** (2009); 2984-2989.

[29] Y. Ishii, Y. Nishiwaki, A. Al-zubaidi, S. Kawasaki, *J. Phys. Chem. C* **117** (2013) 18120-18130.

[30] M. Thommes, K. Kaneko, A. V. Neimark, J. P. Olivier, F. Rodriguez-Reinoso, J. Rouquerol, K. S. W. Sing, *Pure Appl. Chem.* **87** (2015) 1051-1069.

[31] S. Tanaka, A. Doi, N. Nakatani, Y. Katayama, Y. Miyake, *Carbon* **47** (2009) 2688-2698.

[32] W. Libbrecht, F. Deruyck, H. Poelman, A. Verbeckmoes, J. Thybaut, J. de Clercq, P. Van Der Voort, ; *Chem. Eng. J.* **259** (2015) 126-134.

[33] M. Short, P. L. Walker Jr; *Carbon* **1** (1963) 3-9.

[34] A. C. Ferrari, J. Robertson; *Physical Review B* **61** (2000) 14095-14107.

[35] F. Zhang, Y. Meng, D. Gu, Y. Yan, Z. Chen, B. Tu, D. Zhao, *Chem. Mater.* **18** (2006) 5279-5288.

[36] Y. Huang, H. Cai, T. Yu, F. Zhang, F. Zhang, Y. Meng, D. Gu, Y. Wan, X. Sun, B. Tu, D. Zhao; *Angew. Chem*, **119** (2007) 1107-1111.

[37] Z. Wu, P. A. Webley, D. Zhao, *Langmuir*, **26 (12)** (2010) 10277-10286.

[38] M. Seredych, D. Hulicova-Yurcakova, G. Q. Lu, T. J. Bandozs, *Carbon*, **46** (2008) 1475-1488.

[39] J. L. Figueiredo, M. F. R. Pereira, M. M. A. Freitas, J. J. M. Orfao; *Carbon* **37** (1999) 1379-1389.

[40] J. L. Falconer, J. A. Schwarz, *Catal. Rev-Sci Eng*. **25** (1983) 141-227.

[41] H. P. Boehm, *Carbon,* **32** (1994) 759-769.

[42] S. Biniak. G. Szymanski, J. Siedlewski, A. Swiatkowski; *Carbon* **35** (1997) 1799-1810.

[43] Y. Li, G. Lan, G. Feng, W. Jiang, W. Han, H. Tang, H. Liu; *ChemCatChem*, **6** (2014) 572-579.

[44] V. P. Santos, M. F. Pereira, P. C. C. Faria, J. J. M. Orfao; *Journal of Hazardous Materials* **162** (2009) 736-742.

[45] J. S. Noh, J. A. Schwarz, *Carbon* **28** (1990) 675-682.

[46] J. Zhang, D. Su, A. Zhang, D. Wang, R. Schloegl, C. Hebert, *Angew. Chem. Int. Ed*. **46** (2007) 7319-7323.

[47] J. Zhang, X. Liu, R. Blume, A. H. Zhang, R. Schlogl, D. S. Su, *Science* **322** (2008)73-77.

[48] S. Yang, X. Li, W. Zhu, J. Wang, C. Descorme, *Carbon* **46** (2008) 445-452.

[49] D. R. Dreyer, H. P. Jia, C. W. Bielawski, *Agnew. Chem. Int. Ed.* **49** (2010) 6813-6816.

[50] R. P. Rocha, J. Restivo, J. P. S. Sousa, J. J. M. Orfao, M. F. R. Pereira, J. L. Figueiredo; *Catal. Today* **241** (2015) 73-79.

Chapter 3: Catalytic superacid perfluorosulfonic resins

3.1 Introduction

It is widely acknowledged that there is a growing need for more environmentally acceptable process in the chemical industry. This trend towards what has become known as ‘Green Chemistry’ necessitates a paradigm shift from traditional concepts of process efficiency that focus largely on chemical yield to one that assigns economic value to eliminating waste at source and avoiding the use of toxic and/or hazardous substances[1].

Green Chemistry is the design of chemical products and processes that reduces or eliminates the use and the generation of hazardous substances. Green Chemistry efficiently utilizes (preferably renewable) raw materials, eliminates waste and avoids the use of toxic and/or hazardous reagents and solvents in the manufacture and application of chemical products.

Catalysis has played a great role in reducing pollution in our environment. With catalyst, reactions can be more efficient and selective thereby eliminating large amounts of by-products and other waste compounds[2]. Moreover catalysts accelerate reactions by orders of magnitude, enabling them to be carried out under the most favorable thermodynamic regime, and at much lower temperatures and pressures.

Catalysis is of a crucial importance for the chemical industry and is used to make an enormous range of products like heavy commodity and fine chemicals. It is one of the fundamental pillars of Green Chemistry and it is a key factor in reducing both the investment and operation costs of chemical process[3].

Acid catalysis is by far the most important area of catalysis employed by industries in all sectors of chemical manufacturing. A wide range of liquid phase industrial reactions depend on the use of inorganic or mineral acids, while many of these processes are catalytic, some require stoichiometric amounts of acids. Some of the major reaction types which are important in this context are Friedel-Crafts alkylations, acylations and sulfonylations, aromatic halogenation, nitration, isomerisations, and oligomerisation[1].

These reactions are generally catalyzed by mineral acids such as H_2SO_4 and HF, and by Lewis acids such $AlCl_3$ and BF_3. These reagents are hazardous in handling, damaging the plant through their corrosiveness and add process difficulties through the use of quenching and separation stages, which led to large volume of toxic and corrosive wastes.

In this context, solid acid catalysts can be a more environment friendly alternative. The advantages of a solid acid catalyst include reduced equipment corrosion, ease of product separation, less potential contamination in waste streams and recycle of the catalyst[4]. Using a solid it may also increase the number of processing options such as gas flow reactor and a fixed bed. The selectivity may also be improved in going to a solid acid catalyst.

Solid acids can be described in terms of their Bronsted/Lewis acidity, the strength and number of these sites and the morphology of the support (typically in terms of surface area and porosity).

There is a wide range of solid acid catalysts, such as aluminum and silicon pure and mixed oxides, transition metal oxides[5], and the use of ion exchange resins plays a key role. In **Figure *68*** a summary of the families of solid acid catalysts that find industrial applications is reported.

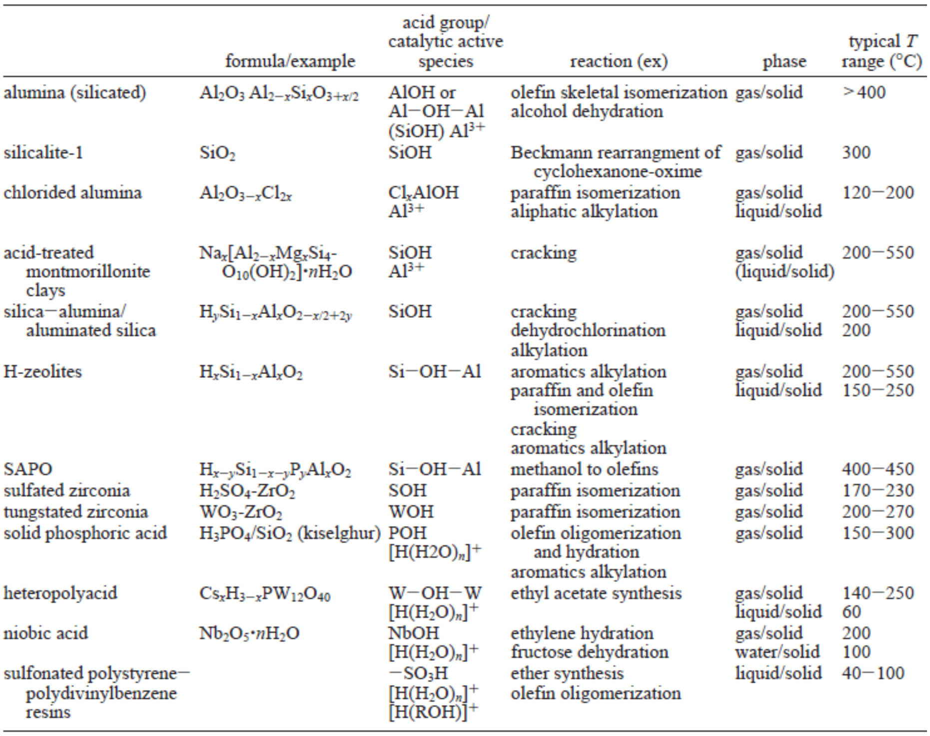

	formula/example	acid group/ catalytic active species	reaction (ex)	phase	typical T range (°C)
alumina (silicated)	Al_2O_3 $Al_{2-x}Si_xO_{3+x/2}$	AlOH or Al−OH−Al (SiOH) Al^{3+}	olefin skeletal isomerization alcohol dehydration	gas/solid	>400
silicalite-1	SiO_2	SiOH	Beckmann rearrangment of cyclohexanone-oxime	gas/solid	300
chlorided alumina	$Al_2O_{3-x}Cl_{2x}$	Cl_xAlOH Al^{3+}	paraffin isomerization aliphatic alkylation	gas/solid liquid/solid	120−200
acid-treated montmorillonite clays	$Na_x[Al_{2-x}Mg_xSi_4O_{10}(OH)_2]\cdot nH_2O$	SiOH Al^{3+}	cracking	gas/solid (liquid/solid)	200−550
silica−alumina/ aluminated silica	$H_ySi_{1-x}Al_xO_{2-x/2+2y}$	SiOH	cracking dehydrochlorination alkylation	gas/solid liquid/solid	200−550 200
H-zeolites	$H_xSi_{1-x}Al_xO_2$	Si−OH−Al	aromatics alkylation paraffin and olefin isomerization cracking aromatics alkylation	gas/solid liquid/solid	200−550 150−250
SAPO	$H_{x-y}Si_{1-x-y}P_yAl_xO_2$	Si−OH−Al	methanol to olefins	gas/solid	400−450
sulfated zirconia	H_2SO_4-ZrO_2	SOH	paraffin isomerization	gas/solid	170−230
tungstated zirconia	WO_3-ZrO_2	WOH	paraffin isomerization	gas/solid	200−270
solid phosphoric acid	H_3PO_4/SiO_2 (kiselghur)	POH $[H(H2O)_n]^+$	olefin oligomerization and hydration aromatics alkylation	gas/solid	150−300
heteropolyacid	$Cs_xH_{3-x}PW_{12}O_{40}$	W−OH−W $[H(H_2O)_n]^+$	ethyl acetate synthesis	gas/solid liquid/solid	140−250 60
niobic acid	$Nb_2O_5\cdot nH_2O$	NbOH $[H(H_2O)_n]^+$	ethylene hydration fructose dehydration	gas/solid water/solid	200 100
sulfonated polystyrene−polydivinylbenzene resins		$-SO_3H$ $[H(H_2O)_n]^+$ $[H(ROH)]^+$	ether synthesis olefin oligomerization	liquid/solid	40−100

Figure 68 Summary of industrial solid acid catalysts[5].

3.1.1 Ion-exchange resins

Ion-exchange resins, introduced in 1960s[5], are insoluble macroporous polymers which are capable of exchanging specific ions with other ions within the polymer itself in a solution or reaction media[1].

In the most of the acidic ion exchangers, the active sites are the sulfonic acid groups that are attached to a solid backbone such as sulfonated coal, sulfonated phenol-formaldehyde resins, or sulfonated styrene-divinylbenzene cross-linked polymers[6].

Normally, sulfonic ion-exchange resins are co-polymers of divinylbenzene (DVB), styrene and sulfonic acid groups[7], belonging to the Amberlyst family. The polymer structure of the resin is mainly characterized by the composition of cross-linking component (normally DVB) which will determine its surface area and pore size distribution[8]. Besides this, their catalytic activity is also strongly dependent on their swelling properties because the swelling capacity limits reactant accessibility to the acid sites and affects their overall activity[9].

Common types of acidic ion-exchange resins commercially available are Amberlyst®-15 and Amberlyst®-35. In particular, Amberlyst®-15 is a macroreticular sulfonated polystyrene-based ion-exchange resin with 20% of divinylbenzene (**Figure *69***).

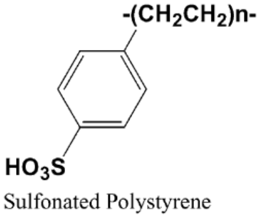

Figure 69 Structural unit of Amberlyst ion-exchange resin.

The acidity of the Amberlyst type materials, having surface area near 50 m^2/g, is associated with the strong acidity of the aryl-sulfonic acid groups Ar-SO_3H. These materials are prepared as “gel” resins in the form of uniform beads and as “macroporous” materials. Due to the restricted diffusion, the acid sites in the gel are accessible only when the beads are swollen. Macroporous resins are prepared with permanent porosity; thus, more acid sites are accessible also in non-swelling solvents, although diffusion of the reactant in the polymer matrix is also determinant[10].

The number of acid sites in sulfonated polystyrene is relatively high, 4.7 equiv/kg for Amberlyst®-15 and 5.4 equiv/kg for the hypersulfonated resin Amberlyst®-36. However the acid strength is considered to be relatively low, the Hammett acidity function being evaluated as H_0=-2.2. Another limit of these materials consists in the limited stability temperature range (150-180°C)[5].

Solutions for the dramatic drawbacks belonging to polystyrene-based sulfonic resins are represented by perfluoropolymer ionomers (where ionomers stands for ion-containing polymers[11]) also known as perfluorosulfonic acids (PFSA). These materials are perfluorinated resinsulfonic acids, mainly used in the form of membranes, finding interesting applications in the field of fuel cells[11].

Perfluoropolymer ionomers are known since the late 1960s, when the Nafion ionomers were developed by the DuPont company.

Nafion resin is a perfluorinated resinsulfonic acids which is a copolymer derived from tetrafluoroethylene and perfluoro-2-(fluorosulfonylethoxy)propyl vinyl ether. After hydrolysis of the sulfonyl fluoride, it yields the strongly acidic terminal -$CF_2CF_2SO_3H$ group (**Figure** ***70***).

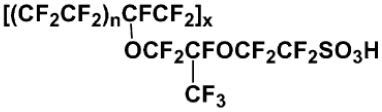

$$[(CF_2CF_2)_nCFCF_2]_x \quad OCF_2CFOCF_2CF_2SO_3H \quad CF_3$$

Perfluorinated resinsulfonic acid

Figure 70 Structural unit of Nafion ion-exchange resin.

This structure provides high acidity sites and at the same time the perfluorinated polymer itself is highly inert and resists acid cleavage.

The equivalent weight of this polymer is typically about 1070[4]. This material is both chemically stable, due to the fluorocarbon nature of the backbone, and thermally stable up to 280 °C, at which temperature the sulfonic acid groups being to decompose[12]. It is commercialized in the form of membranes, beads, and dispersion in water and aliphatic alcohol solutions.

This material is largely used in electrochemical processes as membrane for chloro-alkali cells and as electrolyte for proton exchange membrane fuel cells (PEMFC), but it can also act as a very strong Bronsted acid solid catalyst.

Nafion is definitely more acidic than polystyrene-based sulfonic resins. Indeed it is generally accepted that perfluorinated resin sulfonic acids are very strong acid with values of Hammett acidity function (H_0=-11 to -13[13]) which allow the application of the term “superacid”[5]. However, the surface area of this material is very low and the availability of the protonic sites is very small. Consequently, the specific activity of Nafion, namely, the number of reacting molecules per unit weight, is extremely low.

In order to increase the acid site accessibility of Nafion resin-based catalysts, a new class of solid acid catalyst-based upon high surface area Nafion resin silica nanocomposites, has been developed, where nanometer sized Nafion resin particles are entrapped within a highly porous silica network[14]. This nanocomposite, marked under the trade name of NAFION SAC-13, was developed by Harmer and co-workers[14, 15, 16], using the in situ sol-gel technique. During the process, nanometer-size silica particles were formed, which were aggregated to produce a porous silica network entrapping the Nafion particles.

The nanocomposites have particle size in the range of 2-20 nm and large surface areas (typically 150-500 m^2/g) that is, approximately four orders of magnitude larger than that of the starting Nafion polymer resin.

Synthesis conditions, particularly the choice of the silica source, allow the tailoring of the microstructure, surface area and acidity of the nanocomposites. Furthermore, Nafion loading can also be varied easily up to about 40 wt%. Moreover, Nafion was also embedded into order mesoporous MCM-41 silica material[17, 18].

In more recent years, the growing interest related to cleaner energy production technologies has promoted the consideration and study of ionomers as proton exchange membranes (PEMs) in fuel cells. Again, due to electrochemical stability requirements, perfluorinated materials have been preferred as the best candidates for satisfying the needs of the system and new ionomers have been synthesized[19].

In 1980s, Ballard Power Systems showed significant improvements in fuel cell performance using ionomer membranes obtained from Dow Chemicals[20]. This ionomer, commonly known as the Dow ionomer, is perfluorinated and similar in structure to Nafion, save for a shorter pendant side-chain which carries the functional ion-transporting group (**Figure *71***).

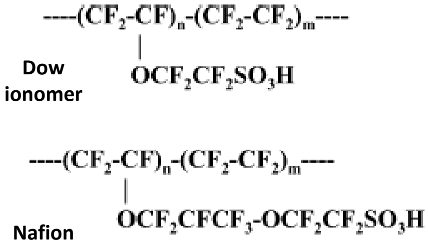

$$\text{----}(CF_2\text{-}\underset{\displaystyle OCF_2CF_2SO_3H}{\underset{|}{CF}})_n\text{-}(CF_2\text{-}CF_2)_m\text{----}$$

$$\text{----}(CF_2\text{-}\underset{\displaystyle OCF_2CFCF_3\text{-}OCF_2CF_2SO_3H}{\underset{|}{CF}})_n\text{-}(CF_2\text{-}CF_2)_m\text{----}$$

Figure 71 Structural unit of Dow ionomer and Nafion.

It has to be stated that the Dow ionomer is known also as the short-side-chain (SSC) ionomer. Correspondingly, Nafion is sometimes referred to as the long-side-chain (LSC) ionomer. Other examples of LSC ionomers are Aciplex (Asahi Chemical), Flemion (Asahi Glass) and Gore- Select (Gore and Associates)[11].

Although demonstration of higher power-generating capability in fuel cell was demonstrated using the Dow ionomer, after the filing of a series of patents by the Dow company[19, 21, 22], the industrial development of this interesting ionomer structure was abandoned. No commercialization of these very promising experimental membranes followed. The complexity of the Dow process for the synthesis of the base functional monomer used for the production of the SSC ionomer caused this interesting development to be abandoned.

Other perfluorinated ionomer membranes, chemically very similar to Nafion, are also commercially available. For example, Aciplex, manufactured by Asahi Chemical Company, is very similar to Nafion, except that it has perfluoropropanesulfonic acid side chain.

Recently, due to a different and more simple route for the synthesis of the base monomer for SSC ionomers, Solvay Specialty Polymers has developed polymer electrolyte membranes based on new perfluorinated ionomer type. The commercial name for this ionomer (and the membranes made therefrom) was Hyflon Ion until 2010, when the ionomer was commercialized with the name of Aquivion® PFSA (**Figure *72***).

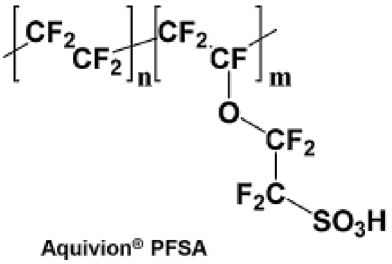

Figure 72 Chemical structure of Aquivion® PFSA.

This innovative material is obtained by the free-radical copolymerization of tetrafluorethylene (TFE) and sulfonyl fluoride vinyl ether $CF_2{=}CF{-}O{-}(CF_2)_2{-}SO_2F$ (SFVE). Starting from the monomers, ionomers are synthesized by taking advantage of a proprietary emulsion polymerization process[23]. The resulting fluoropolymer's functional groups are then converted to their sulfonic acid form $-SO_3H$ by a hydrolysis with strong mineral base (NaOH or KOH) followed by a cation exchange in acid environment[24], as shown in **Figure *73***.

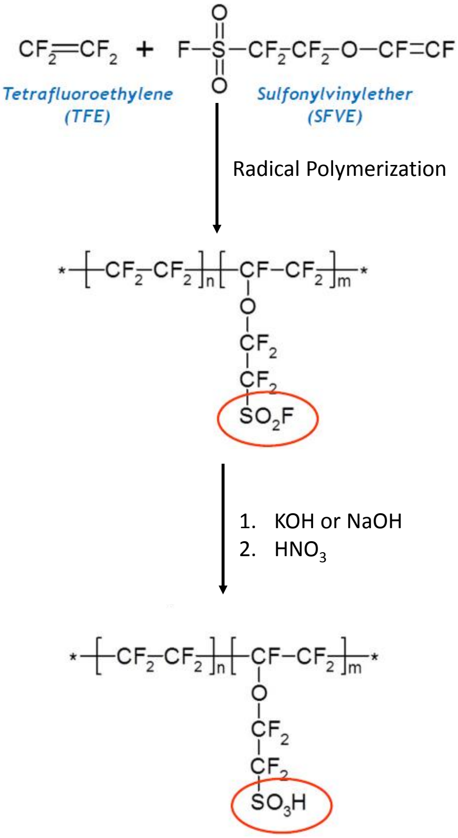

Figure 73 Synthetic steps for Aquivion® PFSA preparation.

Thanks to the strong electronegative effect of fluorine atoms in its perfluorinated structure which leads to a prominent dissociation tendency of $–SO_3H$ group, Aquivion based material is a solid superacid with a Hammett acidity function of -12, which is comparable to the that of pure sulphuric acid[6] (**Figure *74***).

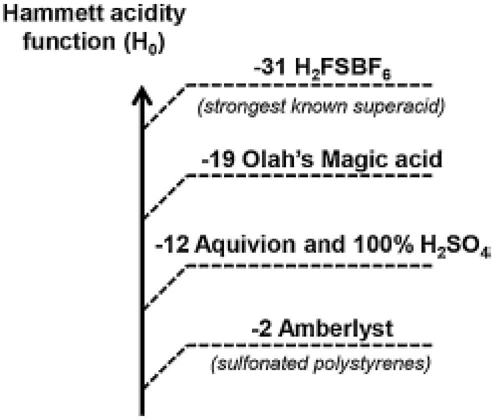

Figure 74 Aquivion® PFSA material classification in the Hammett acidity scale.

Aquivion® PFSA, belonging to SSC ionomer family, has the shortest side chain compared to its commercially available congeners, as Nafion. This feature increases its crystallinity and the glass transition temperature is raised to 140-150°C allowing, when needed, the use at high reaction temperatures without loss in mechanical and chemical integrity[19, 25, 26].

Furthermore, the high chemical inertness given by the perfluorinated structure allows Aquivion PFSA to withstand highly aggressive reaction conditions, thus resisting strong acids, bases and oxidative as well as reductive environments.

Concerning its thermal stability, this polymer starts to decompose at relatively high temperature, near 300°C, showing the main weight loss from 280 to 550°C[25].

Moreover, through the fine-tuning of the copolymer composition, it is possible to tailor the acid loading as well as the mechanical properties of the final material, because they are strongly linked to each other.

Indeed the crystalline portion in Aquivion material is represented by the TFE backbone, while the amorphous part is due to the SFVE side chain which brings the acid functionalities. Consequently, increasing the acid loading and so the SFVE amount, the crystallinity of the final material decreases.

Aquivion PFSA is commercially available in different form, such as powder, pellet, both with different acid loading (from 1.0 to 1.5 mmol/g as grade acid capacity), but also dispersion and membrane. Some applications of this material has been reported in the frame of fuel cells and electrolysers[27, 28], but recent papers investigated its catalytic activity in different reactions[24, 29], also employing Aquivion/silica composites[25].

3.1.2 Catalytic application of ion-exchange resins

Strong-acid cation-exchange resins have been used commercially as solid acid catalysts in many areas[4]. Currently, the largest volume application of acidic ion-exchange resin in catalysis is represented by the coupling of isobutene to form methyl t-butyl ether (MTBE). This catalysts are also used in the dehydration of alcohols to olefins or ethers (for example the t-butanol dehydration to form isobutene) and in alkylation of phenols to alkyl phenols. Moreover they are employed in condensation reactions, olefin hydration to form alcohols and esters hydrolysis.

It is also noteworthy how the use and application of these types of resins grow dramatically as the microstructure of these materials was improved. Prior to about 1960, polystyrene-based resins were essentially gel type resins whose swelling characteristics depended upon the solvent or reactants. In non-swelling media, the active sites were largely inaccessible for reactivity. This problem was overcome with development of “macroporous” ion-exchange resins, consisting of agglomerates of very small microspheres interspersed with macropores[4]. A good understanding and optimization of this materials for a range of catalytic reactions has pioneered the way for these ion-exchange resins to become industrial catalysts of choice in several key areas. Moreover, the design of a nanocomposite material clearly has significant advantages where the reaction studied are essentially non-swelling. For this reason also the composites materials, developed to enhance the catalytic performances of the perfluorinated sulfonic acids, play an important role. For example, Nafion® resin/silica nanocomposite is a very active catalyst for alkylation of benzene with C12 olefins to form linear alkyl benzenes (**Figure** *75*).

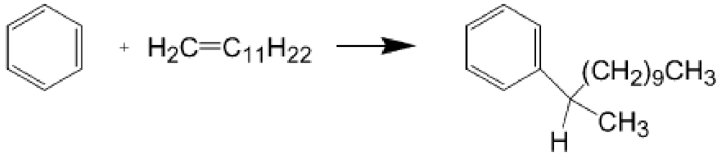

Figure 75 Benzene alkylation with 1-dodecene to 2-phenyl dodecene.

These products, when sulfonated, represent the basis of the detergent industry. In the current commercial process HF is used as catalyst and there is an obvious drive to replace this very hazardous material with a solid acid catalyst. The products of these reactions contain a mixture of alkylbenzenes with phenyl group attached to different C-atoms in the linear hydrocarbon chain. The 2-phenyl isomer is the most preferred product, while branched isomers, coming from skeletal isomerization reaction, are very undesirable due to lower biodegradability. The nanocomposite catalyst was approximately x400 more active than an Amberlyst-based resin and pure Nafion[30].

One class of reactions where there is a large difference in reactivity using perfluorosulfonic type acids is the Friedel- Crafts benzylation of benzene and p-xylene with benzyl alcohol. Amberlyst-type resins are essentially inactive whereas the stronger Nafion-type resins and especially its silica nanocomposites are very active catalysts[31].

Alkylated phenols and derivatives are widely used commercially as antioxidants, herbicides, insecticides, fragrance, polymerization inhibitor, lubricants and so on. Alkylated phenols are typically made by cation-exchange resins (Amberlyst$^{®}$-15, -16) as catalyst for alkylation of phenol with the corresponding olefins and the reaction proceeds preferentially in the para position[32]. The use of a resin catalyst in this reaction has almost entirely replaced H_2SO_4 and BF_3 catalytic systems. Catalyst deactivation is a major concern since the reaction is carried out at the temperature close to the decomposition temperature (> 110°C) of the acid groups in the normal cation-exchange resins. The Nafion-based resin and its composites have some advantages for catalysing this type of reactions due to its higher thermal stability.

Moreover, the Nafion/silica composite was very active catalyst for the olefin isomerization, cis-/trans-transformations and double bond migration. One example is the isomerization of 1-butene to the cis- and trans-2-butene isomers[15]. The composite is also effective for catalysing long chain olefin isomerization such as C12 olefin and higher.

Acidic ion-exchange resins are known to be able to catalyse the oligomerization of olefins, such as oligomerization of C4 alkenes over Amberlyst-type resins and oligomerization of higher olefins (C10-32) over Nafion-type resins. The oligomers from

C4 alkenes can be used as diesel fuels, while the oligomers of higher olefins have been used as lubricant, preferably after hydrogenation.

Ion-exchange resins are effective catalyst for a number of dehydration type chemistries. These include the dehydration of t-butanol to isobutylene and also the dehydration of butane diol to THF. Of course, the most well-known reaction is the formation of bisphenol-A, with the release of one water molecule for each mole of product produced[33].

Concerning Aquivion-type resins, besides their use in the frame of fuel cells and electrolyzers[27, 28], there are some catalytic applications in liquid phase reactions, also in composite form, while gas-phase reactions have never been explored.

Aquivion material has been used as a novel solid and reusable acid catalyst in the synthesis of 2-pyrrolidin-2-ones in flow conditions[29]. In particular, Aquivion PFSA effectively catalysed the diasteroselective nitro-Mannich/lactamization cascade reaction between the imine formed from aldehydes and amines with methyl 3-nitropropanoate (**Figure** *76*).

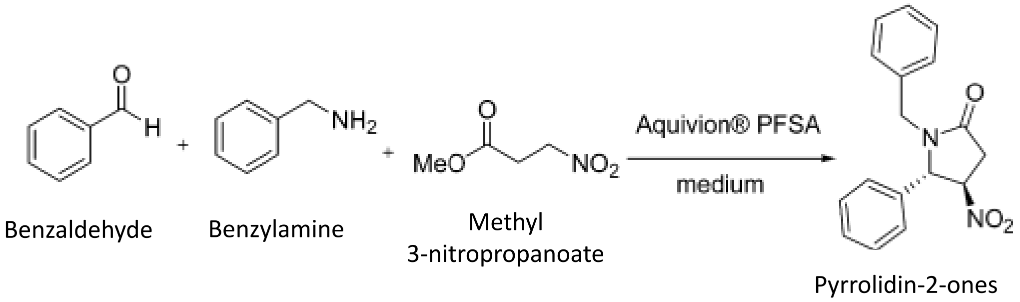

Figure 76 Diasteroselective nitro-Mannich/lactamization cascade reaction.

Pyrrolidin-2-one moiety is a common motif of important biologically active products and pharmaceutical compounds. Furthermore it is a key building block to directly access a large variety of heterocyclic systems. Many synthetic protocols to obtain such a product have been already developed, but the experimental conditions have not been optimized on the sustainability point of views. Through the use of Aquivion-based catalyst, the synthetic protocol was improved in terms of sustainability, employing solvent free or concentrated conditions and flow which replaced the classic magnetic stirring. The Aquivion PFSA catalysed reaction resulted to be stereoselective, as the trans-isomer of the pyrrolidin-2-one has been obtained as the major product and only traces of the cis-isomer were detected. In general, the developed protocol, was very convenient in terms of sustainability and of efficiency. In fact, little amount of catalyst was employed, equimolar amounts of reactants were used, and the procedure to isolate the products was straightforward. Moreover the adoption of the flow technology has allowed the minimization of waste production and the recovery and reuse of the catalyst. Green metrics calculation have been confirmed the significant contribution and improvements of the protocol among the other literature reports on this topic.

Pure Aquivion PFSA material was recently used as heterogeneous catalyst in glycerol oligomerization reaction, as reported by Karam et al.[24]. The catalytic oligomerization of glycerol is a reaction of high interest yielding highly hydrophilic molecules, which exhibit a broad range of applications in various industrial sectors such as cosmetic, food and pharmaceutic industries. Like many polyols, the difficultly to closely control the selectivity of this reaction is the main hurdle faced by catalysis. Indeed glycerol can be oligomerized under basic or acid conditions and many side reactions can take place such as dehydration, dehydrogenation and many others. Heterogeneization of strong acid sites over a solid support would open a convenient way to produce oligoglycerols with a higher efficiency notably by facilitating the recycling of the catalyst at the end of the reaction. Different solid acid catalysts could be used for this reaction, but many of them show dramatic drawbacks. For example, silica-supported sulfonic sites unfortunately suffer from a lack of stability in neat glycerol moisture due to the release of water during the reaction that partly hydrolizes the silica surface. In addition, zeolites often suffer from deactivation in liquid glycerol. Conventional cation exchange resins could be also used, but their thermal instabilities often limit their use on such reactions. The solid superacid Aquivion-based catalyst can be a stable, recyclable and selective catalytic system for the glycerol oligomerization. In the work proposed by Karam et al.[24], Aquivion PFSA, in the form of powder and pellet, was tested in the liquid phase glycerol oligomerization (**Figure** *77*) and compared to Nafion- and Amberlyst-based catalysts.

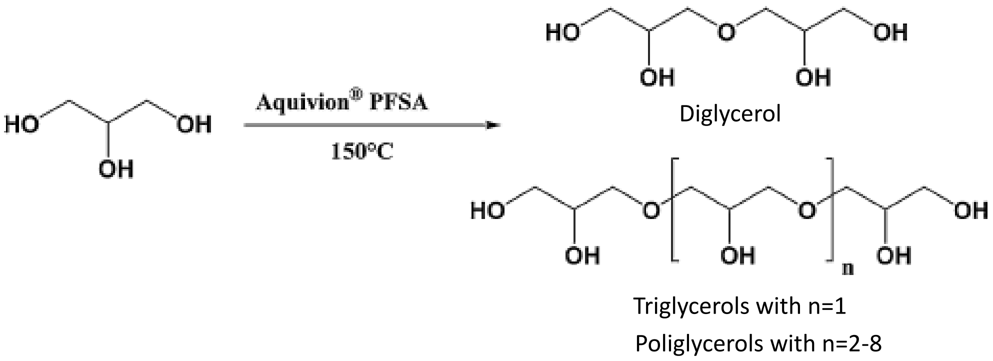

Figure 77 Glycerol oligomerization.

Aquivion PFSA gave not only high selectivity, but also higher activity than previously reported acid catalysts. Moreover, Aquivion powder was slightly more active than the other cation exchange resin (Nafion and Amberlyst). Furthermore, Aquivion catalyst was highly stable in the operating conditions and was successfully recycled at least 10 times without appreciable decrease of activity and selectivity.

Lewis acid catalysed reactions are of a great interest in organic synthesis; however the use of traditional Lewis acid is often characterized by the high amount of waste formation and sometimes by low reaction selectivity. Initially, rare earth triflates were used; then Zn, Fe, Ga and In triflates were preferred due to their lower cost. As recently reported[34, 35], also functionalized polymers have been investigated as Lewis acid, such as Nafion-Fe and Nafion-Ga. These particular catalysts were prepared by cation exchange reaction starting from Nafion-K and metal halogenated precursors with a non-environmentally friendly procedure. Consequently, Tassini et al.[26] investigated the preparation of Aquivion-Fe and Aquivion-Ga with a simpler and more sustainable preparative approach and tested their catalytic performances in Friedel-Crafts acylation reactions. Moreover, the catalytic behaviour of Fe and Ga containing Aquivion was compared to Fe and Ga-containing Nafion catalysts. This study lead to the preparation of Fe and Ga containing ion exchange resin with a simpler approach than that starting from Nafion. Specifically the performance of Aquivion catalysts in Friedel-Crafts acylation of electron rich heterocycles, working under solvent-free conditions or using acylating reagent also as solvent, permitted to obtain products of high purity, good yield, simple work-up and with less waste.

3. Catalytic superacid perfluorosulfonic resins

With the aim to improve the acid sulfonic groups accessibility in Aquivion material, Fang et al.[25] proposed for the first time the synthesis of silica-immobilized Aquivion PFSA, through a template-free sol-gel method, and it use for the direct etherification of glycerol with aliphatic n-butanol. The synthetic protocol was performed using an improved sol-gel method in absence of hydrochloric acid, where the sulfonic groups of Aquivion resin realized the acidic hydrolysis and simultaneous polycondensation of silica precursors. This allowed organosulfonic acid groups to be fixed to silica network via formation of covalent bond and /or electrostatic interactions[36, 37]. TEOS was used as silica source and, during the sol-gel process, it can self-assemble in the presence of Aquivion resin. In such case, Aquivion was expected to cover mainly silica nanoparticles and it was regarded to play the role as a template. The final composite materials showed a large specific surface area (300-360 m^2/g) and a mesoporous structure. Moreover, the Aquivion-silica composites showed a higher thermal stability compared to the bare polymer. In addition, the composite materials were composed of very small silica particles (10-15 nm) and an amorphous morphology.

In the sol-gel prepared catalysts, the SO_3H groups within Aquivion resin were easily accessible to the reactants. The Aquivion-silica solid acid catalysts demonstrated a higher catalytic activity and selectivity in the direct etherification reaction of glycerol with n-butanol compared to typical benchmark homogenous and heterogeneous acid catalysts, making it a candidate of choice for acid-catalysed reactions involving biomass-derived reagents. This can be attributed to a combined effect of the strong acid sites of Aquivion resin and the large porosity of silica. Moreover, the composites catalysts could be reused with no need of regeneration, keeping the integrity of the acid sites and porous structure after six catalytic cycles.

Finally, Aquivion resin was also used for prepare composites with carbon, as reported by Fang et al.[38]. They obtained the Aquivion-carbon composites through a one-pot hydrothermal carbonization (HTC) of guar gum or cellulose[39]. The composite materials exhibited the presence of large meso- and macropores, with a specific surface area higher than the bare polymer, but lower than the silica-based composites.

3.2 Materials and methods

The Aquivion PFSA samples were kindly provided by Solvay Specialty Polymers (Italy), while all the characterizations and catalytic tests were performed in UNIBO laboratories. The Aquivion samples were characterized with different techniques in order to discover their thermal stability, textural properties and swelling behaviour. Finally, the samples were tested in a laboratory-scale plant as heterogeneous catalysts for the model reaction of ethanol dehydration.

For catalytic applications, Aquivion samples are commercially available in different forms (coarsely grained powders, pellets and dispersions) and with different total acid capacities (from 0.98 to 1.43 meq/g).

3.2.1 Aquivion PFSA® samples

In this work, Aquivion with different forms and acid loadings were used, both commercial (in red) and not (in black), as reported in **Table** ***14***.

Sample name	Acid loading (mmolSO_3H/g)	Form	Use
PW98	1,00	powder	Catalytic Test
P98	1,00	pellet (2x2mm)	Catalytic Test
mP98	1,00	micropellet (>1mm)	Catalytic Test
mP98-exp	1,00	expanded micropellet	Characterization
P98-exp	1,00	expanded pellet	Characterization
PW79-S	1,25	stabilized powder	Catalytic Test
PW87-S	1,15	stabilized powder	Catalytic Test
P87-S	1,15	stabilized pellet	Catalytic Test
PW65-S	1,48	stabilized powder	Catalytic Test
Exp98	1,02	expanded pellet	Catalytic Test
PW98-S	1,02	stabilized powder	Catalytic Test
PW87	1,15	powder	Catalytic Test

Table 14 Aquivion samples employed in this work, in red the commercially available samples.

It has to be explained that the samples, named with the final S, were subjected to a stabilization treatment used to transform the –COOH terminal groups, formed by a side-reaction during the polymerization[40], in $-CF_3$ groups carried out in the presence of gaseous fluorine at high temperature[41].

3. Catalytic superacid perfluorosulfonic resins

The catalytic performances and features of the Aquivion samples were also compared to other commercially available ion-exchange resins, reported in **Table *15***.

Sample name	Material	Acid loading (mmol SO_3H/g)	Catalyst form
A15dry	Amberlyst	≥4.7	Pellet
A70wet	Amberlyst	≥2.55	Pellet
NR50	Nafion	≥0.8	Pellet

Table 15 Commercially available ion-exchange resins used in comparison with Aquivion resin.

3.2.2 Characterization methods

The Aquivion material was characterized with different methods. In particular, thorough the porosimetric analysis, it was possible to determine the surface area of this material.

Moreover, the TGA coupled with FT-IR was employed to study the thermal decomposition of the resin and, through the FT-IR, the type of the released gas during the different steps of decomposition.

Finally, the fluorescence microscopy was able to give information about the swelling behaviour of Aquivion.

N_2 adsorption/desorption isotherms (77 K) were performed in a Micromeritics ASAP 2020 instrument. Samples were previously outgassed for 30 min at 100°C and 15 µmHg, and then heated for 30 min at 100°C. Specific surface area values were obtained by multi-point BET equation.

The thermal stability of Aquivion was tested on this material in different form (powder and micropellet) and with different acid loading (from 1.00 to 1.25 mmol SO_3H/g), using the TGA coupled with FT-IR analysis. The analyses were performed heating the samples from RT to 800°C (10°C/min - 5 min at 800°C) both in air and in nitrogen, using a TA Instrument Q600 coupled with a FT-IR spectrometer.

ATR analysis was performed on the Aquivion powders with different acid loading with the aim to understand the degree of hydration. This type of analysis was performed in IR Bruker Alpha Platinum ATR directly on the powder in 500-4000 cm^{-1} range.

The fluorescence microscopy was employed to study the swelling behaviour of Aquivion pellet in solvents with different polarity. The Aquivion pellets were impregnated with solutions of fluorescein. Then they were analysed with fluorescence microscope on the external surface and in the section, with the aim to follow the uptaking of the fluorescein solution from the material through the swelling phenomena.

The samples, prepared in Solvay laboratories using P87-S pellet, are reported in **Table *16*** with the solvent used for the impregnation and the corresponding polarity index.

Sample	Solvent	Polarity index
660/07A	Water	9.0
660/07B	Acetonitrile	5.8
660/07C	Ethanol	5.2
660/45-1	Cyclohexane	0.2
660/45-2	Dichloromethane	2.4
660/45-3	Toluene	3.1

Table 16 Aquivion samples prepared for the study of swelling behaviour.

The samples were prepared following the procedure described below:

- 5 g of pellet in 11 g of solvent with 1g of $1.4*10^{-4}$ M fluorescein solution in ethanol
- Stirring for 3 hours at 60°C or room temperature in the case of dichloromethane
- Drying at 80°C overnight

The analysis were performed in a confocal microscope Zeiss LSM 710, equipped with a 405 nm laser source and different objectives (10x, 20x and 50x). In **Figure *78***, a scheme of the instrument and the structure of fluorescein are displayed.

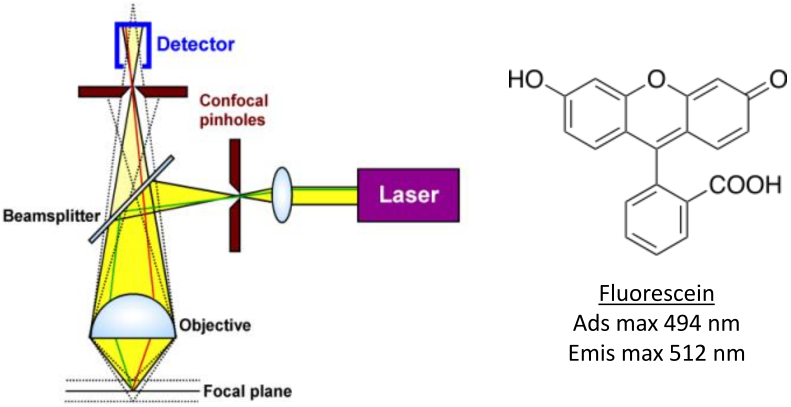

Figure 78 Confocal fluorescence microscope and fluorescein structure.

3.2.3 Catalytic tests

The catalytic behaviour of Aquivion was investigated in the gas phase reaction of ethanol dehydration to ethylene, as a model reaction (**Figure** ***79***).

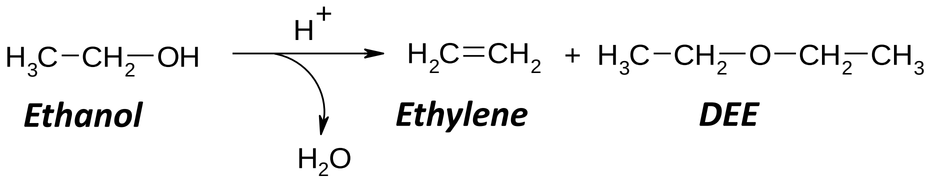

Figure 79 Ethanol dehydration reaction.

The laboratory scale plant was built up with a feeding system, composed by a pump for syringe and gas flow meters of nitrogen or helium, a glass fix-bed reactor and a TCD-gas-chromatograph apparatus for the analysis of the products (**Figure** ***80***).

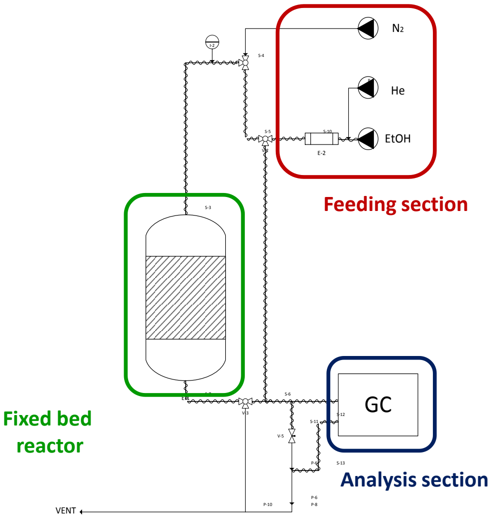

Figure 80 Flow sheet of the laboratory scale plant for the reaction of ethanol dehydration to ethylene.

In particular, helium was used as a carrier for ethanol, while nitrogen was employed as the inert gas for the pre-treatment of the resin, carried out before each catalytic test with the aim to remove the moisture from the Aquivion surface.

The pre-treatment was performed at 150°C for 1 hour with 40 ml/min of nitrogen.

Once developed the laboratory scale plant and the analytical system, many reaction parameters were studied, trying to find the best reaction conditions. In particular, the reaction temperature ranged between 120 and 200°C, while the contact time between 0.5 and 2 seconds.

A generic reaction scheme is reported in **Figure *81***. Many products can be formed on the surface of the catalyst, depending on the characteristics of the catalytic material and the reaction conditions.

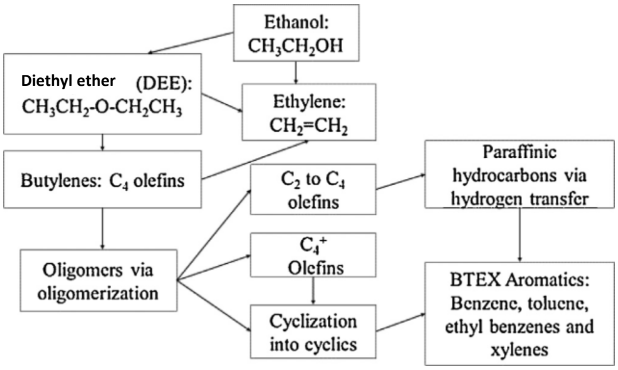

Figure 81 General reaction scheme for the ethanol dehydration reaction.

3.3 Results and discussion

During the last PhD year, the research activity has been focused on the study of the properties of Aquivion® PFSA, a perfluorosulfonic superacid resin (PFSA) provided by Solvay Specialty Polymers and at its testing as acidic catalyst.

The work done was based on two main topics:

i) Characterization of Aquivion material with the aim to understand its thermal properties and its swelling behaviour in different solvents.

ii) Catalytic tests using the dehydration of ethanol to ethylene as model reaction, to study the catalytic behaviour of this material in the gas phase, which has never been explored before.

In particular, for the study, different techniques of characterization were used and a laboratory-scale plant was built and coupled with an appropriate analytical system.

Among the various characterization techniques used, TGA coupled with FT-IR was chosen to follow the thermal behaviour of Aquivion and the compounds released during its decomposition.

Moreover, fluorescence microscopy was employed to study the swelling behaviour of these materials, using fluorescein dissolved in solvents at different polarities.

Finally, porosimetric analysis gave information about the surface area of dried Aquivion.

The behaviour of Aquivion as heterogeneous catalyst was studied in the gas-phase dehydration of ethanol to ethylene as a model reaction; the main products observed during the tests were ethylene and diethyl ether (DEE).

This reaction has reached growing attention due to environmental concerns. Indeed, among the new platform molecules originating from biomass, alcohols are of considerable importance and their dehydration to the corresponding olefins, performed with heterogeneous catalyst in a continuous gas phase process, is becoming an important issue. Over the years, a number of solid acids have been developed with the aim to replace homogeneous material causing corrosive media and difficult separation process. For example, oxides and zeolite have been used, but these materials need very high temperature and suffer from deactivation. Cationic exchange resins have also been tested, but they are only usable at low temperature. In this contest, the use of perfluorosulfonic resins as Aquivion becomes interesting thanks to the higher thermal stability and the super-acid character.

During the catalytic test, the effect of many reaction parameters has been monitored:

- Reaction temperature (from 120 to 200°C) and contact time (from 0.5 to 1 s)
- Catalyst form (pellet, micropellet, powder, etc.)
- Acid loading (from 1.00 to 1.5 mmol SO_3H/g) and stabilization treatment

3.3.1 Characterization of Aquivion material

The porosimetric analysis was performed on Aquivion material in different forms, through N_2 adsorption/desorption after an appropriate degas treatment.

The results are reported in **Table *17***.

Sample	**BET Surface Area (m^2/g)**	**Acid loading ($mmolSO_3H/g$)**	**Note**
PW98	0.3	1.00	Powder
PW79-S	0.2	1.25	Stabilized powder
PW87-S	0.3	1.15	Stabilized powder
P98	0.2	1.00	Pellets
P87-S	0.2	1.15	Stabilized pellets
P98-exp	0.0	1	Expanded pellets
mP98	0.1	1	Micropellets

Table 17 BET surface area of Aquivion samples.

The surface area values for all the analysed samples are very low and similar to each other; nevertheless, some interesting features were observed in the adsorption/desorption isotherms, as shown in **Figure *82***.

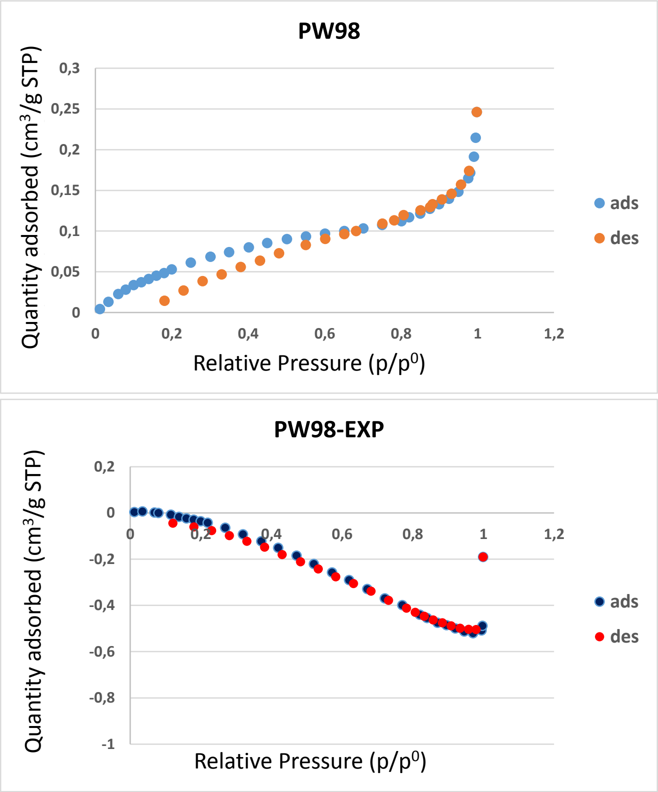

Figure 82 N_2 adsorption/desorption isotherms of PW98 and PW98-EXP samples.

The adsorption and desorption isotherms of PW98 sample are different, suggesting that the material changed after N_2 adsorption through the swelling phenomena. In particular, the desorption curve of PW98 sample is located under the adsorption one, suggesting that during the N_2 adsorption the structure of the material was changed due to swelling phenomena.

The isotherms related to PW98EXP shows negative values, evidencing the evolution of gases coming from inside the material during the analysis. This particular behaviour was due to the procedure used for the preparation of expanded material. The sample during the analysis did not adsorbed nitrogen but released gases.

The thermal stability of Aquivion was tested on this material in different form (powder and micropellet) and with different acid loading (from 1.00 to 1.25 mmol SO_3H/g), using the TGA coupled with FT-IR analysis.

The samples analysed with TGA and FT-IR analysis are reported in **Table *18***.

Analysed Sample	**In air**	**In N_2**	**Acid loading (mmolSO_3H/g)**	**Note**
PW98	X	X	1.00	Powder
PW87-S	X	X	1.15	Stabilized powder
PW79-S	X	X	1.25	Stabilized powder
mP98	X	X	1.00	Micropellet

Table 18 Aquivion samples analysed with TGA coupled with FT-IR analysis.

The analyses were performed heating the samples from RT to 800°C (10°C/min - 5 min at 800°C) both in air and in nitrogen.

The gas flow coming out from the TGA chamber was then analysed with an IR spectrometer.

In **Figure 83** an example of TG/DT profile, obtained with PW98 sample in air, is reported.

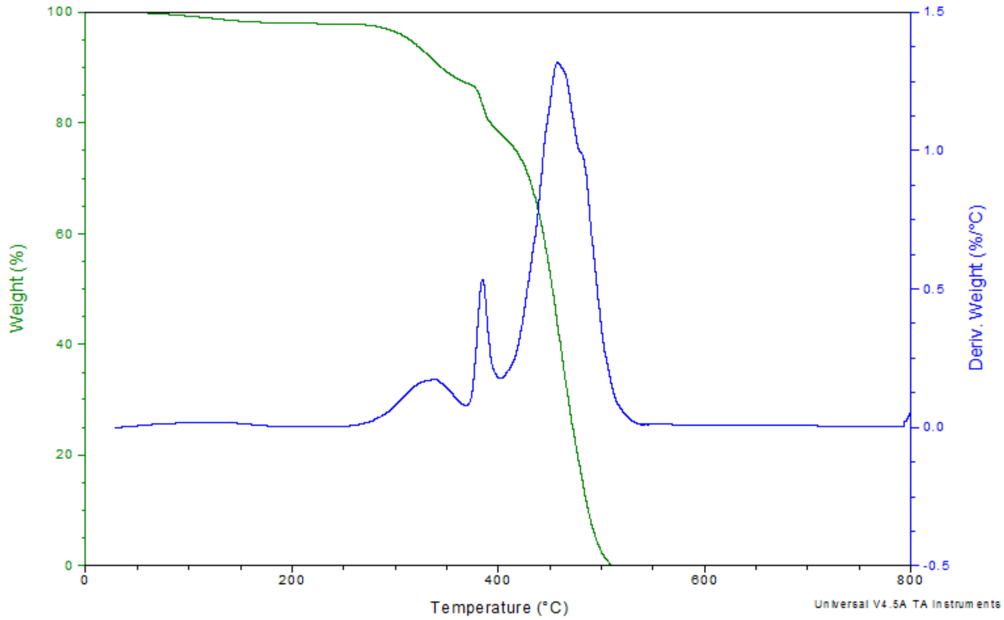

Figure 83 TG/DT profile of PW98 powder in air.

From this profile, three main events can be observed[42]:

- 290-400°C: desulfonation process
- 400-470°C: side-chain decomposition
- 470-560°C: PTFE backbone decomposition

The slight weight loss before 290°C was due to moisture on the surface of the material; all the steps of the decomposition and the moisture loss were observed for all the samples analysed both in air and in nitrogen flow. The FT-IR analysis of the gaseous stream confirmed that the decomposition of Aquivion took place through the events reported before. In **Figure *84***, the FT-IR analysis acquired during each step of decomposition are shown and explained[43].

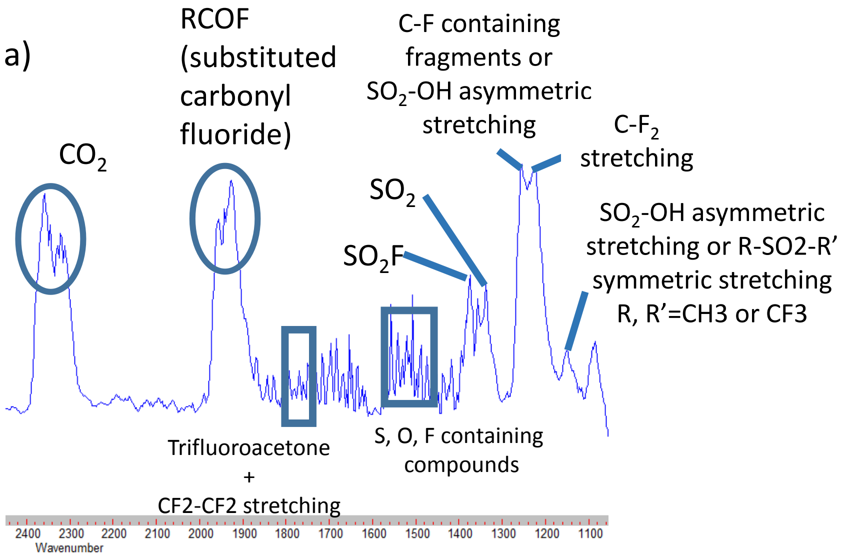
a)
CO_2
RCOF (substituted carbonyl fluoride)
C-F containing fragments or SO_2-OH asymmetric stretching
C-F_2 stretching
SO_2
SO_2F
SO_2-OH asymmetric stretching or R-SO2-R' symmetric stretching R, R'=CH3 or CF3
Trifluoroacetone + CF2-CF2 stretching
S, O, F containing compounds
2400
2300
2200
2100
2000
1900
1800
1700
1600
1500
1400
1300
1200
1100
Wavenumber

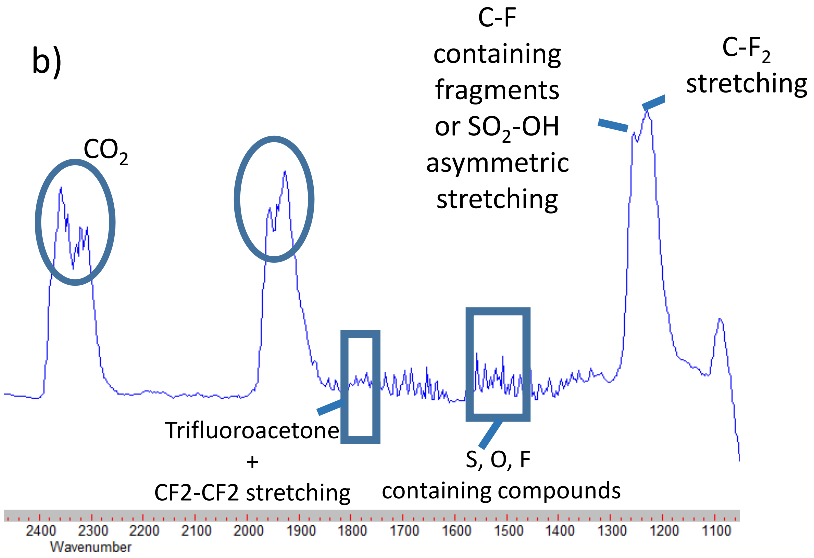
b)
CO_2
C-F containing fragments or SO_2-OH asymmetric stretching
C-F_2 stretching
Trifluoroacetone + CF2-CF2 stretching
S, O, F containing compounds
2400
2300
2200
2100
2000
1900
1800
1700
1600
1500
1400
1300
1200
1100
Wavenumber

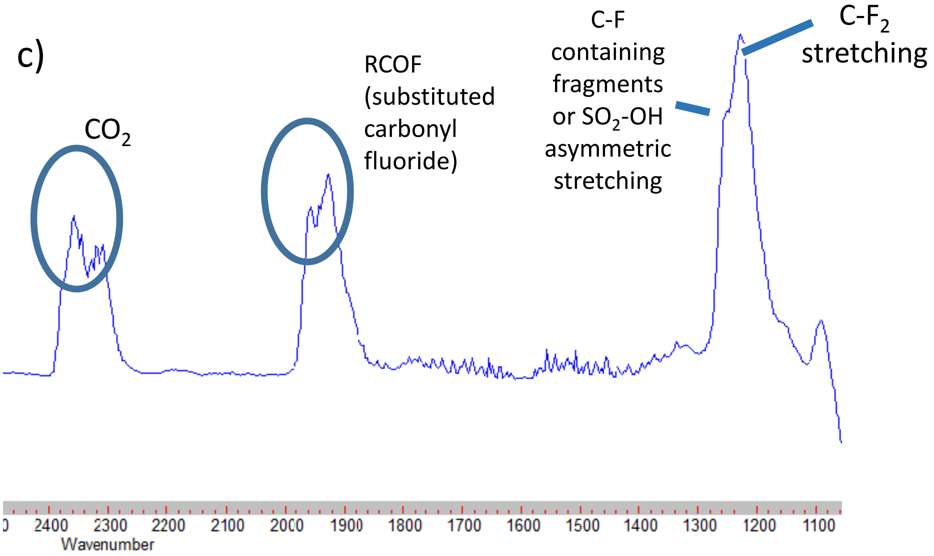

Figure 84 FT-IR spectra acquired during the first (a), second (b) and third (c) step of decomposition for sample PW98 during the TGA in air.

From the FT-IR spectra, it is possible to understand that during the first step of decomposition, corresponding to the desulfonation process, mainly S-containing compounds were released; while during the second and third steps F-containing compounds were detected.

Comparing the profiles obtained during the analysis in air and in nitrogen, some differences can be observed for all the analysed samples. In **Figure *85***, an example of comparison related to PW98 sample profiles is displayed.

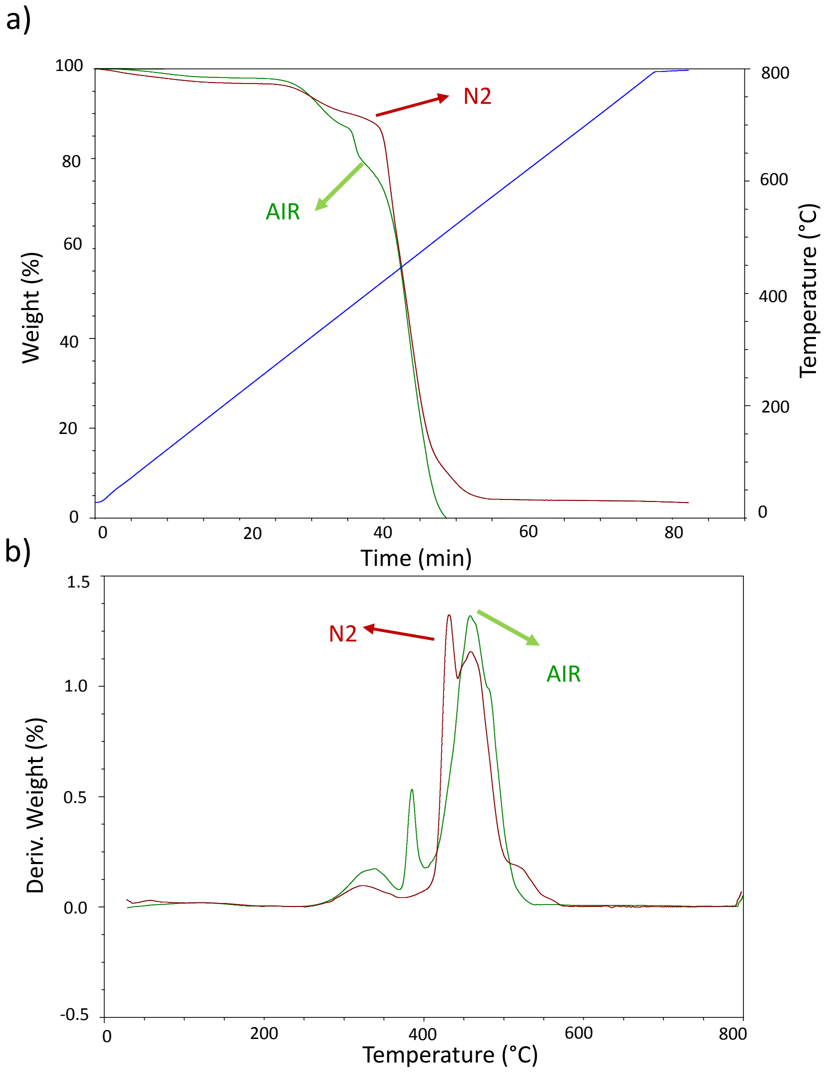

Figure 85 a) TG and b) DT profiles of PW98 powder analysed in air and in N_2.

As expected, the decomposition in nitrogen atmosphere begun at a relatively higher temperature than in air flow; although the type and the order of the events were always the same, as confirmed from the FT-IR analysis.

With the aim to understand the effect of the acid loading on the decomposition profile of Aquivion, in **Figure *86*** are reported the TG profiles of the Aquivion powders with different acid loading obtained in air and in nitrogen flow.

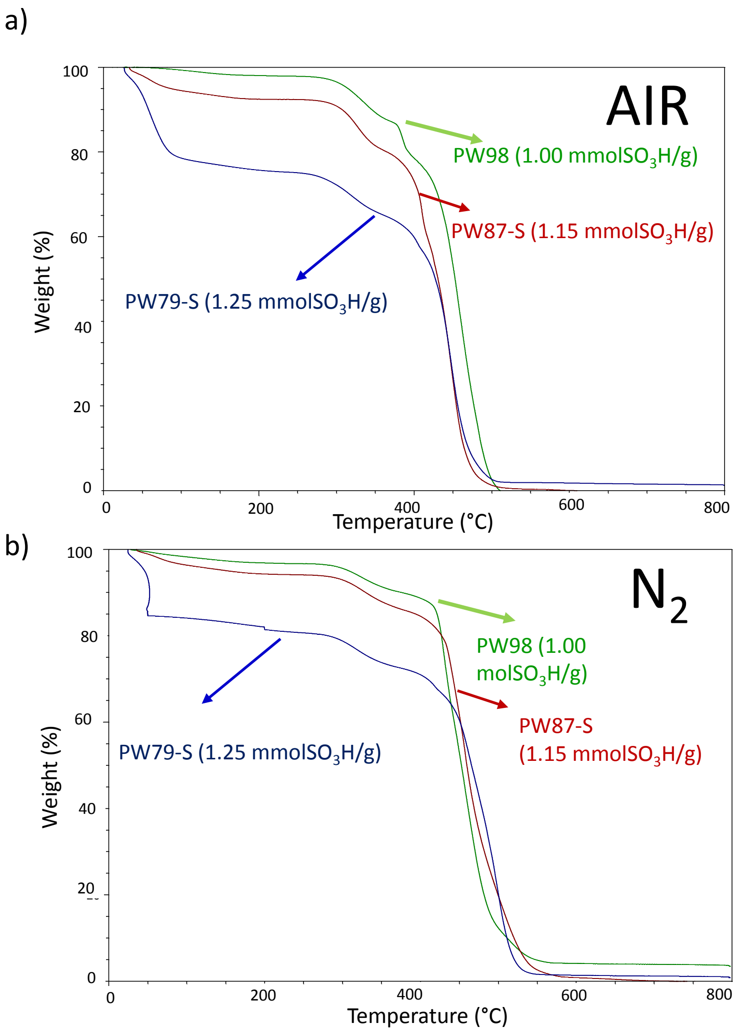

Figure 86 TG profiles in a) air and b) nitrogen of Aquivion samples with different acid loadings.

The differences between the TG profiles, with the acid loading and the kind of atmosphere, can be explained as below:

- About the first weight loss related to the water moisture loss: the higher the acid loading, the greater was the moisture weight loss. As expected, the PW79-S, which is the sample with the higher acid loading, showed the greater weight loss because, having the highest amount of $-SO_3H$ groups, was the most hydrated one.
- About the temperature of the greatest weight loss (the backbone decomposition): in air flow, the order of decomposition was PW87-S~PW79-

S<PW98, while in nitrogen flow was PW79-S<PW87-S<PW98. Although these slight differences, a trend of the backbone decomposition temperature with the acid loading could be observed; in particular, the greater the acid loading, the lower was the temperature of the backbone decomposition.

The degree of hydration of the Aquivion samples with the acid loading was confirmed from the ATR analysis, reported in **Figure *87***, with the corresponding interpretation of the bands[44].

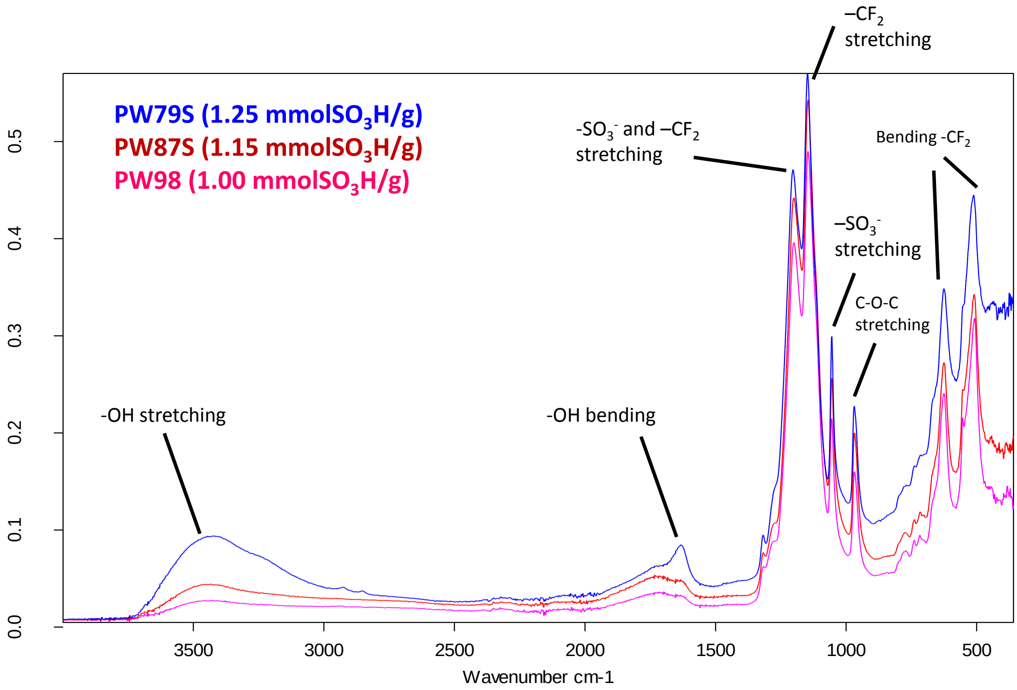

Figure 87 ATR analysis on Aquivion powder with different acid loading.

From the ATR spectra can be observed that the higher the acid loading, the greater was the amount of water, as the bands related to the –OH stretching and bending showed.

Comparing the TG profile related to PW98 (powder) and mP98 (micropellets) in air and in nitrogen (spectra not shown), the effect of the catalyst form can be understand; as expected, the form did not influence the decomposition profiles of the examined samples.

On the contrary, comparing the TG profile of the stabilized (PW87-S) and not stabilized samples (PW98), the effect of the stabilization treatment can be observed (**Figure *88***).

In particular, the attention should be focused on the released CO_2.

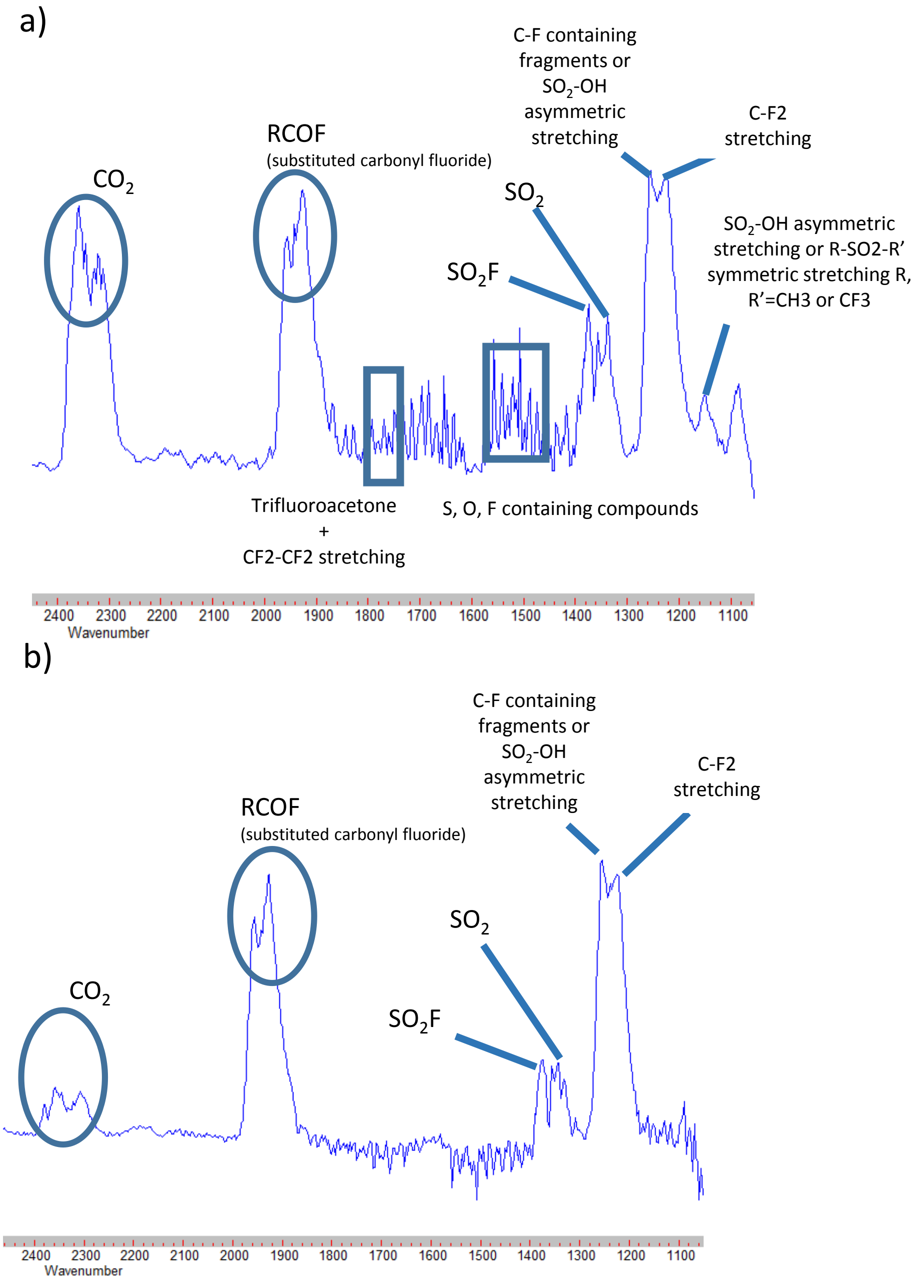

Figure 88 FT-IR spectra recorder for the first step of decomposition during the TGA in air of the sample PW98 (a), not stabilized powder, and PW87-S (b), stabilized powder.

The stabilization treatment is used to transform the –COOH terminal groups, formed by a side-reaction during the polymerization, in $–CF_3$ groups. As a consequence, the released CO_2 during TG analysis should be less for the stabilized samples and, as expected, this trend can be observed from the FT-IR spectra recorded during the first step of decomposition.

The fluorescence microscopy was employed to study the swelling behaviour of Aquivion pellet in solvents with different polarity. The Aquivion pellet were impregnated with solutions of fluorescein. Then they were analysed with fluorescence microscope on the external surface and in the section, with the aim to follow the up-taking of the fluorescein solution from the material through the swelling phenomena.

The prepared and analysed samples are reported in **Table *19*** with the solvent employed for the impregnation and the corresponding polarity index.

Sample	Solvent	Polarity index
660/07A	Water	9.0
660/07B	Acetonitrile	5.8
660/07C	Ethanol	5.2
660/45-1	Cyclohexane	0.2
660/45-2	Dichloromethane	3.1
660/45-3	Toluene	2.4

Table 19 P87-S samples prepared with fluorescein and different solvent for fluorescence microscopy analysis.

Looking at the many images acquired during the analysis, all the samples were fluorescent on the external surface while in the section some differences can be found.

The sample without fluorescein as expected was not fluorescent.

Firstly, considering the sample prepared with polar solvent (water, ethanol and acetonitrile), no differences were observed on the external surface and in the section of the pellet; this means that in polar solvent the fluorescein solution went also inside the pellet, in its inner part through swelling phenomena. The distribution of fluorescein and the intensity of fluorescence was homogeneous in the whole pellet.

Considering the samples impregnated with the more polar solvents (water, ethanol and acetonitrile), their external surface was fluorescent (**Figure *89***).

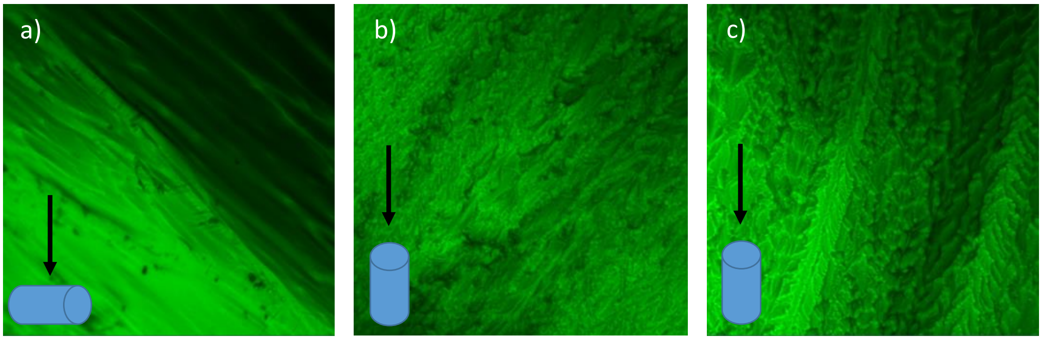

Figure 89 Comparison of the fluorescence images of the external surface of the P87-S pellet impregnated with water (a), acetonitrile (b) ad ethanol (c).

Moreover, the fluorescein solution went also in the inner part of the pellets through swelling phenomena, using the three different polar solvents, as demonstrated by the section images (**Figure *90***).

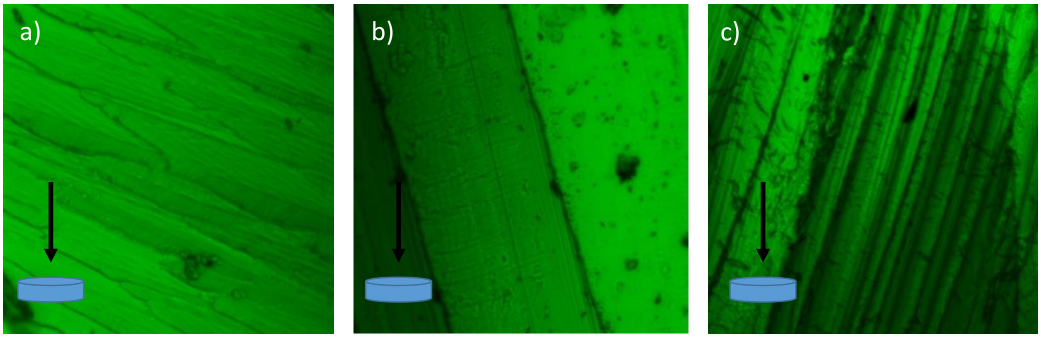

Figure 90 Comparison of the fluorescence images of the section of the P87-S pellet impregnated with water (a), acetonitrile (b) ad ethanol (c).

So using water, ethanol and acetonitrile, the Aquivion pellets showed a very prominent swelling behaviour.

Concerning the samples prepared with less polar solvents (cyclohexane, toluene and dichloromethane), the external surfaces were fluorescent (**Figure *91***), as seen also in the case of the more polar solvents.

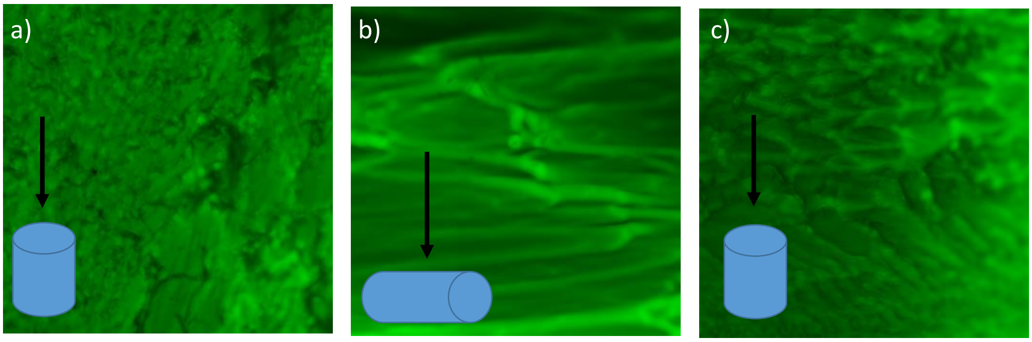

Figure 91 Comparison of the fluorescence images of the external surface of the P87-S pellet impregnated with cyclohexane (a), dichloromethane (b) and toluene (c).

Images belonging to the pellet sections exhibited inhomogeneous fluorescence, in particular for the samples impregnated with cyclohexane and dichloromethane.

This behaviour was probably due to a bad interaction between the resin and the solvents. In the case of these particular samples, the section were obtained into different way, to understand better the distribution of the fluorescein and consequently of the solvent, in the internal part of the pellet. One type was obtained, as the other, cutting the pellet along its diameter, while the other type was obtained cutting the pellet along the longitudinal plane. In **Figure *92*** are displayed, fluorescence image and intensity profile of the longitudinal section of the sample impregnated with dichloromethane.

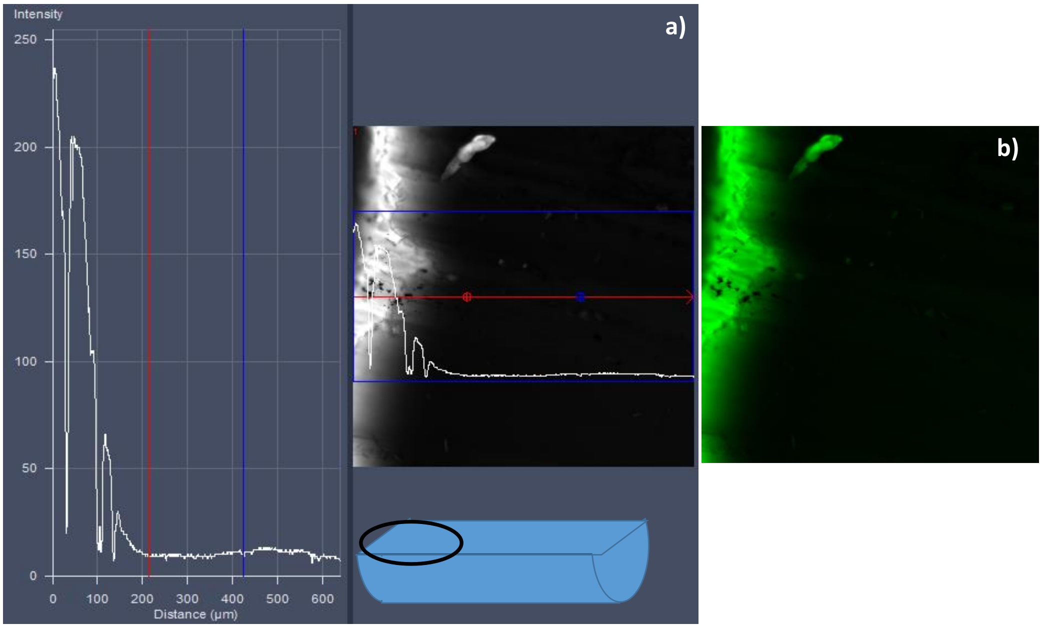

Figure 92 Intensity profile a) and image b) obtained with fluorescence microscopy analysis on the longitudinal section of 660/45-2 sample (impregnated with dichloromethane).

From the image reported above, it appears clear that the fluorescein did not go inside the pellet but only on its external surface. Indeed, considering the intensity profile, moving from the external surface to the inner part, the intensity decreased dramatically. A similar behaviour can be observed also in the longitudinal section of the sample prepared with cyclohexane (**Figure** *93*).

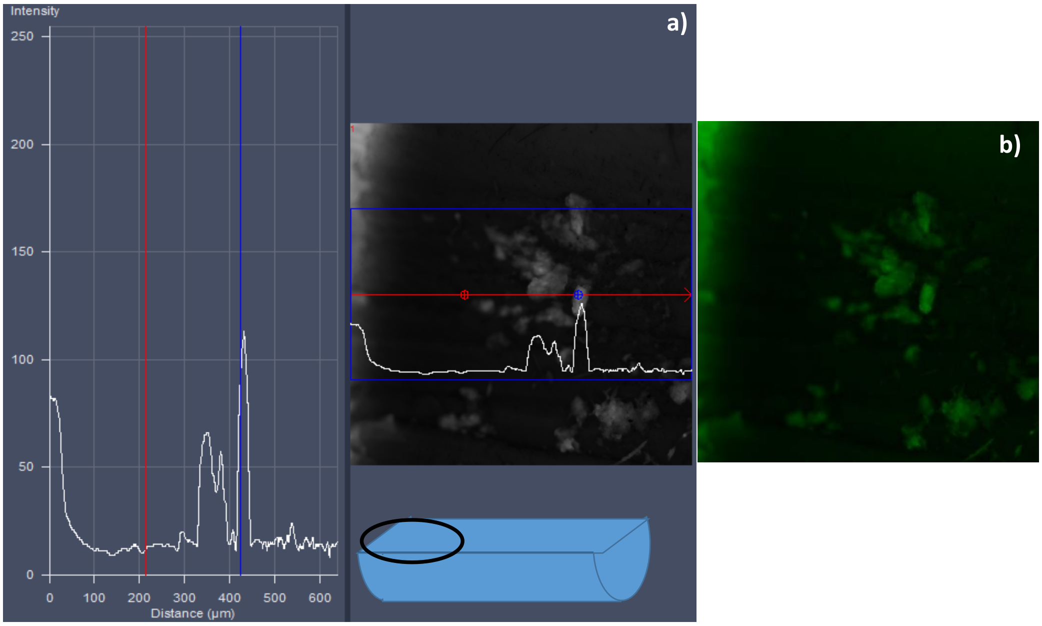

Figure 93 Intensity profile a) and image b) obtained with fluorescence microscopy analysis on the longitudinal section of 660/45-1 sample (impregnated with cyclohexane).

Also in this case, the profile intensity shows that the fluorescence intensity decreased going in the inner part of the pellet where the fluorescence was not homogenous. Among the less polar solvents tested, the only one, which assured a homogeneous fluorescence outside and inside the pellet, was toluene, as shown in **Figure** *94* in comparison with the other samples with inhomogeneous fluorescence.

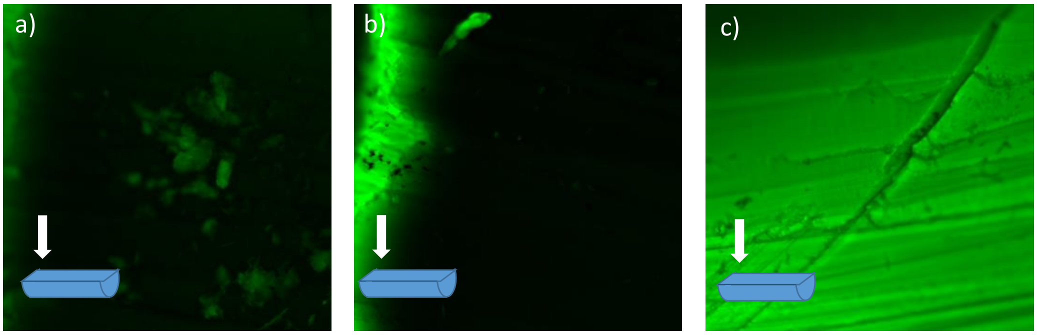

Figure 94 Comparison of the fluorescence images of the section of the P87-S pellet impregnated with cyclohexane (a), dichloromethane (b) and toluene (c).

In conclusion, the prominent swelling behaviour was guaranteed by the use of water, ethanol and acetonitrile; while employing less polar solvents, such as dichloromethane and cyclohexane, the fluorescein was not homogenously distributed inside the Aquivion pellets.

3.3.2 Catalytic tests in gas-phase ethanol dehydration

The catalytic behaviour of Aquivion in the gas phase reaction of ethanol dehydration to ethylene was investigated, changing different reaction parameters such as temperature, contact time, catalyst form, acid loading and feeding stream composition.

Effect of reaction temperature

The effect of the reaction temperature on the catalytic performances was studied on different Aquivion based catalysts, which are reported in **Table *20*** with the temperature used in each catalytic tests.

Catalyst	**T range (°C)**	**Acid loading ($mmolSO_3H/g$)**	**Note**
P98	150-180-200	1.00	Pellet
PW98	120-150	1.00	Powder
PW98-S	120-150	1.00	Stabilized powder
PW87-S	120-150	1.15	Stabilized powder
PW79-S	120-150	1.25	Stabilized powder
PW65-S	120-150	1.40	Stabilized powder
P87-S	150-180-200	1.48	Stabilized pellet

Table 20 Aquivion samples used for the study of the reaction temperature effect.

The effect of the temperature was monitored on the powder and on the pellet form, stabilized or not, and on the stabilized powder with different acid loading.

In general, from the obtained results it was possible to understand that for all the tested catalysts, the ethanol conversion and the ethylene selectivity increased with increasing temperature, while the DEE (diethyl ether) selectivity decreased. These results agreed perfectly with the ones reported in literature and obtained with other kind of material[45, 46, 47]. Indeed, the reaction that leads to the formation of DEE is a condensation reaction between two ethanol molecules and it is exothermic, consequently not favoured with increasing temperature; while ethylene is formed via dehydration reaction, which is an endothermic reaction. As an example, the trend of the catalytic activity, in terms of ethanol conversion and products selectivity, of P98 as a function of temperature is displayed in **Figure *95***.

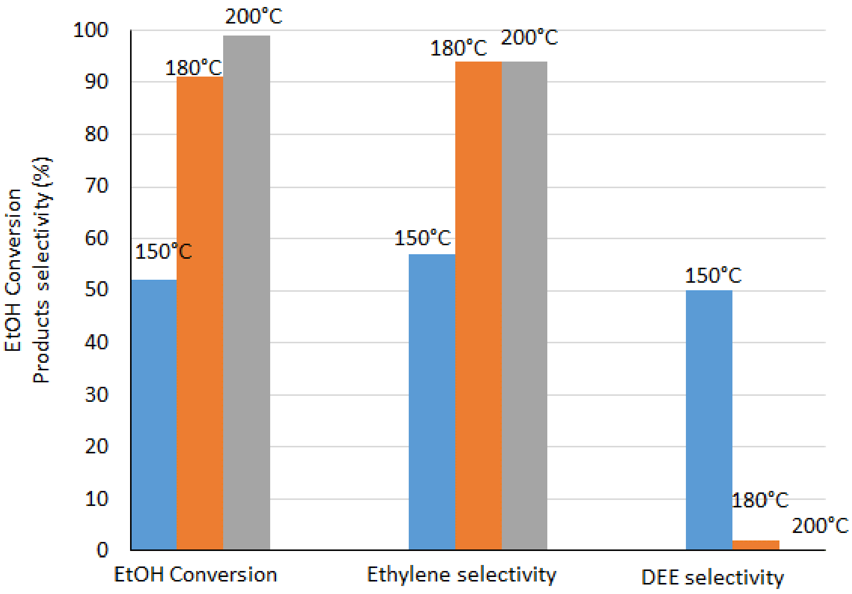

Figure 95 Trend of the catalytic activity of P98 with 1% of ethanol in the gas stream and 1s as contact time.

It should be underlined that the ethanol conversion was high at relatively low temperature; at 150°C, the conversion already reached 50%. Moreover, the conversion was around 100% at 200°C.

The effect of temperature was the same on stabilised and not stabilised catalysts. For example, comparing the catalytic performances of PW98-S and PW98, it was possible to observe the same trend of conversion and products selectivity with increasing temperature.

Concerning the different acid loading, the increase of the reaction temperature led to the same effect on the catalytic performances of Aquivion, even if the acid loading changed.

In conclusion, the best catalytic performances in terms of ethanol conversion and ethylene selectivity, were obtained at the highest temperature, 200°C for pellet form and 150°C for powder form. Moreover, the catalysts provided stable performance for different hours.

Effect of contact time

The effect of the contact time was studied on P98 catalyst changing the catalyst amount and keeping constant the total flow and vice versa, in order to obtain a contact time of 0.5, 1 and 2 seconds.

When the contact time was increased, increasing the catalyst amount or decreasing the total flow, the conversion of ethanol increased, while the selectivity in the main product did not change so evidently, even if at the lower temperature some differences could be observed. The effect of the contact time was studied feeding 1% of ethanol in the gaseous stream at 150, 180 and 200°C. As expected, for each temperature, the effect of the contact time was similar. As an example, in **Figure *96*** is reported the study of the influence of the contact time on P98 performances at 150°C, changing the catalyst amount and keeping constant the total flow.

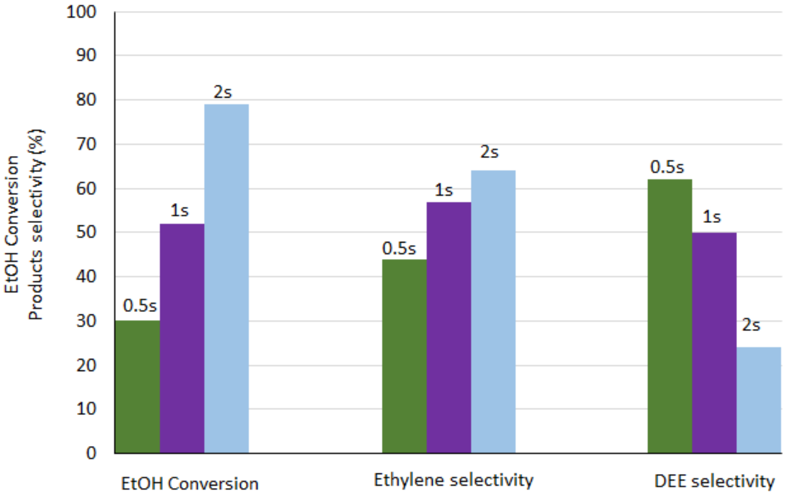

Figure 96 Effect of contact time on P98 performances at 150°C and 1% of ethanol.

As expected[47], increasing the contact time with the amount of catalyst, the ethanol conversion increased. At 150°C the effect of the contact time was clearly visible, while at 180 and 200°C there was only a slight influence. This was probably due to the fact that at higher temperature the ethanol conversion and ethylene selectivity were so high that little changes could not be easily noticed.

Effect of catalyst form

The influence of the catalyst form was monitored on the catalytic performances of catalysts belonging to the 98 series, so with the same acid loading (1.00 mmolSO_3H/g), but in different forms (***Table 21***).

Sample	**Catalyst form**	**τ (s)**	**Catalyst amount (g)**
PW98	Powder	1.20	0.7
mP98	Micropellet	0.95	0.7
P98	Pellet	1.00	0.7
EXP98	Expanded pellet	3.50	0.7
EXP98	Expanded pellet	1.00	0.2

Table 21 Catalyst and reaction conditions used for the study of the influence of the catalyst form.

The catalytic tests were performed at 150°C with 1% of ethanol concentration in gaseous stream, in two different ways in order to have a comparison between the different forms of catalyst. In one case, the catalyst amount was kept constant, in the other one, the contact time was maintained the same, having the catalyst different bulk density. The results obtained in the first case are displayed in **Figure *97***, where on the two Y axes can be found respectively the ethanol conversion and the ratio between DEE and ethylene selectivity. Consequently, the best catalyst should show higher value in ethanol conversion (orange line) and lower value in DEE/ethylene ratio (blue line).

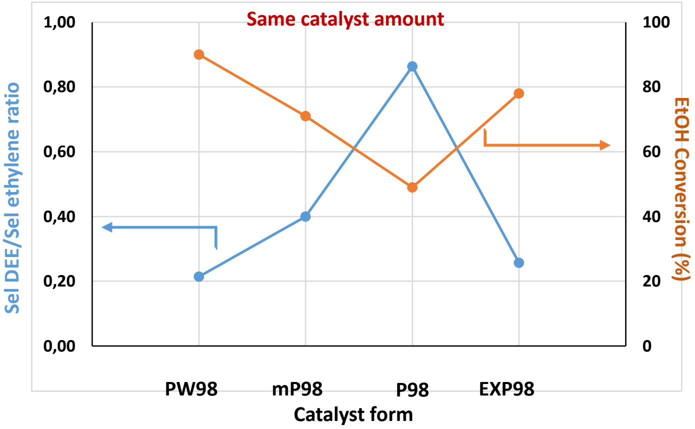

Figure 97 Study of the effect of the catalyst form with catalyst amount constant at 150°C and 1% of ethanol. The product selectivity is reported as the ratio between DEE and ethylene selectivity.

In this case, the best catalyst was PW98 (the powder form) followed by EXP98, mP98 and P98. In this type of study, the catalyst amount was the same for the different forms and the contact time was similar, except for EXP 98 sample; consequently, it seemed that the powder form showed more available acid sites than the other forms.

The effect of the catalyst form was studied also keeping constant the contact time (***Figure 98***).

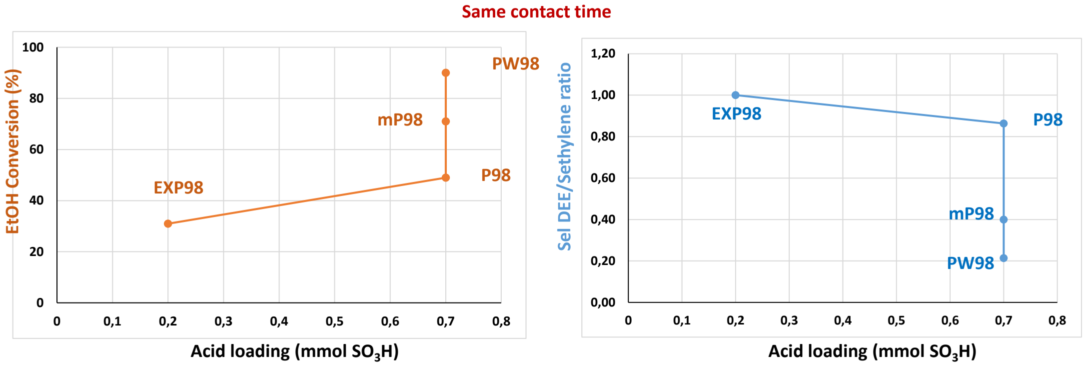

Figure 98 Study of the effect of the catalyst form with contact time constant at 150°C and 1% of ethanol.

The results are shown in function of the real acid sites amount used for each catalytic test. Indeed, with the aim to maintain constant the contact time, the amount of catalyst had to be change because of the different bulk densities.

Also in this case, the best catalyst was PW98 which provided the highest ethanol conversion with the lowest DEE/ethylene selectivity ratio. The catalytic performances of PW98 were followed by those of mP98, P98 and EXP98. This trend was probably due to the same reason of the previous case; the powder form showed more accessible acid sites.

In conclusion, the form of the catalyst had a great effect on the catalytic activity which was favoured by the form with fine particle size and/or more active surface.

Effect of acid loading

The influence of the acid loading was studied on the stabilized powder (**Table *22***) at 120 and 150°C with 1% of ethanol in the gaseous stream. The catalytic tests were performed also at 120°C with the aim to have a lower catalytic activity and discriminate better the differences among the catalysts.

Catalyst	Acid loading (mmolSO$_3$H/g)
PW98-S	1.00
PW87-S	1.15
PW79-S	1.25
PW65-S	1.48

Table 22 Catalyst powders used for the study of the influence of the acid loading.

The catalytic tests were performed in two different ways: keeping constant the contact time or the catalyst amount. The expected trend was in function of the acid loading: higher the acid loading, better the catalytic activity. PW65-S gave the best catalytic performances, but also PW87-S unexpectedly showed a high ethanol conversion and ethylene selectivity. As an example, the comparison among the different catalyst at 120 °C with 1% of ethanol and 0.7g of catalyst is showed in **Figure *99***.

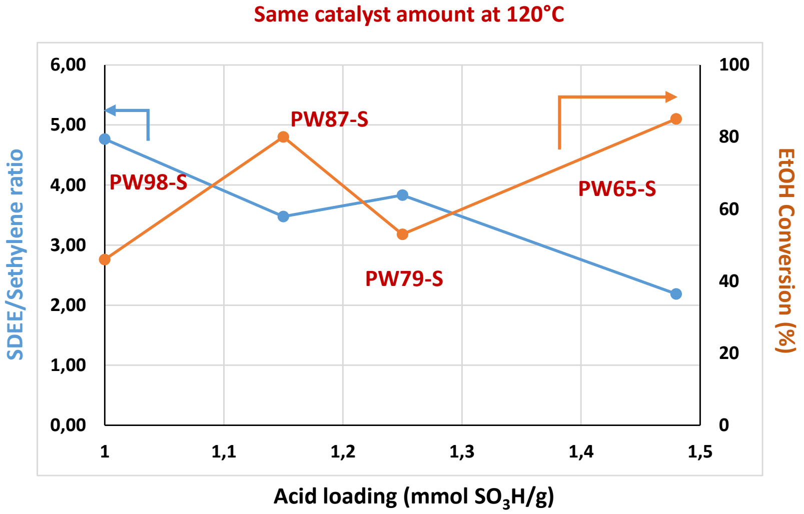

Figure 99 Effect of the acid loading at 120 °C, with 1% of ethanol and 0.7 g of catalyst.

The results obtained are reported in function of the acid loading, the ethanol conversion and the ratio between DEE and ethylene selectivity. Consequently, the best catalyst should show higher value in ethanol conversion (orange line) and lower value in DEE/ethylene ratio (blue line). The differences among the catalysts can be better observed at 120°C where PW87-S and PW65-S gave the best catalytic performances.

The change in the acid loading had a similar effect also in the tests performed at 120 and 150°C with the same contact time; PW65-S and PW87-S showed the best catalytic performances in terms of ethanol conversion and ethylene selectivity. The behaviour of the catalyst with different acid loading was expected, except for PW87-S which provided catalytic performances similar to PW65-S probably due to a better accessibility of the acid sites.

In conclusion, a trend of the catalytic performances with the acid loading could be found considering PW98-S, PW79-S and PW65-S catalytic performances, only the behaviour of the PW87-S did not respect this trend, due probably to a better accessibility of the active sites.

Effect of catalyst type

Different types of acid catalyst were tested with the aim to discover if Aquivion could provide improved catalytic performances compared to similar materials in the reaction of interest.

3. Catalytic superacid perfluorosulfonic resins

Between the ion exchange resins, Amberlyst and Nafion type were chosen. The former is a resin composed by styrene and divinylbenzene and cannot be used at high temperature; the latter, is composed by F-containing polymer, as a consequence, has a great thermal stability and can be used at higher temperature.

The catalysts used for the comparison of Aquivion with other kind of material are reported in **Table** ***23***.

Catalyst	Material	Acid loading (mmol SO_3H/g)	Catalyst form
A15dry	Amberlyst	≥4.7	Opaque spherical beads
A70wet	Amberlyst	≥2.55	Dark brown spherical beads
NR50	Nafion	≥0.8	Pellet
P98	Aquivion	1.00	Pellet
P87-S	Aquivion	1.15	Pellet

Table 23 Materials used for the study of the influence of the catalyst type.

The Amberlyst catalysts possess a very high acidity and they are available into two forms: wet and dry. A70 wet catalyst has around 50% of moisture content (mainly water); for this reason, it was pre-treated at 120°C overnight before being loaded in the reactor, to obtain the dry form. Both Amberlyst catalysts were used only at 150°C because they have a low thermal resistance. Instead, Nafion catalyst could be used until 200°C, as Aquivion.

The catalytic activity of all these different catalysts at 150°C, 1% of ethanol and 1s as contact time is displayed in **Figure** ***100***.

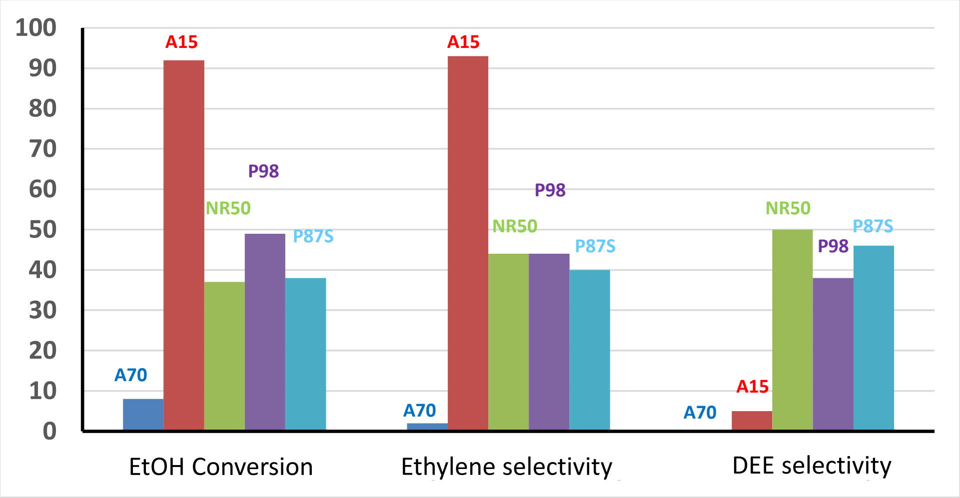

Figure 100 Catalyst type influence on catalytic performances at 150°C, 1% of ethanol and 1 s of contact time.

From these data, it is clearly evident that dry Amberlyst (A15) gave the best catalytic performances, followed by Aquivion (P98), while the wet Amberlyst A70 was the worst catalyst. The catalytic behaviour of Amberlyst A15 could be explained considering its higher surface area (50 m^2/g) and acid loading (≥4.7 $mmolSO_3H/g$) compared to Nafion and Aquivion materials.

Effect of water presence in the feeding stream

In order to investigate the influence of water in the feeding stream, many catalytic tests were performed in the same laboratory-scale plant on Aquivion pellet form (P87-S), feeding a mixture composed by 1% of ethanol and 1% or 0.5% of water in He, with the aim to mime a sort of feeding stream coming from biomass fermentation. The reaction temperature was in the range of 120-200 °C and the contact time was 1 second.

In general, the water had a slightly negative effect on the catalytic behaviour of Aquivion, mainly in ethanol conversion and ethylene production; nevertheless, the catalysts maintained stable conversion and yields (**Figure *101***).

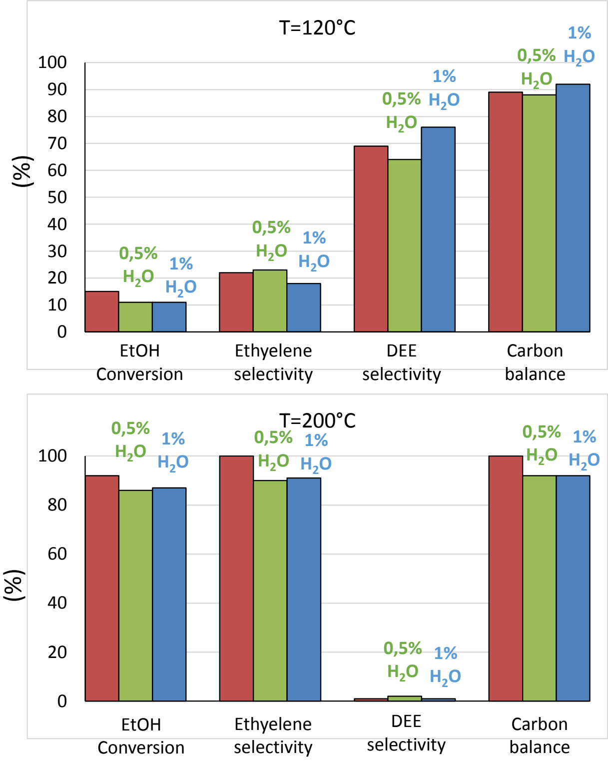

Figure 101 Catalytic tests on P87-S for the study of the water influence (120-200°C, 0-1% water and 1s as contact time).

In the considered range of temperature, water had a slight negative effect on the catalytic performances because the ethanol conversion and ethylene selectivity in general were lower than the values obtained in absence of water. This behaviour was probably due to the fact that water was expected to adsorb more strongly than ethanol on catalyst surface, causing reduction in the number of available active sites for the chemisorption of ethanol[47]. Moreover, water is a coproduct of the dehydration reaction, so a negative effect could be expected.

In conclusion, water had a slight negative effect on the catalytic behaviour of Aquivion catalyst; nevertheless, the catalytic performances were stable, without showing any deactivation phenomena.

3.4 Conclusions

In general, Aquivion material showed interesting catalytic properties in the gas-phase ethanol dehydration and very good swelling properties. Although the very low surface area, this material provided high ethanol conversions at relatively low temperature and stable performances for different hours, without showing any deactivation trends.

Concerning the characterization, Aquivion material showed a high thermal stability thanks to its structure. Moreover, this material displayed interesting swelling properties when put in contact with polar solvents.

The catalytic performances were monitored in many different conditions. In particular, the ethanol conversion and the ethylene selectivity increased with increasing temperature, while the DEE (diethyl ether) selectivity decreased; while, increasing the contact time with the amount of catalyst, the ethanol conversion increased.

In addition, the form of the catalyst had a great effect on the catalytic activity which was favoured by the form with fine particle size and/or more active surface, consequently the powder form provided the best catalytic performances.

The behaviour of Aquivion catalysts with different acid loading was similar to the expected one, except for PW87-S which provided catalytic performances similar to PW65-S (with the highest acid loading) probably due to a better accessibility of the acid sites.

From the comparison of the catalytic activity of Aquivion with other ion exchange resin, emerged that dry Amberlyst (A15) gave the best catalytic performances, followed by Aquivion (P98), while the wet Amberlyst A70 was the worst catalyst. The catalytic behaviour of Amberlyst A15 could be explained considering its higher surface area; nevertheless this type of material could be used only at low temperature. Nafion material instead could be employed in the same temperature range of Aquivion and provided catalytic performances similar to Aquivion material.

Finally, in the considered range of temperature, water had a slight negative effect on the catalytic performances because the ethanol conversion and ethylene selectivity in general were lower than the values obtained in absence of water. This behaviour was probably due to a stronger adsorption of water on the active sites with respect to ethanol.

References

---

[1] P. Gupta, S. Paul, *Catal. Today* **236** (2014) 153-170.

[2] M. Lancaster, Green Chemistry: An Introductory Text, Royal Society of Chemistry, Cambridge, 2002.

[3] P. T. Anastas, M. M. Kirchhoff, T. C. Williamson, *Appl. Catal. A: Gen.* **221** (2001) 3-13.

[4] M. A. Harmer, Q. Sun, *Appl. Catal. A: Gen.* **221** (2001) 45-62.

[5] G. Busca, *Chem. Rev*. **107** (2007) 5366-5410.

[6] G. A. Olah, G. K. S. Prakash, A. Molnar, J. Sommer, *Superacid Chemistry*, Wiley, Hoboken, 2009.

[7] N. Ozbay, N. Oktar, N. A Tapan, *Fuel* **87** (2008) 1789-1798.

[8] P. K. Paakkonen, A. O. I Krause, *Appl. Cata. A: Gen.* **245** (2003) 289-301.

[9] Y. Feng, B. He, Y. Cao, J. Li, M. Liu, F. Yan, *Bioresour. Technol.* **101** (2010) 1518-1521.

[10] P. F. Siril, D. R. Brown, *J. Mol. Catal. A: Chem.* **252** (2006) 125-131.

[11] V. Arcella, T. Troglia, A. Ghielmi, *Ind. Eng. Chem. Res.* **44** (2005) 7646-7651.

[12] S. R. Samms, S. Wasmus, R. F. Savinell, *J. Electrochem. Soc.* **143** (1996) 1498-1504.

[13] G. A. Olah, G. K. S. Prakash, J. Sommer, *Science* **206** (1979) 13-20.

[14] M. A. Harmer, Q. Sun, W. E. Farneth, *J. Am. Chem. Soc.* **118** (1996) 7708-7715.

[15] Q. Sun. M. A. Harmer, W. E. Farneth, *Chem. Commun*, (1996) 1201-1202.

[16] M. A. Harmer, W. E. Farneth, Q. Sun, *Adv. Mater* **10** (1998) 1255-1257.

[17] M. Fujiwara, K. Shiokawa, Y. Zhu, *J. Mol. Catal. A: Chem.* **264** (2007) 153-161.

[18] M. Fujiwara, K. Kuroaka, T. Yazawa, Q. Xu, M. Tanak, Y. Souma, *Chem. Commun.* (2000) 1523-1524.

[19] A. Ghielmi, P. Vaccarono, C. Troglia, V. Arcella, *J. Power Sources* **145** (2005) 108-115.

[20] K. Prater, *J. Power Sources* **29** (1990) 239–250.

[21] B.R. Ezzell, W.P. Carl, W.A. Mod, US Patent 4,330,654 (1982).

[22] B.R. Ezzell, W.P. Carl, US Patent 4,940,525 (1990).

[23] M. Apostolo, V. Arcella, (Ausimont S.p. A.). European Patent No. 1 172 382 A2, 2002.

[24] A. Karam, N. Sayoud, K. D. O. Vigier, J. Lai, A. Liebens, C. Oldani, F. Jerome, *J. Mol. Catal. A: Chem.* 422 (2016) 84-88.

[25] W. Fang, S. Wang, A. Liebens, F. De Campo, H. Xu, W. Shen, M. Pera-Titus, J. M: Clacens, *Cat. Sci. Technol.* **5** (2015) 3980-3990.

[26] R. Tassini, V. D. Rathod, S. Paganelli, E. Balliana, O. Piccolo, *J. Mol. Catal. A: Chem.* **411** (2016) 257-263.

[27] C. D'urso, C. Oldani, V. Baglio, L. Merlo, A. S. Aricò, *J. Power Sources* **272** (2014) 753-758.

[28] A. Donnadio, M. Pica, S. Subianto, D. J. Jones, P. Cojacaru, M. Casciola, *ChemSusChem* **7** (2014) 2176-2184.

[29] L. Bianchi, E. Ballerini, M. Curini, D. Lanari, A. Marrocchi, C. Oldani, L. Vaccaro, *ACS Sustainable Chem. Eng.* **3** (2015) 1873-1880.

[30] M. A. Harmer, Q. Sun, A. J. Vega, W. E. Farneth, A. Heidekum, W. F. Hoelderich, *Green Chem.* **6** (2000) 7-14.

[31] Q. Sun, M. A. Harmer, W. E. Farneth, *Ind. Eng. Chem. Res.* **36** (1997) 5541-5544.

[32] C. B. Campbell, A. Onopchenko, D. C. Young, *Ind. Eng. Chem. Res.* **29** (1990) 642-647.

[33] A. Chauvel, B. Delmon, W. F. Hoelderich, *Appl. Catal. A* **115** (1194) 173-217.

[34] G. K. S. Prakash, I. Bychinskaya, E. R. Marinez, T. Mathew, G. A. Olah, *Catal. Lett.* **143** (2013) 303-312.

[35] G. K. S. Prakash, H. Lau, C. Pania, I. Bychinskaya, S. K. Ganesh, B. Zaro, T. Mathew, G. A. Olah, *Catal. Lett.* **144** (2014) 2012-2020.

[36] H. Zou, S. Wu, J. Shen, *Chem. Rev.* **108** (2008) 3893-3957.

[37] X. Zhang, F. Su, D. Song, S. An, B. Lu, Y. Guo, *Appl. Catal., B* **163** (2015) 50-62.

[38] W. Fang, Z. Fan, H. Shi, S. Wang, W. Shen, H. Xu, J-M. Clacens, F. De Campo, A. Liebens, M. Pera-Tituts, *J. Mater. Chem., A* **4** (2016) 4380-4385.

[39] M. M. Titirici, M. Antonietti, *Chem. Soc. Rev.* **39** (2010) 103-116.

[40] M. I. Bro, C. A. Sperati, *J. Polym. Sci.* **38** (1959) 298-295.

[41] M. Pianca, E. Barchiesi, G. Esposto, S. Radice, *J. Fluorine Chem.* **95** (1999) 71-84.

[42] S. H. De Almeida, Y. Kawano, *J. Therm. Anal. Calorim.*, **58** (1999) 569-577.

[43] Q. Deng, C. A. Wilkie, R. B. Moore, K. Mauritz, *Polymer*, **39** (1998) 5961-5972.

[44] A. Gruger, A. Regis, T. Schmatko, P. Colomban, *Vibr. Spectrosc.* **26** (2001) 215-225.

[45] A. Galadima, O. Muraza, *J. Ind. and Chem*. **31** (2016) 1-14.

[46] T. T. Nguyen, V. Ruaux, L. Massin, C. Lorentz, P. Afanasiev, F. Maugè, V. Belliere-Baca, P. Rey, J. M. M. Millet, *Appl. Catal., B* **166-167** (2015) 432-444.

[47] D. Varisli, T. Dogu, G. Dogu, *Chem. Eng. Sci.* **62** (2007) 5349-5352.

General Conclusions

In this PhD work, different topics were developed mainly dealing with mesoporous materials and fluorinated compounds.

In the first part of the PhD work, PdCu/MCM-41 systems were successfully prepared as mesoporous catalysts for hydrodechlorination (HDC) reaction for the production of fluorinated monomers. Indeed, this study demonstrated the possibility of obtaining bimetallic catalysts with ordinated structure through sol-gel method and the direct insertion of the metallic precursors during MCM-41 synthesis[1, 2]. Nevertheless, the calcination at high temperature (T=540°C) for the removal of the template provoked the segregation of oxides and large Pd/Cu particles. To control the active phase composition and particle size, the ionic exchange, using ethanol and ammonium nitrate at 60°C, was employed as an alternative method for the template removal. Moreover, with the aim of optimizing the distribution of bimetallic Pd/Cu species over the support, Pd/Cu nanoparticles (PdCu NPs) were employed as metal precursors (**Scheme *1***).

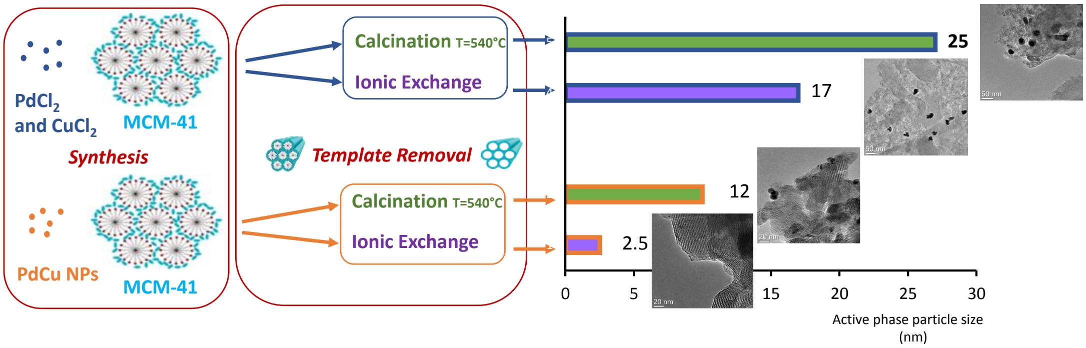

Scheme 1 Summary of the synthetic procedure for PdCu/MCM-41 catalysts.

This optimized method of synthesis permitted to avoid the aggregation of metals the first stage of the MCM-41 preparation. Moreover, the use of ionic exchange treatment avoid the growth of metallic nanoparticles during the template removal.

Finally, the catalysts were tested in the hydrodechlorination (HDC) reaction of $CF_3OCFClCF_2Cl$ (AM) to $CF_3OCF=CF_2$ (MVE) showing interesting behaviour. Higher

AM conversion was provided by bimetallic nanoparticles-containing catalyst due to the lower particle size and through the ionic exchange the MVE selectivity was enhanced[3].
Although the mesoporous features of MCM-41 based catalysts, the catalytic performances in the reaction of interest were not comparable to the results obtained using active carbon as support for Pd/Cu active phase[4]. Consequently, trying to enhance the catalytic activity, the research work was moved from mesoporous silica to mesoporous carbon materials, combining the mesoporous features of the silica with the catalytic behaviour provided by carbon based catalysts.

Concerning the mesoporous carbon material, soft-template method, using greener phenolic resins precursors, was an efficient synthetic route for the preparation of this kind of material (OMC), having ordered structure and high surface area[5]. Moreover, through post-synthesis oxidation treatments with HNO_3 or H_2O_2, it was possible to create new surface functional groups, useful for enhancing the catalytic activity (**Scheme *2***).

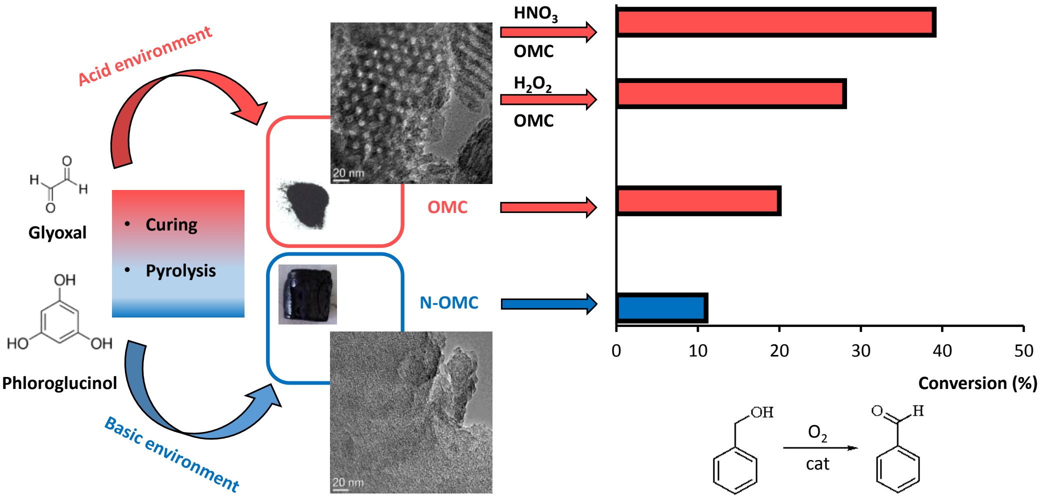

Scheme 2 Synthetic procedure and catalytic performances of mesoporous carbon catalysts.

In addition, synthetic route involving the use of amine was developed with the aim of introducing basic functionalities (N-OMC); nevertheless, this method led to microporous materials. Finally, through the catalytic tests, the role of the surface functional groups in the benzyl alcohol oxidation model reaction was demonstrated.

The last part of the work dealt with a topic that has never been explored before: the investigation of catalytic properties of Aquivion® PFSA in gas-phase dehydration reaction (**Scheme *3***).

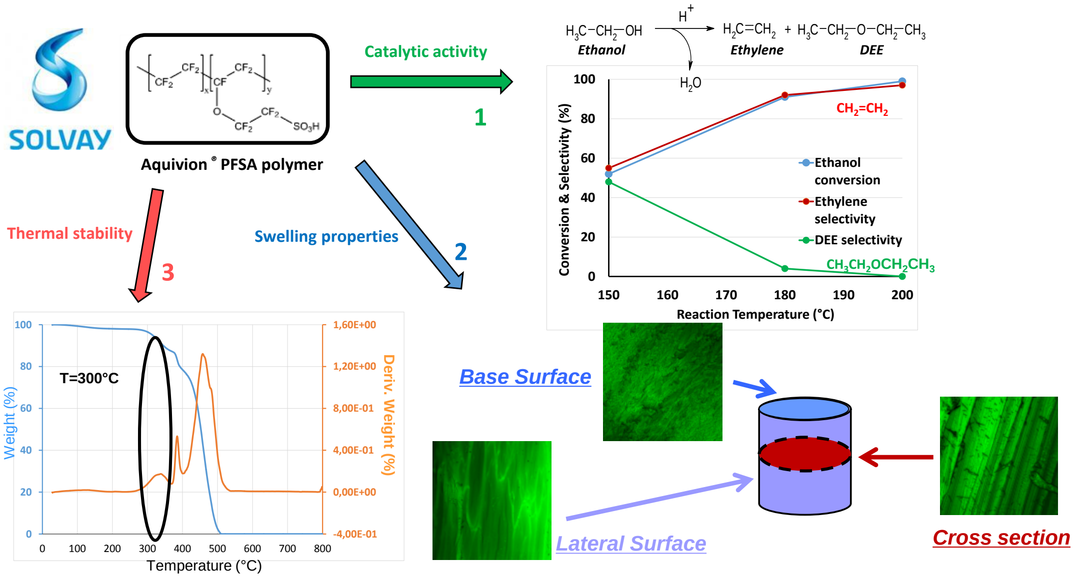

Scheme 3 Graphical abstract concerning the research work on Aquivion PFSA materials.

This innovative material is a perfluorosulfonic superacid resin produced by Solvay Specialty Polymers and it was tested in the model reaction of ethanol dehydration to ethylene, providing high ethanol conversion at relatively low temperature and stable performances for different hours (**Scheme *3***, part 1), although its very low surface area. Moreover, these catalytic systems showed interesting swelling properties, investigated performing fluorescence microscopy analysis on Aquivion pellet impregnated with solution of fluorescein and solvents with different polarity (**Scheme *3***, part 2). Moreover, the thermal behaviour of this material was followed through TGA coupled with FT-IR spectrometer (**Scheme *3***, part 3), showing high thermal resistance. From the study of Aquivion features and catalytic properties emerged that this material could have possible application as heterogeneous acid catalyst in gas-phase reactions.

References

---

[1] P. Benito, M. Gregori, S. Andreoli, G. Fornasari, S. Millefanti, F. Ospitali, S. Albonetti, *Catal. Today* **235**, 134-143 (2014).

[2] P. Benito, M. Gregori, S. Andreoli, G. Fornasari, F. Ospitali, S. Millefanti, M. S. Avila, T. F. Garetto, S. Albonetti, *Catal. Today* **246**, 108-115 (2015).

[3] M. Blosi, S. Ortelli, A. L. Costa, M. Dondi, A. Lolli, S. Andreoli, P. Benito, S. Albonetti, *Materials* **9**, 550 (2016).

[4] European Patent No.16179182.7-1451, assigned to Solvay Specialty Polymers Italy S.p.A. (13/07/2016).

[5] S. Andreoli, M. V. Solmi, S. Albonetti, G. Fornasari (submitted).

Acknowledgements

Solvay Specialty Polymers SpA is acknowledged for financing this PhD project. Thank you to Manuel Gregori, Stefano Millefanti and Claudio Oldani from Solvay Specialty Polymers.

INSTM is acknowledged for co-financing this PhD project.

The Department of Industrial Chemistry “Toso Montanari” is acknowledged for accommodating this project. A special acknowledgment goes to my supervisors, professors Stefania Albonetti and Giuseppe Fornasari.